

Electronic Thesis and Dissertation Repository

---

12-12-2012 12:00 AM

## Optimal Inertial Sensor Placement and Motion Detection for Epileptic Seizure Patient Monitoring

Babak Kamalizonouzi  
*The University of Western Ontario*

Supervisor  
Dr. Samuel F. Asokanthan  
*The University of Western Ontario*

Graduate Program in Mechanical and Materials Engineering  
A thesis submitted in partial fulfillment of the requirements for the degree in Master of Engineering Science  
© Babak Kamalizonouzi 2012

Follow this and additional works at: <https://ir.lib.uwo.ca/etd>



Part of the [Biomechanical Engineering Commons](#), and the [Biomedical Devices and Instrumentation Commons](#)

---

### Recommended Citation

Kamalizonouzi, Babak, "Optimal Inertial Sensor Placement and Motion Detection for Epileptic Seizure Patient Monitoring" (2012). *Electronic Thesis and Dissertation Repository*. 990.  
<https://ir.lib.uwo.ca/etd/990>

This Dissertation/Thesis is brought to you for free and open access by Scholarship@Western. It has been accepted for inclusion in Electronic Thesis and Dissertation Repository by an authorized administrator of Scholarship@Western. For more information, please contact [wlsadmin@uwo.ca](mailto:wlsadmin@uwo.ca).

**Optimal Inertial Sensor Placement and Motion Detection for Epileptic Seizure  
Patient Monitoring**

(Spine title: Optimal Sensor Placement and motion Detection for Epileptic Patient)

(Thesis format: Monograph)

by

**Babak Kamalizonouzi**

Graduate Program in Engineering  
Department of Mechanical and Materials Engineering

A thesis submitted in partial fulfillment  
of the requirements for the degree of  
Master of Engineering Science

The School of Graduate and Postdoctoral Studies  
The University of Western Ontario  
London, Ontario, Canada

© Babak Kamalizonouzi 2012

THE UNIVERSITY OF WESTERN ONTARIO  
School of Graduate and Postdoctoral Studies

**CERTIFICATE OF EXAMINATION**

Supervisor

Examiners

\_\_\_\_\_  
Dr. Samuel F. Asokanthan

\_\_\_\_\_  
Dr. Shaun Salisbury

Supervisory Committee

\_\_\_\_\_  
Dr. Liying Jiang

\_\_\_\_\_  
Dr. Anand V. Singh

\_\_\_\_\_  
Dr. Ken McIlsac

The thesis by

**Babak Kamalizonouzi**

entitled:

**Optimal Inertial Sensor Placement and Motion Detection for  
Epileptic Patient Monitoring**

is accepted in partial fulfillment of the  
requirements for the degree of  
Master of Engineering Science

\_\_\_\_\_  
Date

\_\_\_\_\_  
Chair of the Thesis Examination Board

## Abstract

Use of inertial sensory systems to monitor and detect seizure episodes in patients suffering from epilepsy is investigated via numerical simulations and experiments. Numerical simulations employ a mathematical model that is able to predict human body dynamic responses during a typical epileptic seizure. An optimized inertial sensor placement procedure is developed to address achievement of highest possible sensing resolution in determining angular accelerations with minimal errors. In addition, a joint torque estimation procedure is formulated to assist in the future development of a possible detection scheme. Experimental motion data obtained from an epileptic seizure patient as well as a healthy subject via a cluster of inertial measurement sensors formed a basis for proposing a suitable detection scheme based on non-linear response analysis. In particular, preliminary experimental data analysis has shown that the proposed modified Poincaré Map based scheme can become an effective tool in detecting of seizure via inertial measurements.

Key words: Human body modeling, multi-body dynamics, epileptic seizure, sensor placement optimization, inertial measurement, gyroscopes, joint torque estimation, Lyapunov exponent, Poincaré map, seizure detection.

## Dedications

I am grateful to my loving parents who have always believed that I can achieve anything that I set my mind to. Their inimitable confidence in me continues to be a driving force in both my personal and professional life. I thank you for all your faith, love, support and patience and I dedicate this thesis to you.

## Acknowledgments

I would like to thank my supervisor, Professor Samuel F. Asokanathan. His thoughtfulness and kindness will be remembered fondly. I owe a debt of gratitude to him since he went beyond the call of duty to help me with this dissertation and his constant support and encouragement were indispensable factors behind the successful completion of this research.

Further, I should also thank Dr. McLachlan to devote his time to us to guide and assist us on various epileptic seizure topics as well as providing the opportunities to conduct experiments with his patient.

I would like to thank Jiamming (Bryan) Ma and Joel Book for their active support in Dynamics and Systems Sensing Lab (DSSL). Especially, Joel's experience with different software as well as lab equipments helped me tremendously during my research work.

I would also like to thank my friends and fellow lab mates for their valuable inputs and suggestions.

Finally, I would like to thank organizations such as the National Sciences and Engineering Research Council (NSERC) of Canada discovery grant, The University of Western Ontario's Academic Development Fund/Small Grants and Western Graduate Research Scholarship (WGRS) from the University of Western Ontario, as this research work was partly funded by them.

# Table of Contents

CERTIFICATE OF EXAMINATION .....	ii
Abstract.....	iii
Dedications .....	iv
Acknowledgments.....	v
Table of Contents .....	vi
List of Tables .....	x
List of Figures .....	xi
List of Appendices .....	xvi
Nomenclature .....	xvii
Acronyms .....	xxi
Chapter 1 .....	1
1 Introduction, Background and Related Work .....	1
1.1 Motivation.....	2
1.2 Human Body Dynamic Modeling and Simulation.....	4
1.2.1 Review of Human Body Dynamic Models.....	5
1.2.2 Forward vs. Inverse Dynamics .....	6
1.2.3 Kane’s Method and Application to Human Body Modeling.....	7
1.2.4 Simulation Software.....	8
1.3 Epileptic Seizure Classification and Definition .....	11
1.3.1 Facts about Epilepsy .....	11
1.3.2 Epileptic Seizure Generalized Types .....	13
1.3.3 Current Detection and Monitoring Systems for Epilepsy Studies .....	15
1.4 Inertial Sensor Selection and Placement.....	18

1.4.1	State-of-the-art in wearable inertial sensors and their medical applications .....	18
1.4.2	Review of current Products.....	20
1.4.3	Sensor Placement.....	24
1.5	Seizure Detection using Inertial Sensors .....	25
1.5.1	Seizure Detection Techniques.....	26
1.6	Thesis Aims and Outline.....	28
1.6.1	Thesis Aims .....	28
1.6.2	Thesis Outline .....	30
Chapter 2	.....	31
2	Human Body Modeling and Epileptic Seizure Simulation .....	31
2.1	Preliminary Anatomical Principles.....	31
2.1.1	Planes of Movement .....	32
2.1.2	Axes of Movement.....	32
2.1.3	Movements in the Sagittal Plane about the Coronal Axis .....	33
2.1.4	Movements in the Frontal Plane about the Sagittal Axis.....	34
2.1.5	Movements in the Transverse Plane about the Vertical Axis.....	35
2.2	Model Description .....	37
2.2.1	Modeling Assumptions .....	37
2.2.2	Segments.....	38
2.2.3	Degrees of Freedom and Segment Connections .....	40
2.2.4	Model Anthropometry .....	41
2.2.5	Passive Joint Moments.....	42
2.3	Epileptic Seizure Model.....	44
2.3.1	Muscle Contraction.....	45
2.3.2	Mechanical Model of the Arm.....	48



2.3.3	Moment Estimation for Myoclonic Epileptic Seizure Model.....	51
2.4	Dynamic Simulation Results.....	52
2.4.1	Motion Genesis™ Code.....	52
2.4.2	Simulation Results .....	55
2.5	Closure .....	63
Chapter 3	.....	64
3	Optimization of the Sensor Placement.....	64
3.1	Model Used to Place Inertial Sensors .....	64
3.1.1	Model Assumptions .....	64
3.1.2	Formulation of Arm Acceleration Uncertainties .....	65
3.2	Constrained Optimization for Sensing Angular Acceleration .....	71
3.2.1	Simulated Annealing Overview .....	71
3.2.2	Genetic Algorithm Overview.....	72
3.2.3	Objective Function.....	72
3.2.4	Results.....	73
3.3	Sensitivity Analysis .....	74
3.3.1	Sensitivity to the Joint Torque and Damping Coefficients.....	75
3.3.2	Sensitivity to the Arm Geometry and Mass .....	75
3.3.3	Sensitivity to the Inertial Sensor’s Uncertainty .....	76
3.4	Closure .....	77
Chapter 4	.....	78
4	Seizure Detection via Inertial Measurement based Torque Estimation .....	78
4.1	Joint Torque Estimation.....	78
4.1.1	Joint Angle Estimation Using Accelerometers and Magnetometers .....	79
4.1.2	Angular Rate Estimation using Accelerometers .....	83
4.1.3	The Procedure for Joint Torque Estimation.....	84

4.2 Closure .....	86
Chapter 5 .....	87
5 Motion Based Identification for Epilepsy .....	87
5.1 Inertial Sensory Detection System.....	87
5.1.1 Subjects and Attachment Locations.....	90
5.1.2 Synchronized Inertial and EEG .....	91
5.2 Inertial Measurement Results and Discussion .....	92
5.2.1 Node 01 on the Forearm .....	95
5.2.2 Node 05 on the Leg.....	97
5.3 Data Analysis .....	99
5.3.1 Fast Fourier Transform Analysis of the Data .....	100
5.3.2 Pseudo-Phase-Space Method.....	106
5.3.3 Lyapunov Exponent .....	108
5.3.4 Poincaré Map .....	110
5.3.5 Moment of Inertia Based Approach.....	113
5.3.6 Discussion.....	115
5.3.7 Limitations .....	116
5.4 Closure .....	117
Chapter 6.....	118
6 Conclusion and Recommendations for Future Work.....	118
6.1 Summary of Research.....	118
6.2 Thesis Contributions .....	119
6.3 Recommendations for Future Work.....	119
References.....	121
Appendices.....	131
Curriculum Vitae .....	152

# List of Tables

Table 1-1: Comparison of Dynamic Formulation Methods.....	8
Table 1-2: Commercial and non-commercial Multi-body Modeling and Simulation Software .....	10
Table 1-3: Statistical representation of inertial sensors selection for epilepsy studies in different papers .....	20
Table 1-4: Comparison of different commercial inertial sensor packages .....	24
Table 1-5: Comparison of the placement methods in different papers .....	25
Table 2-1: Anatomical planes and axes and type of motions in which everyday activities are involve.....	36
Table 2-2: Joints and joint degrees of freedom used in the present model.....	40
Table 2-3: Model anthropometry data used in the model [5] .....	41
Table 2-4: Coefficients for passive joint moments .....	44
Table 3-1: Optimal Sensor Placement Predictions .....	73
Table 3-2: Optimization sensitivity to the joint torque and damping coefficients .....	75
Table 3-3: Optimization sensitivity to the arm geometry and mass .....	76
Table 3-4: Optimization sensitivity to the inertial sensor's uncertainty .....	77
Table 5-1: Motion Node™ data output.....	89
Table A-1: Partial velocity for the two degree of freedom system.....	136

## List of Figures

Figure 1-1: Different techniques for simulation of human body motion.....	7
Figure 1-2: Application of LifeMOD to assess the kinematic and dynamic changes in the posture of an elderly person with an assistive device .....	9
Figure 1-3: Epilepsy Facts for Canada [22] .....	12
Figure 1-4: Schematic representation of body movements during simple motor seizure [33]	15
Figure 1-5: Electrodes placed at a number of locations on the scalp [37] .....	17
Figure 1-6: An EEG trace of a healthy individual at rest with their eyes closed [37] .....	17
Figure 1-7: An EEG trace of during an (absence) epileptic seizure [37].....	17
Figure 1-8 a, b: Xsens™ MVN [68] (a), MTx unit [69] (b) .....	22
Figure 1-9, AIRCAST™ Pneumatic Armband arm band used for attaching the sensor unit to the body [71] .....	22
Figure 1-10 a, b: Motion Node™ Bus on the wrist [70] (a), Motion Node™ unit and the Bus wireless system [70] (b) .....	23
Figure 2-1: Three major planes of movement: sagittal plane, coronal plane and transverse plane [97] .....	33
Figure 2-2: Movements in the sagittal plane about the coronal axis [98].....	34
Figure 2-3: Movements in the frontal plane about the sagittal axis [98] .....	35
Figure 2-4: Movements in transverse plane about the vertical axis [98].....	36
Figure 2-5 a, b: 15 segment of human body of Hanavan [96] (a), 17 segment of human body of Huston [100] (b) .....	39

Figure 2-6 a, b: 17 segment of human body model of Hatze [101] (a), 16 segment of human body model used in this text (b).....	40
Figure 2-7: Head/Neck model of Huston [100] .....	40
Figure 2-8: Joint resistance torque modeled with a non-linear torsional spring and damper .	43
Figure 2-9: Penalty moment for the elbow joint.....	43
Figure 2-10: Development of a mathematical model for muscle by Hill [107].....	46
Figure 2-11: Hill's muscle model.....	46
Figure 2-12: Time- course of the isometric twitch in which $a = 0.95, \beta = 0.08, f = 2.5gsmm, K1 = 69gmm, K2 = 2.0gmm,$ and $x - x_0 = 9 mm$ [109].....	48
Figure 2-13: Schematic overview of the biomechanical arm model in [75].....	49
Figure 2-14: Flowchart of the simulation procedure developed in Motion Genesis™ .....	54
Figure 2-15: Wrist angular velocity in the x-direction .....	56
Figure 2-16: Wrist angular velocity in the y-direction .....	57
Figure 2-17: Wrist angular velocity in the z-direction.....	57
Figure 2-18: Elbow angular velocity in the z-direction .....	58
Figure 2-19: Shoulder angular velocity in the z-direction .....	59
Figure 2-20: Hand acceleration in the x-direction .....	60
Figure 2-21: Hand acceleration in the y-direction .....	60
Figure 2-22: Hand acceleration in the z-direction .....	61
Figure 2-23: Forearm acceleration in the x-direction .....	62
Figure 2-24: Arm acceleration in the x-direction .....	62

Figure 3-1: Arm angular velocity components in the x directions .....	67
Figure 3-2: Arm angular velocity components in the y directions .....	67
Figure 3-3: Arm angular velocity components in the z directions.....	68
Figure 3-4: Configuration of accelerometer placement within the space available on the arm .....	69
Figure 4-1: The elbow virtual sensor and three forearm physical sensors .....	80
Figure 4-2: Analysis of the elbow joint angle using the double virtual sensors considered to be on the elbow .....	82
Figure 4-3: Kane’s equation of motion to calculate the joint torques.....	84
Figure 4-4: The actual and estimated torques at the elbow .....	85
Figure 5-1: Principle of seizure detection inertial sensory system .....	88
Figure 5-2: Sensors attachment on the body.....	91
Figure 5-3: X, Y, and Z definition for each Motion Node™ sensor [1].....	93
Figure 5-4: Magnitude of the acceleration and components in X, Y, and Z directions for the sensor unit placed on the forearm for seizure measurement.....	94
Figure 5-5: Magnitude of the angular rate and components in X, Y, and Z directions for the sensor unit placed on the forearm for seizure measurement.....	95
Figure 5-6: Acceleration magnitude of the Node 1 attached to the forearm .....	96
Figure 5-7: Gyroscope magnitude of the Node 1 attached to the forearm.....	97
Figure 5-8: Acceleration magnitude of the Node 5 attached to the leg .....	98
Figure 5-9: Gyroscope magnitude of the Node 5 attached to the leg .....	99

Figure 5-10: FFT spectrum of Node 01 (accelerometer output in the y-direction) on the forearm for seizure without high pass filter .....	101
Figure 5-11: FFT spectrum of Node 01 (accelerometer output in the y-direction) on the forearm for seizure with high pass filter .....	101
Figure 5-12: FFT spectrum of Node 01 (accelerometer output in the z-direction) on the forearm for seizure .....	102
Figure 5-13: FFT spectrum of Node 01 (gyroscope output in the y-direction) on the forearm for seizure.....	103
Figure 5-14: FFT spectrum of Node 01 (accelerometer output in the z-direction) on the forearm for rhythmic motion .....	104
Figure 5-15: FFT spectrum of Node 01 (gyroscope output in the y-direction in the z-direction) on the forearm for rhythmic motion .....	104
Figure 5-16: FFT spectrum of Node 05 (accelerometer output in the z-direction) on the leg for seizure.....	105
Figure 5-17: FFT spectrum of Node 05 (accelerometer output in the z-direction) on the leg for walking .....	105
Figure 5-18: Pseudo-Phase-Space method for Node01 (accelerometer output in the z-direction) on the forearm .....	107
Figure 5-19: Pseudo-Phase-Space method for Node05 (accelerometer output in the z-direction) on the leg .....	107
Figure 5-20: Lyapunov exponent for different activities .....	110
Figure 5-21: Poincaré map for the Node 01 on the arm .....	112
Figure 5-22: Poincaré map for the Node 05 on the leg.....	113
Figure 5-23: Moment of Inertia based approach.....	114

Figure 5-24: Proposed method for the detection..... 116



## List of Appendices

Appendix A: An example of application of Kane's method.....	131
Appendix B: Joint Torque Estimation Procedure Developed in Motion Genesis™ .....	139
Appendix C: Experimental plots and Poincaré Plots .....	147

## Nomenclature

$F(t)$	Second-order critically damped impulse response
$F_o$	Constant for given motor unit
$t$	Time in seconds
$\tau_{sum}$	Twitch Time (time for tension to reach maximum)
$g(t)$	Active state of the muscle
$\alpha, \beta$	Muscle characteristic coefficient
$F_m$	Force generated by the muscle
$K_1$	Slope of nonlinear springs and dampers at the linearization point of load-extension curve of the muscle
$K_2$	Slope of nonlinear springs and dampers at the linearization point of tension-length curve of the muscle
$f$	Slope of nonlinear springs and dampers at the linearization point of force-velocity curve of the muscle
$x_o$	Unstretched length of the muscle
$x(t)$	Length of the muscle at time $t$
$F_{ag}$	Agonist muscle force
$F_{ant}$	Antagonist muscle force
$F_{sum}$	Constant for the agonist and antagonist muscle impulse response
$A, B$	Dimensionless constants for the agonist and antagonist muscle impulse response
$k_{1j}, k_{2j}, k_{3j}, k_{4j}$	Constants of joint $j$ for determination of the profile of the ligament's moment-angle relationship
$\theta_{1j}, \theta_{2j}$	Initial angles of joint $j$
$c_j$	Damping coefficient of joint $j$
$\dot{q}_j$	Angular change of joint $j$
$T_{lig,j-1}$	Net ligament moment applied about joint $j$
$T_{lig,j-2}$	Damping torque /moment of joint $j$

$x(t)$	Displacement of arm
$e_1(t), e_2(t)$	Moving frame of reference for arm model
$v(t)$	Linear velocity of arm
$\omega$	Angular velocity of moving frame
$\alpha(t)$	Angular acceleration of arm
$a(t)$	Linear acceleration of arm
$A_t(t)$	Tangential component of arm linear acceleration
$A_n(t)$	Normal component of arm linear acceleration
$I$	Mass moment of inertia
$d_{ag}$	Distance from elbow joint to the action point of the agonist muscle force
$d_{ant}$	Distance from elbow joint to the action point of the agonist muscle force
$L$	Rigid rod length
$m$	Mass of arm/rod
$R$	The distance from elbow to wrist
$K$	Constant for epileptic seizure acceleration model
$A_i$	Acceleration of accelerometer number $i$
$A_j$	Acceleration of accelerometer number $j$
$P_{ij}$	Position vector from $i$ th to $j$ th sensor
$a_{i,x,y,z}$	Linear acceleration of accelerometer $i$
$\sigma_{\alpha_{x,y,z}}$	Overall uncertainties in $x, y, z$ angular acceleration components
$\sigma_{i,x,y,z}$	Uncertainty values of each accelerometer in the $x, y, z$ directions
$\sigma_{\alpha}$	Magnitude of overall uncertainty in angular acceleration
$l, m, n$	Sensor non-dimensional location variables in the range of $[0 \dots 1]$
$A_{i,x,y,z}$	Equivalent acceleration at point $i$ where $i$ th sensor is located
$g$	Gravitational acceleration
$\ddot{R}_{i,x,y,z}$	Acceleration of point $i$ relative to global coordinate system

$R$	Global coordinate
$A_{forearm}$	Acceleration of the virtual sensor at the elbow joint and in the direction of the forearm
$A_{arm}$	Acceleration of the virtual sensor at the elbow joint and in the direction of the arm
$\theta_{x,y,z}$	Rotation angles about x, y and z directions
$M_{forearm}$	Magnetic vector of the virtual sensor at the elbow joint and in the direction of the forearm
$M_{arm}$	Magnetic vector of the virtual sensor at the elbow joint and in the direction of the arm
$N$	Number of replacement steps in Lyapunov exponent calculation
$\lambda$	Lyapunov exponent
$d(t_k)$	Measure of initial distance between the two starting points at a small but later time
$d_o(t_{k-1})$	Measure of the initial distance between the two starting points
$J_{2xx}, J_{2yy}$	Second moment of inertia measure
$\vec{F}_j^c$	Constraint forces associated with $j$ th segment
$\vec{F}_j^*$	Inertia force associated with $j$ th segment
$\vec{F}_j^e$	external forces associated with $j$ th segment
$\vec{M}_j^e$	Constraint torques associated with $j$ th segment
$\vec{M}_j^c$	Inertia torques associated with $j$ th segment
$\vec{M}_j^*$	external torques associated with $j$ th segment
$\delta w$	Virtual work
$\delta r$	Virtual displacement
$F_r$	Generalized inertia force
$F_r^*$	Generalized active force
$v_j$	Virtual linear velocity
$M_r$	Generalized inertia torque

$M_r^*$	Generalized active torque
$\bar{I}$	Inertia dyadic of $j$ th body relative to the center of mass
$G_j$	Center of mass of $j$ th body
$R$	Global coordinate system
$u_j$	Generalized speed of the $j$ th body
$\hat{n}_1\hat{n}_2$	Global Coordinate system
$\hat{a}_1\hat{a}_2$	Coordinate system of body A
$\hat{b}_1\hat{b}_2$	Coordinate system of body B

# Acronyms

<b>MEMS</b>	Micro Electro Mechanical Systems
<b>EEG</b>	ElectroEncephaloGraphy
<b>ECG</b>	ElectroCardioGraphy
<b>EMG</b>	ElectroMyoGraphy
<b>IMU</b>	Inertial Measurement Unit
<b>PD</b>	Parkinson Disease
<b>PE</b>	Parallel element
<b>SE</b>	Series Element
<b>CE</b>	Contractile Element
<b>RSS</b>	Root of the Sum of the Squares
<b>GA</b>	Genetic Algorithm
<b>SA</b>	Simulated Annealing
<b>FFT</b>	Fast Fourier Transform
<b>DOF</b>	Degree of Freedom
<b>CSV</b>	Comma Separated Values
<b>FBX</b>	Filmbox, file format (.fbx) developed by Autodesk
<b>Collada</b>	COLLABorative Design Activity

## Chapter 1

### 1 Introduction, Background and Related Work

Epilepsy is one of the most common neurological disorders and it is known to affect almost one percent of the population which results in significant social and economic impact [1]. The main challenge for epileptic patients and their families is that seizures which are sudden and unpredictable make the patient unconscious and as a result vulnerable to risks such as severe trauma and even death. This problem justifies the search for new monitoring systems that unlike the current ones are not limited to the hospital so that they can be used during daily activities.

In an effort to address the above requirement, the present thesis focuses on the development of a wearable sensory system for detection of epileptic seizure using commercially available MEMS (*Micro Electro-Mechanical Systems*) inertial sensors. This system if further developed, enables the patient to live independently and the hospital staff or relatives to monitor the patient involuntary movements while undergoing an epileptic seizure.

For the purposes of development of such a detection system, a mechanical model of human body is first developed so that involuntary movements during an epileptic seizure can be understood via simulation. Based on the model predictions as well as the choice of inertial sensors, an optimal strategy for the placement of sensors is proposed. In order that this system can be implemented, a detection methodology to distinguish between normal activities and seizure episodes is proposed and tested via experimental data. This chapter first presents the motivation behind the proposed method and then followed by a review of relevant scientific papers which provide sufficient background information regarding the human body dynamic modeling, Epilepsy classification, state-of-the-art in wearable inertial sensors and their motion-based medical applications. Further, the objectives and assumptions of the current research are also illustrated.

## 1.1 Motivation

Epilepsy is a neurological disorder in which the tendency of the brain to generate epileptic seizures causes involuntary movements. Approximately thirty percent of the epileptic patients continue to have seizures despite using appropriate medications. Many of these onsets are sudden and unpredictable in nature and are known to make the patient lose consciousness and present the potential risk of severe trauma and even death. In some cases, when patients are unsupervised seizures may pass unnoticed, especially during sleep, making the prescription and monitoring purposes more difficult. Under these circumstances, lack of immediate medical assistance can also potentially lead to high risk of mortality. Hence, it is envisaged that the development of a system which is capable of detecting and recording the seizure as well as triggering an alarm in life-threatening occasions, can prove to be effective in reducing the above risks. For example, an alarm can warn staff at the hospital or relatives at home giving a clear knowledge of how often, when and in which incidents the seizure is likely to happen for a particular patient.

Even though there are currently a variety of alarm systems available including patient's bed shaking analysis, rhythmic movement detection by video algorithms, seizure associated Electroencephalography (EEG) pattern recognition, audio sensitive seizure detection devices, and heart rate, rhythm, or regularity analysis, they are found to be not reliable owing to their low sensitivity and false detection sequences. In the case of video detection, regular rhythmic movements can be recognized across pixels of digital image by image processing techniques, but such recognition obviously fail when patients are under a cover. Bed shake detectors are also not very practical since they are only limited to detection of seizures that manifest as repetitive physical movements and not the non-repetitive seizure manifestations.

Hence, this problem justifies the search for new detection systems that are based on inertial sensors that have recently become commercially successful for many mechanical, aerospace, robotic and medical applications. The fact that the epileptic seizure is a motor phenomenon makes the movement-based detection systems an alternative to the current devices. Even though some practice of using inertial sensors in biomechanical and



biomedical studies has recently been established, the work on these systems still seems to be on early stages of its development. Indeed a wave of gathering interest is propelling the field in a variety of directions mostly fueled by cooperation between two fields of engineering and medical studies. For instance, inertial sensors are now used in a wide range of medical application areas for monitoring and studying hand tremors, gait analysis, falling from bed alarms and Parkinson's disease.

It is known that, the efficiency of a detection sensory system depends on the information it can retrieve from a seizure episode. Since the information from a detection system should be sufficient but not excessive, an increased number of sensors alone do not guarantee that the detection system will have a better performance. The relevance of the information brought by an additional sensor must also be taken into account and economic issues may also be considered. When designing a sensor system, one must search for those combinations (numbers and placements) of sensors that can provide the highest possible detection level at the lowest possible cost.

Question at this stage would be: what type of inertial sensors should be used for the detection system? Different combinations of sensors, from using just accelerometers, to the combination of accelerometers, gyroscopes and magnetometers have been suggested in the recent past. Generally in the combined ones, the recent efforts have gone towards extracting an extra piece of information which cannot be derived by using just accelerometers or magnetometers. Even though utilization of the combined inertial sensors, including accelerometers, magnetometers and gyroscopes has been shown to reduce the drift but still the uncertainties of each sensor are known to cause detection errors. In order to quantify and account for errors induced by the placement of each sensor, one needs to develop relationships between human body model and noise level associated with each sensor. Hence, development of a suitable human body model becomes necessary so that explicit dynamic equations that govern the body motion can be derived and employed for suitable sensitivity analysis.

Employing dynamic response simulations via human body model and a suitable detection system, one must also be able to distinguish between the epileptic seizure onset and

normal activities of a patient. This is the area that mostly discussed among the researchers and it seems to be still a challenging topic. Based on the literature search performed in this area to date, there appears to be no accurate and efficient method available to detect the epileptic seizure via inertial sensors. Most of the detection systems employed at present relies on the use of video recording or EEG in conjunction with inertial sensors to detect epileptic episodes. However, this approach on the contrary negates the initial purpose of using inertial sensors which are proposed due to the advantage they offer for portability. Hence, the need for a detection system that is online, immediate, reliable, comfortable and solely rely on the data from inertial sensors prevails.

## 1.2 Human Body Dynamic Modeling and Simulation

The subject of human motion analysis has fostered a dramatic growth of biomechanics researcher interests in simulation and modeling of human body for years and as a matter of fact human body musculoskeletal models and computer simulations have served many purposes in biomechanical research. Numerous models have been used to predict, estimate and define human mechanisms in events that involve body movement. The power of modeling is increasingly accredited in the field of biomechanics with the advent of sophisticated software for human modeling. These types of simulation software provide a realistic and economical set of tools to maintain and improve the skills of healthcare providers and add an invaluable significance to medical education, training and research. As human biomechanical model is a multi degree of freedom system with many unique complexities, one of the main challenges in developing such models is to make the model consistent with the real physical activity to be mimicked [2]. Biomechanical models can replace some of the experimental measurements such as the internal forces in the skeleton and muscular actions, which may be difficult to carry out any other way [3]. Furthermore, biomechanical models can be employed to provide more quantitative explanations and analysis of how the neuromuscular and musculoskeletal systems interact to create movement [4]. Therefore, mathematical and computational tools in general, and multi-body dynamics in particular have been widely applied to build biomechanical models.

There are two main streams of modeling in the human body simulation: inverse dynamics and forward dynamics. In the following sections first previously developed biomechanical models are reviewed then brief discussion on two popular dynamic formulation methods namely, Newton-Euler and Kane's approach will be presented. The section will proceed with a concise review of Kane's method and concludes by providing an overview of common biomechanical simulation software.

### 1.2.1 Review of Human Body Dynamic Models

One of the major issues in biomechanics has been the creation of mathematical models that resemble the human body, in a manner that gives the researchers an opportunity to recreate, simulate or analyze human body movements. As a matter of fact, over the recent years modeling of the human body movement has received significant attention from many researchers. This interest is motivated by a wide variety of applications such as athletic performance analysis, surveillance, research and development, military, human-machine interface, welfare and rehabilitation robotics, and prosthetics.

Anderson et al. [5] developed a human model that consists of 10 rigid bodies, actuated by 54 muscles to simulate maximum vertical jump. Similar to this work, 35 degrees of freedom, three-dimensional human skeletal model was presented by Nagano et al [6] to simulate motion during the jump action using AutoLev software. In their research, Bei et al. [7], created a musculoskeletal multi-body knee model consisting of two rigid bones and one deformable contact surface to predict muscle forces and contact pressures in the knee joint during gait. Sasaki et al. [8], using the forward dynamics technique, a developed 2-dimensional musculoskeletal human model consisting of seven rigid bodies and 15 Hill-type musculotendon actuators at each leg to identify differences in muscle function in walking and running. Huang et al. [9] followed Kane's method to develop a finite-segment, 17 segments human-body model for studying whole body response to jarring and jolting. Nonlinear springs and dampers were used at the joints to represent soft tissue restraint forces and the model was tested and validated with experimental data. In their analyses, Gallenstein et al. [10] studied human motion with straight knees, bent knees, and legs without feet during swimming by applying Kane's method on the 15 segment human body model.

In addition, multi-body biomechanical models have been applied to passive human motion in order to study different injury scenarios such as impact or falling down. For example, Silva et al. [11] have studied injury scenarios for the human head during impact simulation using a three-dimensional biomechanical model consisting of 12 rigid bodies with passive torque applied at each of the 11 joints.

### 1.2.2 Forward vs. Inverse Dynamics

Inverse dynamics is a method that is commonly used in the biomechanical analysis of human movements to assess the net joint torque or muscle induced moments due to the contraction of muscles at each joint using the experimental data from motion, electromyography (EMG) or sensory measurements. This method uses kinematic, kinetic, and anthropometric information as input to solve the equations of motion for each body segment [12]. The inconsistency between the measured data due to modeling error as well as the indeterminate muscle tensions due to actuation redundancy are two main sources of error in inverse dynamics approach. Optimization techniques are applied in order to obtain a unique solution for the latter problem. Other sources of error are also reported which includes inaccuracy in movement coordinate data that is due to the error in marker location. The inherent motion capture system noise and also skin movement artifact, estimations of body segment parameters, and identification of joint center of rotation locations are also reported as sources of errors [13].

Forward dynamics computation, on the other hand, is performed to simulate the motion assuming a muscle activation pattern or even neglecting the effects of the muscle and soft tissue and just considering the joint torques. Actuated forward dynamics simulations are particularly powerful because they allow for the identification of the relationships between the torque applied to the joints, and the specific task movement. Understanding these relationships without simulation analyses is challenging because of the highly complex, nonlinear and multi degree of freedom nature of the human body system. Simulations also allow estimation of quantities that are difficult or impossible to measure in vivo, such as the applied joint torque by using the measurable quantities such as angular acceleration and angular displacement of the joints, and acceleration of the segments along with the forward dynamics equations of motion. A similar procedure is

developed in chapter 4. Figure 1-1 summarizes the simulation techniques that are traditionally employed for human body modeling.

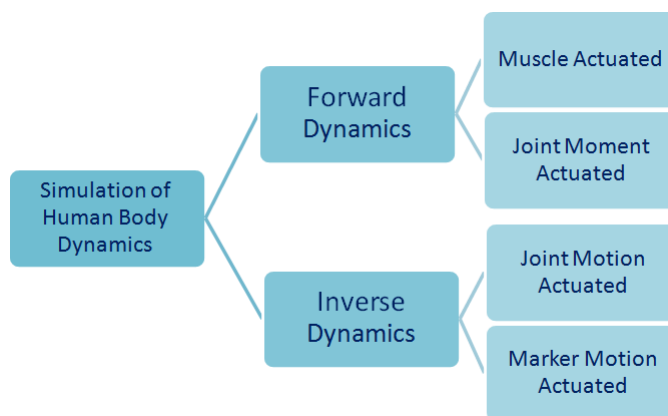


**Figure 1-1: Different techniques for simulation of human body motion**

### 1.2.3 Kane's Method and Application to Human Body Modeling

In 1961, Professor Thomas Kane published a paper ‘‘Dynamics of Non-holonomic Systems’’ [14] in which he described a new method for formulating the equations of motion of complex multi-body dynamical systems. This new method was a Lagrangian form of D’Alembert’s principle which allowed dynamical equations to be generated without differentiation of kinetic and potential energy. Later, in 1965 Kane and Wang published a paper ‘‘On the Derivation of Equations of Motion’’ [15] and described the use of ‘generalized speeds’. These two papers formed the foundation of what has since become known as Kane’s method for multi-body dynamics.

Although application of Kane’s method has advantages over other methods available such as Newton-Euler and Lagrange for formulating dynamical equations (Table 1-1) [16], the importance and ease of Kane’s method was not fully recognized until the advances in the space industry of 1960s and 1970s. At that time, reducing the cost of simulation as well as making the equations of motion suitable for modeling and computer programming lead to the use of Kane’s method. For instance, in references [17], [18] and [19] funded by NASA, researches modeled a human in freefall (weightlessness) by using Kane’s method.

Later, researchers used this method in other areas involving human activities; for example Lemmon et al [20] studied the dynamics of a car crash victim, or Gallenstein et al [10] analyzed the swimmer motion and more recently Nagano et al [6] applied this method to study the jumping dynamics of a human body.

**Table 1-1: Comparison of Dynamic Formulation Methods**

Method	Basis	Advantages	Disadvantages
<b>Newton-Euler</b>	Free-Body Analysis	- Yields good physical understanding	- The interactive forces between the bodies are included in the analysis - Looks at the system in parts
<b>Lagrange</b>	Virtual Work	- Eliminates non-working interactive forces at the joints	- Require differentiation of scalar energy functions. - Requires use of virtual work approach, which can be vague - Requires introduction and elimination of Lagrange multipliers for closed-loop systems
<b>Kane</b>	Partial Velocities	- non-working interactive forces between the bodies are automatically eliminated without the need for tedious differentiations of scalar energy functions - Highly systematic- leads to expressions which are easily converted joint algorithms and can be implemented via computer codes.	- Physical insight can be limited

#### 1.2.4 Simulation Software

Many commercial software such as LifeMOD have been developed based on multi-body dynamics theories in order to enhance the development of biomechanical modeling. For example, Figure 1-2 shows a graphic representation of a full body human musculoskeletal model which has been developed based on multi-body dynamics commercial software and is used to test and verify assistive device applications.

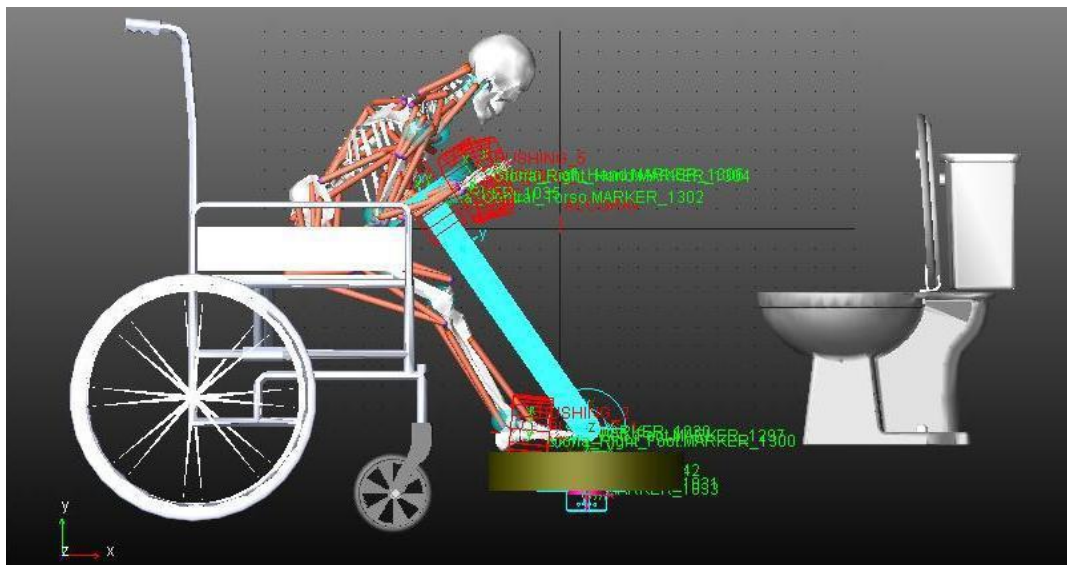


**Figure 1-2: Application of LifeMOD to assess the kinematic and dynamic changes in the posture of an elderly person with an assistive device**

As discussed in Table 1-2, Kane's method has found its way to computer implementation and simulation programs such as ADAMS, Motion Genesis™, Working Model, LifeMOD, etc which are proficient in algebraic manipulations and benefit from this approach. These programs are able to calculate the entire set of dynamics equations in an algebraic form for open-chain linked-segment models, making it possible to utilize models with more segments and more degrees of freedom.

Unlike other biomechanics software such as LifeMOD and ADAMS, Motion Genesis™ provides a step by step approach to Kane's method which allows some insight into the nature of the derived equations. As stated in the user's manual, "Motion Genesis™ was created to facilitate analyses based either on Kane's method or on Newton-Euler equations." Components such as the mass, inertia values, dimensions of each segment as well as the coordinates and the input functions are all entered in a systematic way. Once these components are entered, Motion Genesis™ can generate sets of equations of motion as MATLAB™ or C++ code. The generated code actually integrates Motion Genesis™ equations forward in time using a fourth-order Runge Kutta integration scheme. This numerical method can solve a wide range of equations such as ordinary and nonlinear differential equations. In addition, the generated MATLAB™ code is an optimal one

which reduces the time of calculation effectively. Thus Motion Genesis™ has been the choice of program for the present study since it provides a step by step approach to Kane's method which allows some insight into the nature of the equations derived and is considered to be a valuable tool for the present research.

Table 1-2 shows a brief comparison of the common multi-body software used for human body modeling.

**Table 1-2: Commercial and non-commercial Multi-body Modeling and Simulation Software**

<b>Simulation Software</b>	<b>Method Used</b>	<b>Output</b>
ADAMS MSC Software Corporation, USA	Kane's Method/ Newton-Euler Method	Capable of importing the full body musculoskeletal CAD model, output is in the form of graph or rough data.
AnyBody AnyBody Technology, Denmark	Not given	Musculoskeletal, full body Musculoskeletal CAD based Model/graphs in which joints, constraints and initial values are selectable from the library or can be defined.
Motion Genesis™ USA	Kane's Method	Symbolic sets of equations of motion, MATLAB™ and C++ code.
SIMM MusculoGraphics	Kane's Method	Musculoskeletal, full body CAD based Model/graphs in which joints, constraints and initial values are selectable from the library or can be defined.
Pro/ENGINEER formerly Pro/MECHANICA PTC, USA	Kane's Method	Musculoskeletal, full body CAD based Model/graphs in which joints, constraints and initial values are selectable from the library or can be defined.
SD/FAST (Dynamic software for mechanical systems), PM, USA	Kane's Method	The full nonlinear equations of motion for that system. C++ or Fortran code.
SimMechanics Simulation Toolbox for MATLAB™	Kane's Method, Lagrange Method or Newton-Euler	Symbolic sets of equations of motion, MATLAB™ but very limited compared to others.
Working Model 2D and 3D simulation software from MSC Software Corporation	Kane's Method	Less sophisticated version of ADAMS with output in the form of graph or rough data.



## 1.3 Epileptic Seizure Classification and Definition

Epilepsy has been defined as a medical condition characterized by sudden, brief and recurrent seizures due to the excessive irregular discharge of neurons present in the brain [21]. Seizure itself occurs when a strong wave of electrical activity causes an extreme discharge of neurons in the brain, causing a variety of clinical signs that can be detected either by movement analysis using inertial sensors or brain wave analysis by EEG. Seizure is like a brief electrical storm within the brain and typically lasts from a few seconds to a few minutes.

### 1.3.1 Facts about Epilepsy

Epilepsy affects almost 60 million people worldwide and it has an important social and economic impact on the people concerned [1]. Particularly in Canada, almost 0.6% of the population is known to have the condition of epilepsy. However, due to the encompassing public stigma and the prejudice with which people with epilepsy has historically been treated in society, many with the disorder are resentful to embrace their condition or to seek for treatment. Thus, the prevalence of epilepsy is likely much higher. Figure 1-3 summarizes the facts about epilepsy in Canada as reported by Epilepsy-Canada in [22].

Interestingly, it may be noted that a number of past world leaders and notable people are known to have suffered from epilepsy. In fact, a possible link between epilepsy and greatness has attracted biographers and physicians for centuries. For instance, McLachlan [23] states that Julius Cesar's disease and its consequences possibly altered the course of his life and consequently the history. The French 17th century physician Jean Taxil in his Treatise on Epilepsy refers to Aristotle's "famous epileptics". This list includes Julius Caesar and Roman Emperor Caligula, Drusus, Petrarch, Hercules, Ajax, Bellerophon, Socrates, Plato, Empedocles, Maracus of Syracuse, and the Sibyls [24].

There are number of factors which may trigger the epileptic seizure including stress, poor nutrition and skipped meals, missed medication, flickering lights, illness, fever and

allergies, lack of sleep, emotional involvements such as anger, worry and fear, heat and/or humidity[25]. In almost half of epileptic patients, the cause of epilepsy is unknown. However, in the other half, brain tumor and stroke, and head trauma of any type are most common causes. Other cases that are listed as possible causes of epilepsy include [22]:

- Injury; the more severe the injury, the greater the chance of developing epilepsy
- Infection or systemic illness of the mother during pregnancy
- Brain injury to the infant during delivery may lead to epilepsy
- Aftermath of infection (meningitis, viral encephalitis)
- Poisoning, from substance abuse of alcoholism

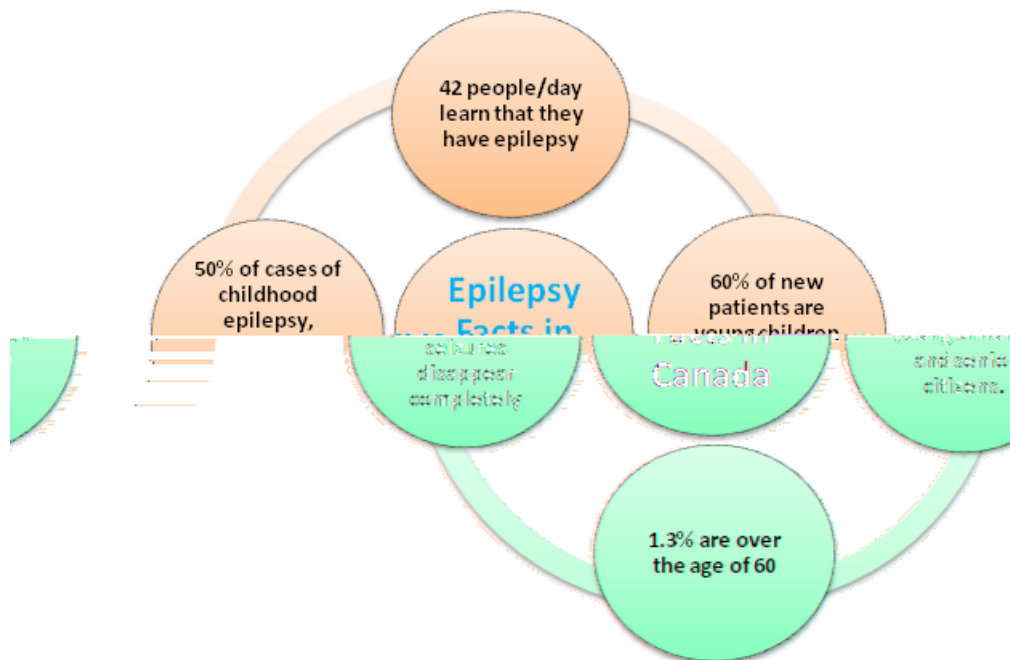


**Figure 1-3: Epilepsy Facts for Canada [22]**

The major form of treatment is long-term drug therapy. However, drugs are not a perfect cure and can have numerous and sometimes severe, side effects. In some severe cases, when the medication fails and the epileptic patient classified as the drug-resistant, brain surgery may be recommended. Surgery consists of the removal, disconnection or coagulation of the brain areas from where seizures arise. The surgery on these areas, so

called epileptogenic zone, will be done only when the seizures are confined to one area of the brain in which the brain tissue can be safely removed without damaging personality or function. Such an approach requires a precise localization of the epileptogenic zones.

Although some segments of the population affected can be treated successfully with drug therapy or neurosurgical procedures, approximately a quarter of the affected patients cannot be treated via any available therapy [1]. These people are at high risk for physical as well as mortal injuries. They are often unable to live independently and a large number is institutionalized. Hence, for the epileptic patients in general, and in particular to the class mentioned above, the instantaneous detection of an epileptic seizure can play a significant role in shaping their well-being. Such a detection unit can be made to trigger an alarm system to get the right assistance in situations that require immediate intervention. This is especially important in institutions where many patients with severe epilepsy live together. Due to lack of resources, the patients are not continuously supervised by nurses especially at night, hence justifying the need for design and development of robust sensing/alarm systems.

### 1.3.2 Epileptic Seizure Generalized Types

Use of inertial sensors which is the main focus of thesis can only allow detection of the type of seizures that express themselves in movements or alternatively the type of seizures which disturb the normal movement patterns. Motor seizure is the term which describes the seizures in which the main clinical manifestations are movements [26]. These kinds of so called “motor seizures” can be divided into two major subgroups, simple motor seizures and complex motor seizures. Simple motor seizures involve motor movements that are relatively ‘simple’ and unnatural. In addition, simple seizures are not accompanied by loss of consciousness and are caused by a relatively massive discharge in the motor structures of the cortex [27]. Whereas complex motor seizures are seizures in which the movements are relatively complex and simulate natural movement, except that they are inappropriate for the situation. These seizures often arise from the limbic system and they are accompanied by loss of consciousness [28]. The focus of this thesis is on the simple motor seizures. This focus actually justifies the application of inertial sensors to model, observe and eventually detect the epileptic seizure. Simple motor

seizures can be subdivided into the following types: myoclonic, clonic, tonic, and tonic-clonic seizures. Primarily simple seizures can be sub-classified into a number of categories, depending on their frequency of movement, the duration of muscle contractions and the muscle involved.

#### 1.3.2.1 Myoclonic Seizures

Myoclonic seizure involves an extremely brief ( $< 100$  ms) muscle contraction with the frequency of 50 Hz [29]. The seizure can result in jerky movements of a few adjacent muscles, for example, only one antagonistic pair muscles or muscle groups. The surface EEG associated with a myoclonic seizure shows a poly/spike wave correlate [30]. EMG-signals reveal synchronous muscle activation in both agonist and antagonist muscle of the affected muscle group. In myoclonic seizure, the flexion of the elbow and the movement arm movement are dominant over other parts of body movements.

#### 1.3.2.2 Clonic Seizures

Clonic seizures consist of regularly repeated myoclonus contractions recurring at intervals between 0.2 and five times per second (i.e. 0.2-5 Hz). During a clonic seizure the affected parts of the body show repetitive jerking [31]. During the clonic seizures (poly) spike-wave complexes were observed in the EEG [32]. Here again the bursts of muscle activation occurred synchronously in agonistic and antagonistic muscles and were separated by periods of complete muscle relaxation in all muscles. A distinguishing factor between clonic and myoclonic seizure is that myoclonic seizures involve only one or a few twitches or jerks without any particular rhythm whereas clonic seizure is rhythmic.

#### 1.3.2.3 Tonic Seizures

During tonic seizures a sustained sudden contraction of multiple muscle groups is observed. Tonic seizures typically have a duration that is from 10 to 20 seconds, but can also be subject to some variations [26]. Tonic seizures most often occur during sleep and usually involve all or most of the parts of brain, affecting both sides of the body. If the

person is standing or walking at the instant the seizure starts, he or she often falls. However, consciousness is usually preserved.

#### 1.3.2.4 Tonic-Clonic Seizures

Tonic-Clonic seizures involve an initial contraction of the muscles similar to the tonic seizure during which the patient has the legs and arms in extension with the arms adducted and crossed in front of the body; this phase lasts 5 to 10 seconds. It is then followed by a series of rhythmic, tremor-like muscle contractions. In which muscle contractions are similar to the clonic seizure. The movements of the arms increase progressively in amplitude as the repetition rate diminishes. This type of seizure may involve tongue biting, urinary incontinence and the absence of breathing. Figure 1-4 shows a schematic representation of body movement during tonic and clonic phases.

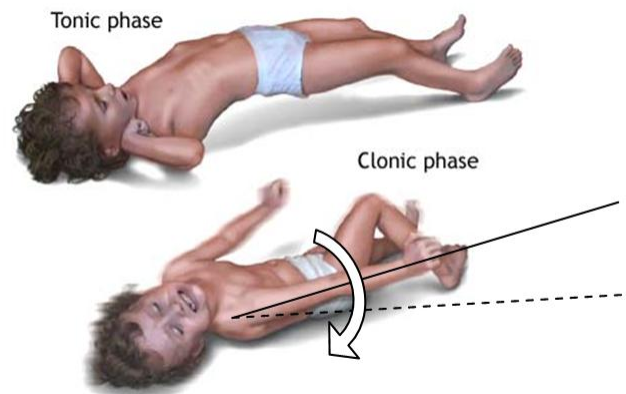


**Figure 1-4: Schematic representation of body movements during simple motor seizure [33]**

#### 1.3.3 Current Detection and Monitoring Systems for Epilepsy Studies

Currently, the primary method used for epileptic seizure characterization relies on recording of electrical activity of the brain through EEG electrodes which are attached to the scalp. The electrical activity is created by the stimulation of neurons in the brain. A routine clinical EEG recording with the preparation typically lasts 45 minutes and usually involves recording from more than 15 scalp electrodes that are attached to the head as

shown in Figure 1-5. EEG recordings require either an invasive recording which is called “intracranial electrodes” in medical terms or placement of several scalp electrodes which is less stable over time. The patient may also be uncomfortable wearing electrodes on the scalp since they are very noticeable for others. In EEG plots, seizures are generally characterized by a high degree of synchronization across the electrode array and an abnormal degree of periodic regularity as shown in Figure 1-6 and Figure 1-7.

Despite the fact that the EEG method is considered to be the gold standard for epilepsy diagnosis and studies, it does not necessarily seem to be the best option for a seizure alarm outside of the hospital. Further, various references discussed the limitations of the EEG even in the hospital, for example [34] mentioned that some people without epilepsy may have abnormal EEG results. They also stated that about 25% of people with epilepsy will have normal EEG results even after undergoing several EEG tests. Today there are some portable EEG devices available, however other than being less reliable than customary EEGs, they have some drawbacks which include [35][36]: when used over a period of time, an increase in the contact resistance and thereby degrading of signal quality occurs since the gels used in the electrodes dry out, and also the gels used in the electrodes cause irritations and rashes when used for longer durations.

When the medical history and repeated EEGs are not enough to figure out what kinds of seizures the patient is having or in the cases which EEG does not give satisfactory results, simultaneous video and EEG recording are used. This method can be also useful for diagnosing other types of seizures from epileptic ones. However, these methods can only be used in a room where a camera is available and during the monitoring phase, a patient must not use any body cover such as a blanket. Further, knowing that the person is under surveillance makes some of the patients uncomfortable and consequently this method is considered not suitable for the intended purpose.



Figure 1-5: Electrodes placed at a number of locations on the scalp [37]

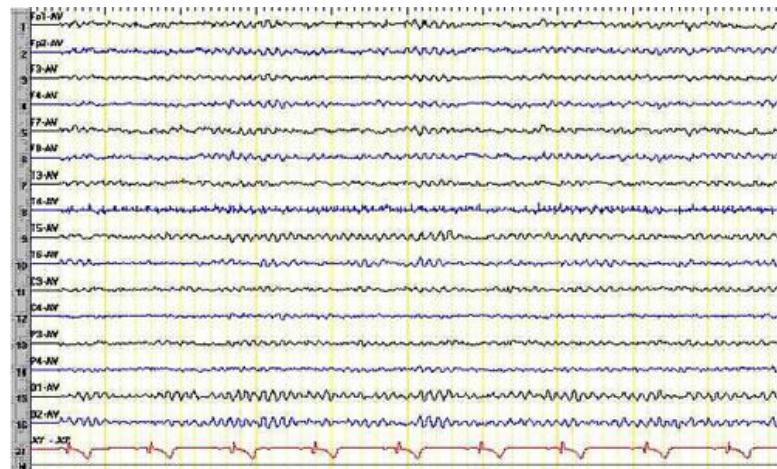


Figure 1-6: An EEG trace of a healthy individual at rest with their eyes closed [37]



Figure 1-7: An EEG trace of during an (absence) epileptic seizure [37]

## 1.4 Inertial Sensor Selection and Placement

Many of epileptic seizure symptoms involve movement of the human body parts as described in section 1.3. In technical terms these symptoms are referred as motor ones. As a result, seizure can be captured and analyzed with several technologies based on motion studies such as video and inertial sensors. In fact owing to the recent developments in the area of micro-electro-mechanical systems (MEMS) based inertial sensors, as well as their desirable size, cost and power consumption, researchers are considering these sensors a good choice for human body motion kinematic studies especially in the form of wearable inertial motion sensors. This form of inertial motion sensors have recently become commercially available and use a combination of accelerometers, gyroscopes and magnetometers.

The placement of inertial sensors on the body is an area which still needs further research as it is often hard to predict which locations on the body can provide the most relevant features with respect to sensitivity limitations of the wearable inertial sensors. On the other hand, placing sensors on several locations of the body can be cumbersome and also prone to errors. It is clear from various studies that the placement of the sensors plays a significant role in activity classification for this type of measurement. Although the wearable sensory system is widely used in human body motion recognition, there appears to be no comparative work performed thus far for investigating optimal sensor placement that is based on motion presented via mechanical equations of motion.

### 1.4.1 State-of-the-art in wearable inertial sensors and their medical applications

Recently, inexpensive in-chip inertial sensors including gyroscopes and accelerometers have gradually found practical applications in human motion analysis. Schepers et al [38] proposed a combination sensor system including six degrees of freedom force sensors and miniature inertial sensors to estimate joint moments and powers of the ankle. Tong and Granat [39] proposed a measurement device using two gyroscopes, one placed on the thigh and the other on the shank, which can estimate knee rotation angle during walking. This system has been shown to detect different phases of human walking.



On the other hand, wearable inertial motion sensors consisting of accelerometers, gyroscopes and magnetic sensors are readily available nowadays [40]. Although these devices which are manufactured using MEMS technology have received commercial success, in particular for applications that require moderate accuracy (see, e.g.,[41]), this class of sensor systems for medical applications started entering the market only in the last year or so. However, the recently developed complete sensor systems that are primarily designed for predicting 3D position/orientation for human movement applications have opened a variety of possibilities for medical applications. For example, inertial sensors are being used in a wide range of medical applications for monitoring and studying hand tremors, gait analysis, falling from bed alarms and Parkinson's disease. In Parkinson's disease, studies aim at distinguishing pathological and normal movements [42][43]whereas in hand tremor studies, the goal is to distinguish between different types of hand tremor using inertial sensors [44]. In these cases, acquiring accurate knowledge of the angular motion of the arm is extremely important. Angular velocities are typically measured using rate gyroscopes which are particularly susceptible to drift [45]. Accelerometers, on the other hand, cannot be used alone since they don't provide sufficient information and they need to be combined with other sensors such as microphones [46], gyroscopes [47], [48] and Electrocardiography (ECG) sensors [49] to provide more accurate activity classification.

The use of inertial sensors has become a prevalent practice in ambulatory motion analysis [50]. In fact, several methods have been proposed for accurate and drift free orientation estimation by combining the signals from tri-axial gyroscopes, accelerometers and magnetometers [51][52]. Accelerometers are normally used to determine the direction of the local vertical by sensing acceleration due to the gravity. Magnetometers provide stability in the horizontal plane by sensing the direction of the earth magnetic field. In other word, magnetometer acts like a compass. Data from these inertial sensors can be used to eliminate drift by continuous correction of the orientation obtained by integrating gyroscope's data.

Only recently sensor configurations that focus on the clinical symptoms and signs of seizures have become more popular [53]. Thus detection of epileptic seizures based on

inertial sensors is a research field that is open for discovery. The feasibility of seizure detection based on tri-axial inertial sensors has been discussed in [54]. For epileptic seizure analysis, various types of inertial sensors have been used as shown in Table 1-3. Some statistics within eleven epilepsy-related papers from references is provided in the same table and in most studies accelerometers are the most frequently used sensors. Almost all the research papers mentioned the usage of accelerometers for this purpose. However to achieve better results, accelerometers are typically used with gyroscopes, to construct an Inertial Measurement Unit (IMU). When a number of these sensor combinations are to be used, it also brings up the need for data fusion [55][56]. Motor characterization of epileptic seizures with inertial sensors has already given rise to several scientific contributions. For instance, Becq et al. [57] provided a study about the motor characterization of epileptic motion analysis performed in a care unit and Jallon et al [58] proposed an algorithm based on mathematical models for seizure detection.

**Table 1-3: Statistical representation of inertial sensors selection for epilepsy studies in different papers**

Category	Discussed by Papers
Accelerometer	[59],[60],[61],[62],[57],[63],[58],[64],[65],[53],[66],[54]
Gyroscope	[66]
IMU	[59],[61],[62],[57],[63],[58]

#### 1.4.2 Review of current Products

A unit of inertial sensor including tri-axial accelerometer, tri-axial gyroscope and tri-axial magnetometer can be easily built by preparing each set of tri-axial sensors from supplier such as Analog Devices [67]. However, it can be quite challenging to get useful information from a sensor combination. This issue becomes even more important when considering motion measurement from several parts of human body, simulation for the optimization purposes and epileptic seizure detection technique that are all needed for introducing a suitable package for the epileptic patient's monitoring. In order to address these short comings, commercial sensory unit packages combining the three sensors mentioned above and having suitable sensor fusion techniques implemented have been

chosen for the present studies. For deciding on the sensory system several factors such as accuracy, sensitivity, noise level, maximum catchable frequency, availability and maintenance service, and the cost of unit are considered important. In this section, a brief overview of the two major inertial sensory units is given and the section as well concludes with a comparative table giving information on the available sensors as described in Table 1-4.

### **XSENS™**

The MVN inertial wearable system is fully ambulatory, body worn array of sensors. Data is transmitted by a wireless connection to the laptop computer on which the processing is performed and visualized. With the MVN Studio software, the user can easily observe, record and export the movements in three dimensional. The approximate price for the standard MVN Development Kit is around \$20k and it includes:

- 17 MTw's are small wireless and highly accurate 3D motion trackers. The output of each MTw is accurate 3D orientation and calibrated sensor data (acceleration, rate of turn, magnetic field and barometer) at high update rates. Internal sampling of almost 120 Hz together with pre-processing ensures accuracy under challenging dynamic conditions.
- The Awinda station is a wireless receiver for up to 32 MTw's which connects to the pc. It charges the sensors simultaneously and has multiple hardware connections for digital I/O for time synchronization with compatible auxiliary systems.
- A set of click-in full-body straps which are easy to use click-in body straps for quick and sturdy mounting the MTw's to the subject's body.
- MT Manager Software is an intuitive user interface for configuring and real time visualization of the MTw orientation and calibrated sensor data. Record and export data as ASCII format.
- MT Software Development Kit is a software package which allows gaining real-time access to the capabilities of the MTw's. This also allows easily integrating the MTw's into user's own application. Example code is provided for MATLAB™, Lab VIEW, Excel, C/C++

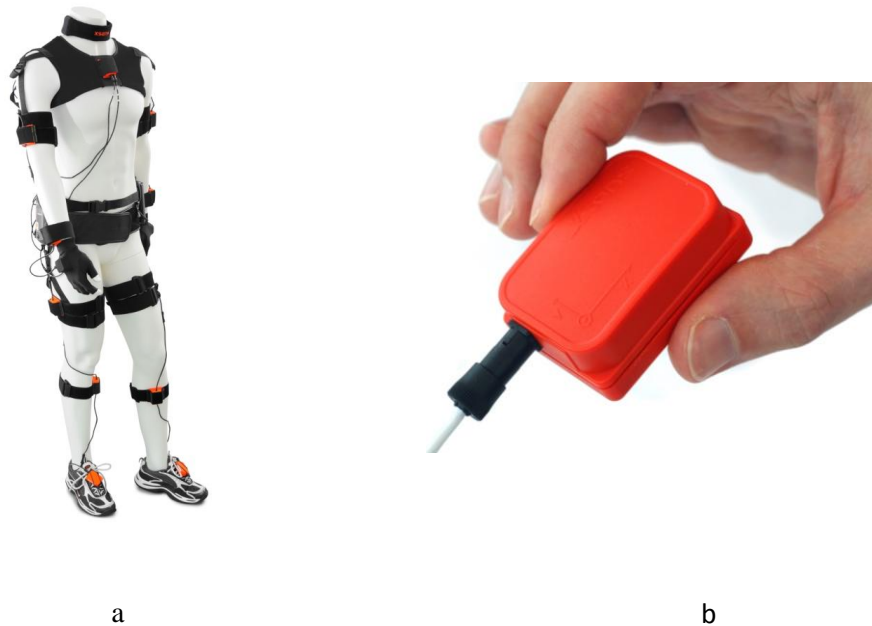


**Figure 1-8 a, b: Xsens™ MVN [68] (a), MTx unit [69] (b)**

### **Motion Node™**

The Motion Node™ system consists of 5 inertial sensor packages with one Motion Node™ Bus [70]. Each package is an inertial measurement unit and contains tri-axial gyroscopes, tri-axial accelerometers and tri-axial magnetometers (35×35×15 mm, 10 g). The sensor modules are connected in a chain to the Motion Node™ Bus, meaning that only one cable leads to each segment. The Motion Node™ Bus synchronizes all sensor sampling, powers the sensors and makes the wireless communication with the stationary unit which can be either PC or laptop.



**Figure 1-9, AIRCAST™ Pneumatic Armband arm band used for attaching the sensor unit to the body [71]**



a



b

**Figure 1-10 a, b: Motion Node™ Bus on the wrist [70] (a), Motion Node™ unit and the Bus wireless system [70] (b)**

The software package which comes with the sensor provides a simple interface to preview, record, and export inertial measurement data to FBX, COLLADA, BVH, and CSV. These output data can be analyzed in MATLAB™, Lab View and Excel. It also adjusts sensitivity and filtering parameters for different application requirements. In addition, sensor fusion algorithms implemented in the software on the sensor results ensure highly accurate output.

For quick and convenient placement, the sensors and cables can be attached to body segments using AIRCAST™ Pneumatic Armband [72] as illustrated in Figure 1-9 with the Motion Node™ Bus mounted on the wrist (Figure 1-10 a, b). The armband is of universal fit type and it guarantees a minimal skin motion artifact. It also provides less restriction and its breathable material enhances comfort and wearability which is highly important in the project to guarantee patient's comfort during the experiment. Straps can also be worn over normal clothing.

The system is also very quick and easy to set up typically in less than 10 minutes by a non-technical person. The total weight of the system (including batteries) is 1.9 kg. Five sensor modules can be placed on the right arm, forearm (2 sensors), head, and chest.

Battery life for 5 sensors is approximately 7 hours which seems to be quite satisfactory for the purpose of monitoring during night.

**Table 1-4: Comparison of different commercial inertial sensor packages**

Sensor	Maximum Range			size	Sampling Rate	Battery Life	Weight
	Accelerometer	Gyroscope	Magnetometer				
Motion Node™	$\pm 6g$	$\pm 2000^\circ/s$	$\pm 100\mu T$	35X35X 15 mm	100 Hz	7 hours	1.9 kg
XSENS™	$\pm 18g$	$\pm 1200^\circ/s$	$\pm 150\mu T$	38X53X 21 mm	120 Hz	3 hours	1.93 kg
INTERSE NSE	-	$\pm 1200^\circ/s$	-	60X54X 32 mm	180 Hz	8 hours	0.5 kg
BIOSYN STEM	$\pm 6g$	$\pm 2000^\circ/s$	$\pm 150\mu T$	19X19X 10 mm	120 Hz	3 hours	1.93 kg
MEM SENSE	$\pm 10g$	$\pm 1200^\circ/s$	$\pm 190\mu T$	19X19X 10 mm	50 Hz	N/A	N/A

### 1.4.3 Sensor Placement

In an effort to formulate a method to place the sensors, some researchers have resorted to statistical or classification methods. For instance, L. Atallah et al. [73] presented a framework for the investigation of feature relevance as well as sensor positioning for a set of wearable accelerometers. Their work was based on the activity classification by applying three feature selection methods: Relief-F, Simba, and mRMR to assess the relevance of features for discriminating 15 different activities. All these three methods achieved similar performance. Bao & Intille [74] employed five bi-axial accelerometers placed on the user's right hip, wrist, upper arm, ankle, and thigh in order to collect data from 20 users. Using decision tables, instance-based learning, C4.5 and Naïve Bayes classifiers, they created models to distinguish twenty daily activities from each other. Their results indicated that the accelerometer placed on the thigh was most powerful for distinguishing between activities.

In particular, for the case of epileptic seizure detection, researchers often chose to use sensors in predefined locations on the body such as wrist, forearm and arm. For instance, Nijsen et al. [63] have developed a detection algorithm to discriminate between data with and without subtle nocturnal motor activity for epileptic seizure. Five accelerometers were attached to the body, two to the ankles, two to the wrists, and one to the chest. In another study, Nijsen et al. [75] attached an accelerometer to the arm of the patient and fitted the output results' curve with exponential function. Jallon et al. [58] and Cuppens et al. [76] also studied the detection of epileptic seizures with accelerometers and Conradsen et al. [66] used a multi-modal approach. Table 1-5 summarizes some of the most significant recent work using sensors for activity recognition, and Parkinson's disease as well as epileptic seizure detection.

**Table 1-5: Comparison of the placement methods in different papers**

Researchers	Type of Sensors	Placement
Atallah et. Al. [73]	Accelerometer	Different locations for different types of activities
Bao et al. [74]	Accelerometer	hip, wrist, ankle, arm and thigh
Yang et al. [77]	Accelerometer	wrist
Hester et al. [78]	Accelerometer	ankle
Mathie et al. [79]	Accelerometer	waist
Attallah et al. [80]	Accelerometer	Ear-worn
Karantonis et al. [81]	Accelerometer	waist
Schulc et al. [65]	wii remote (Accelerometer)	forearm
Nijsen et al. [75]	Accelerometer	arm
Conradsen et. al. [66]	Xsens™ (Accelerometer, Gyroscope and Magnetometer)	
Becq et al. [57]	Accelerometer, Magnetometer	wrist and head
Jallon et. Al. [60]	Motion Pod (Accelerometer and Magnetometer)	wrist
Keijsers et. Al. [82]	Accelerometer	upper arms, upper legs, wrist, and trunk

## 1.5 Seizure Detection using Inertial Sensors

Epileptic seizure is considered to depict a non-chaotic rhythmic behavior whereas normal activities such as walking are assumed to be chaotic by many researchers. Indeed, the

chaotic study of the epilepsy has attracted the attentions towards studying the EEG signals to derive an expression for the brain functionality during seizure in terms of chaotic or non-chaotic behavior. Lyapunov exponent, Pseudo-Phase-Space and Poincaré map have been the most common tools employed for studying the chaotic behavior of the system. Even though, studying the chaotic level of the response of the brain may be advantageous for the identification of the seizure onset but due to the complex function of the brain, these studies often yield no satisfactory results. However, the application of the chaotic identification to the inertial sensor's output is a novel approach that seems not to be explored enough. Patients with epilepsy are reported to be at an increased risk of physical injury, usually arising as a direct consequence of their epilepsy. In particular, Tonic clonic and myoclonic seizures cause most injuries in the epileptic patients due to the sudden falls [83]. In the following sections, a review of the current seizure detection is presented.

### 1.5.1 Seizure Detection Techniques

The analysis of potentially chaotic behavior in biomechanics and biomedical fields for the purpose of system identification has attracted great interest in recent years [84]. Although no universally accepted mathematical definition of the term chaos exists, chaos is normally defined as aperiodic long-term behavior in a deterministic system that exhibits sensitive dependence on initial conditions [85].

Chaotic analysis of the time series data is a newly presented approach for the study of complex systems. According to the chaos theory, the degree of chaos can be presented both graphically and numerically (i.e. Lyapunov exponent). When studying highly complex systems, an established graphical procedure to reduce the system's multidimensional continuous trajectory in state space to a discontinuous low dimensional projection known as Poincaré map can be useful. Poincaré map is generally applied on the experimental data to analyze the dynamic systems by showing periodicity and is obtained by representing pairs of consecutive time series differences in the coordinate or by plotting one quantity against the differentiation of that quantity. These Poincaré maps can sometimes be used to distinguish between various qualitative states of motion such as periodic, quasi periodic, or chaotic. Finally, if the Poincaré map does not consists of



either a finite set of points or a closed orbit, the motion may be chaotic. Poincaré technique is commonly applied in the field of cardiology and more recently, the technique is used for the indication of the sudden cardiac death risks [86]. For example, Freeman [87] simulated the chaotic EEG patterns with a dynamic model of the olfactory system.

Chaos is defined as aperiodic long-term behavior. Aperiodic long-term behavior means that trajectories do not converge to a fixed point, but instead exhibit irregular unpredictable behavior. The Poincaré map is commonly used to interpret the behavior of groups of trajectories, relating the states at one point in time to a set of future states forward along the path. One of the advantages of the Poincaré map lies in its power as a visualization tool. Such a map reduces the order of the problem, condensing quantities of information into a lower-dimensional image. Poincaré maps reveal, at a glance, various characteristics of individual trajectories or groups of trajectories, whose features are otherwise difficult to isolate within the vast quantity of available information. Lyapunov exponents, on the other hand, provide a direct measure of separation of the trajectories that start arbitrarily near to each other by quantifying the exponential rates at which neighboring orbits on an attractor diverge (or converge) as the system evolves in time. Lyapunov exponent calculations have been applied to a wide range of biological and biomedical phenomena.

Researchers have used Lyapunov exponents to analyze mathematical models of individual neurons and neural networks[88], examine experimental molecular and cellular dynamics including gas transport through blood cells[89], study the dynamics of blood flow [90], investigate human hand writing [91] and apply on the control of oscillatory limb movements [92]. One of the biggest areas of focus has been in understanding heart rate variability and analyzing functional brain activity through ECG and EEG, respectively [93]. An extensive recent review by Stam [94] summarizes the findings of nonlinear analyses of these signals in healthy subjects during a wide variety of cognitive states and in a wide range of patients with various pathologies, ranging from seizures to degenerative diseases like Alzheimer's or Parkinson's disease and even to psychiatric disorders. Although the evidence seems to point toward a view of brain

activity as being far more complex and less stationary than can be reasonably modeled by any low-dimensional deterministic model such as chaotic model, both reviews remain optimistic about the future applications of nonlinear analyses in understanding brain function. Particularly, Stam [94] suggests that the most promising potential clinical applications appear to be in identifying and predicting epileptic seizures and sleep disorders. As a result of the inherent computational difficulties in estimating the full Lyapunov spectrum and since the estimation of the maximum Lyapunov exponent is often considered to be of interest to the determination of chaos, many algorithms have been proposed for this purpose. Perhaps the most well-known of these algorithms is from Wolf et al [95].

## 1.6 Thesis Aims and Outline

### 1.6.1 Thesis Aims

In clinical applications the quantitative characterization of human kinematics and kinetics can be helpful for clinical doctors in monitoring patients' recovery status, prescribing the right medicine and notifying the medical personnel rapidly in emergency situations. In diseases such as epilepsy, 24/7 monitoring of patients is needed. However, the use of monitoring instruments during daily activities of the patients is often difficult since these devices are mainly limited to the hospital or laboratory use. The purpose of the present thesis is then on investigating the utilization of a monitoring inertial based sensory system to improve the life of epileptic seizure patients. The present research will primarily focus on patients suffering from epilepsy, although such a system can be used for a variety of patient illnesses such as Parkinson Disease (PD), hand tremor, etc. To achieve this goal, the following objectives have been identified.

1. *Development of a human body dynamic model that can be used for optimization of the sensor placements on the body, torque estimation of joints during different activities and characterization of the human body response during the seizure episode.*

The human body model should be able to mimic the nonlinearities of the joints and muscles and reflect their influences on the response and performance of the body during seizure. To achieve this, springs/dampers that can exhibit nonlinear

characteristics of the human body must be considered and a dynamical approach for developing the equations of motion must be properly represented.

2. *Study of the epileptic seizure classification and dynamics and development/adoption of a suitable dynamic based seizure model for utilizing in the human body model.*

The seizure model should be simple while accurately reflecting the real seizure dynamics. In addition, as only the passive behavior of the human body model is considered, the neuron's function during epileptic seizure and consequently the active state of muscles are omitted. Hence, the seizure model should only involve the muscular behavior of the body during seizure.

3. *Choice of an optimal number and placement locations of inertial sensors on the body to achieve highest sensing resolution.*

Some undesirable issues, such as noise, drift, and uncertainties in the human body model as well as sensors characterizations should be considered in the model to show the suitability of the inertial sensors for detection purposes. The experimental data can assist in validating the predictions made via modeling of the human dynamics for the purposes of determining optimal sensor locations for patient-specific activities.

4. *Simulation of the modified Motion Genesis™ procedure in the symbolic math toolbox available in MATLAB™, MuPAD to estimate the joint torques during seizure.*

The proposed approach can be utilized in the experimental study for comparison of different activities based on the joint torque that is involved in each activity. In order to do so, an approach based on the sensor outputs should be developed. It will be also advantageous if the integration and differentiation of the raw data is avoided so that the errors due to these operations are eluded.

5. *Analysis of the experimental data and proposition of an identification approach*

As the human body is highly nonlinear, complex system, the response of the human body during normal and involuntary movements typically exhibits that of a nonlinear system. Hence, a nonlinear response based approach can be useful in characterizing the seizure as well as normal activities. Lyapunov exponent,

Poincaré map and Pseudo-Phase-Space methods are common nonlinear based methods that can be employed to study resulting experimental data. Outputs of these approaches can lead to development of a new experimental based method for epileptic seizure detection.

### 1.6.2 Thesis Outline

In the second chapter, the human body modeling and simulation is described. For this purpose, biomechanical model for human body and the approach to develop such a model is presented. More detailed information on the segments, each joint's degree of freedom and subsequently the complete model degree of freedom, model anthropometry data and joint torques are presented.

Chapter 3 discusses methods for optimal placement of inertial sensors to be placed on the arm, as well as a technique to form a suitable objective function for the optimization process. The optimal placement strategies are evaluated using the global optimization toolbox that is available in the MATLAB™ environment. A sensitivity analysis is also performed to quantify the sensitivity of the procedure to the joint torque and damping coefficients, arm geometry and mass, and the inertial sensor's uncertainty.

In the fourth chapter, the emphasis is placed on proposing a technique for detecting the epileptic seizure using measured output signal from inertial sensors via joint torque predictions. The advantage of using this technique over using the conventional method of the integration of the output results of gyroscope and acceleration is also discussed.

Chapter five includes some preliminary experimental data derived from an epileptic seizure patient along with representative normal activity data from a healthy subject. In this chapter first a brief comparison between the normal and seizure signals is presented. Finally, a non-linear response based detection technique for the classification of the activities in a quantitative manner is presented together with the basis behind this method.

Chapter six includes some concluding remarks on the research performed in the present thesis along with some suggestions for future research directions.

## Chapter 2

### 2 Human Body Modeling and Epileptic Seizure Simulation

In order to design a suitable detection system for epileptic seizure, a mathematical model that represents the dynamics of the human body is developed. The model is investigated to assist in the overall understanding of the human body seizure motion response as well as in the prediction of optimal placement of sensors. Biomechanical multi-body models of humans are typically more complicated than other multi-body systems, as they involve a larger variety of joint types, body segments, and complex actuators formed by muscles and related soft tissues as well as higher degrees of freedom. This fact justified the use of suitable software for modeling purposes.

The human body model can become useful prior to any experimental work, in terms of predicting the body segment's response to a specific input, detection algorithm design, and deciding optimal placement for the sensors. In this chapter, a procedure is developed for simulating the human body dynamics employing the commercial package Motion Genesis™. The human body model is demonstrated on a modified Hanavan's model [96] with 16 segments and the epileptic seizure torque model is adopted based on research performed by Nijsen et al [75]. First, some basic anatomical terms are introduced together with the concept of the agonist and antagonist forces and their interactions. This brief introduction is intended for presenting a better understanding of the model for simulating the arm movement during epileptic seizure. Further, corresponding Motion Genesis™ code and results are provided and the chapter is then concluded with some concluding remarks of the analysis.

#### 2.1 Preliminary Anatomical Principles

For the sake of explicit and unambiguous definition of the movements of the human musculoskeletal system in everyday activity such as running, walking, etc. as well as involuntary movements such as tremor, seizure, etc., it is necessary to define an appropriate scientific terminology. While using terms such as 'bending knees' and

‘raising arms’ may be acceptable in everyday conversation, the latter is ambiguous and the former is often assumed to be scientifically unacceptable.

So as to make up a distinct nomenclature to describe areas of the body, to provide orientation when describing parts of human anatomy, and to distinguish different movements of the body, human anatomical terms are introduced. An understanding of these terms is necessary to study the human body in depth. In the following sections an overview of technical terms used to define human motion is presented which is later utilized in the determination of the degrees of freedom.

### 2.1.1 Planes of Movement

To facilitate the understanding of the relation of structures one to another and the movement of one segment with respect to another, imaginary reference planes that pass through the body are presumed. The planes, in which joint movements occur, are mutually perpendicular to each other. To describe the three mutually orthogonal intersecting planes various terms are used. Obviously, many such orthogonal systems can be described, depending on their common point of intersection. This is most appropriately defined as the centre of the joint being studied. Three major planes as illustrated in Figure 2-1 include:

- The sagittal plane also known as lateral, is a longitudinal plane passing from posterior (rear) to anterior (front) dividing the body of a bilaterally symmetrical animal/human into left and right sections.
- The coronal plane, also known as frontal, is a vertical plane that passes from left to right of the body and divides it into posterior and anterior portions.
- The transverse plane, also known as axial or horizontal, divides the body into superior (upper) and inferior (lower) parts.

### 2.1.2 Axes of Movement

Movements at the joints of the musculoskeletal system are largely rotational, and take place about a line perpendicular to the plane in which they occur. This line is known as an axis of rotation. Three axes can be defined by the intersection of pairs of the above planes of movement (Figure 2-1).

- The sagittal axis passes horizontally from posterior to anterior and is formed by the intersection of the sagittal and transverse planes.
- The coronal axis passes horizontally from left to right and is formed by the intersection of the coronal and transverse planes.
- The vertical or longitudinal axis passes vertically from inferior to superior and is formed by the intersection of the sagittal and coronal planes.

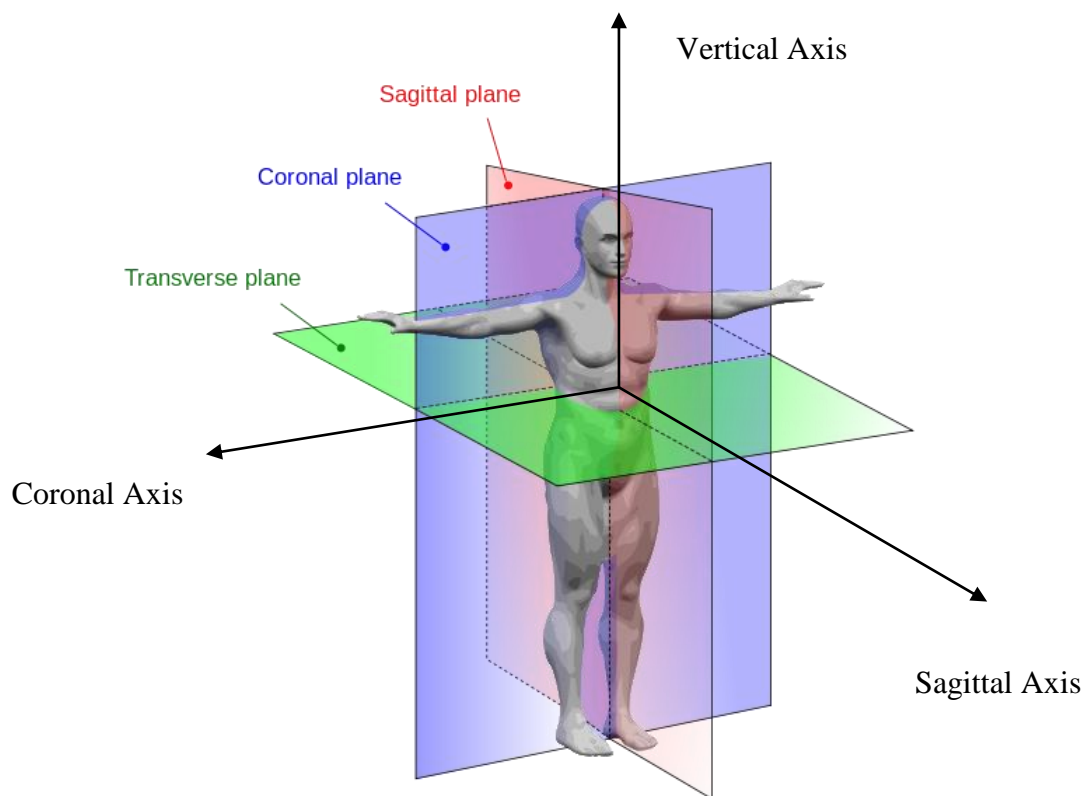


**Figure 2-1: Three major planes of movement: sagittal plane, coronal plane and transverse plane [97]**

### 2.1.3 Movements in the Sagittal Plane about the Coronal Axis

Flexion (Figure 2-2) is a movement allowed by certain joints of the skeleton movement in which the angle between the two adjoining bones decreases. In simple words, it is actually a ‘bending’ movement such as bending the elbow, which decreases the angle between the arm and the forearm. If the movement of flexion continues past the anatomical position, it is called hyper-flexion. The movement is usually to the anterior (except for the knee, ankle and toe). Extension (Figure 2-2) is the reversal movement

from flexion. For example, bending the head toward the chest is flexion and so is the motion of bending down to touch the foot, in which the spine is said to be flexed, whereas extension reverses these movements. Continuation of extension beyond the reference position is termed hyperextension. It is clear that flexion and extension movements occur parallel to the sagittal plane. Dorsi-flexion and plantar-flexion (Figure 2-2 (g)) are normally used to define extension (foot moving towards the anterior surface of the leg) and flexion (foot moving towards the posterior surface of the leg) of the ankle joint respectively. All these terms are schematically shown in Figure 2-2.

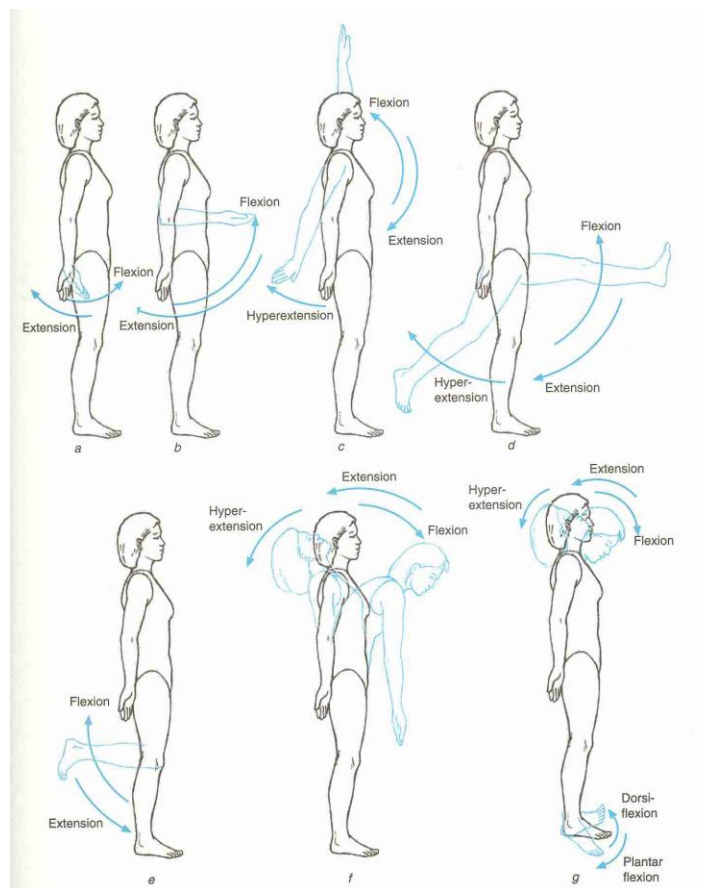


**Figure 2-2: Movements in the sagittal plane about the coronal axis [98]**

#### 2.1.4 Movements in the Frontal Plane about the Sagittal Axis

Abduction and adduction (Figure 2-3 (a)) are the movements of the limbs in the frontal plane. Abduction is movement away from the vertical axis of the body whereas adduction is moving the limb towards the vertical axis. Swinging the arm to the side is an example



of abduction whereas bringing it back towards the body constitutes adduction. Sagittal flexion (Figure 2-3 (d, e)) refers to the upper-body movement away from the vertical axis. It can also be defined as moving the spine to the side (left or right) and the neck towards the shoulder.

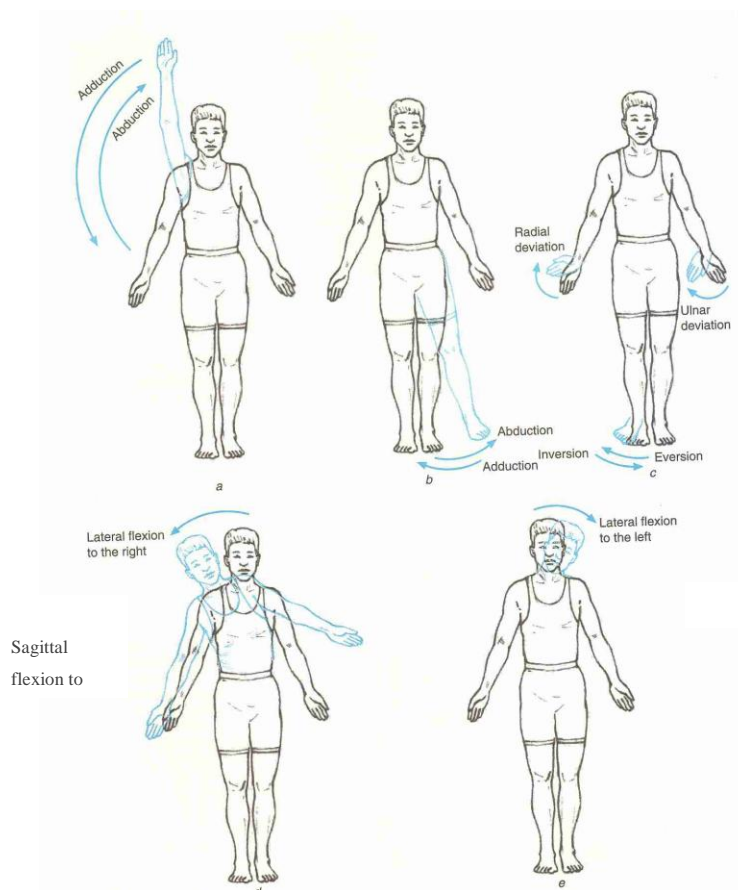


**Figure 2-3: Movements in the frontal plane about the sagittal axis [98]**

### 2.1.5 Movements in the Transverse Plane about the Vertical Axis

Internal rotation (Figure 2-4 (a, b)) is a rotary movement around the vertical axis of the bone toward the center of the body such as turning the thigh or pelvis inward. External rotation (Figure 2-4 (a, b)) is a rotary movement around the vertical axis of the bone away from the center of the body such as turning the thigh or pelvis outward. Pronation (Figure 2-4 (d)) refers to the internal rotation of the forearm resulting in the palm moving posteriorly, or down whereas supination (Figure 2-4 (d)) is the external rotation of the forearm resulting in the palm moving anteriorly, or up.

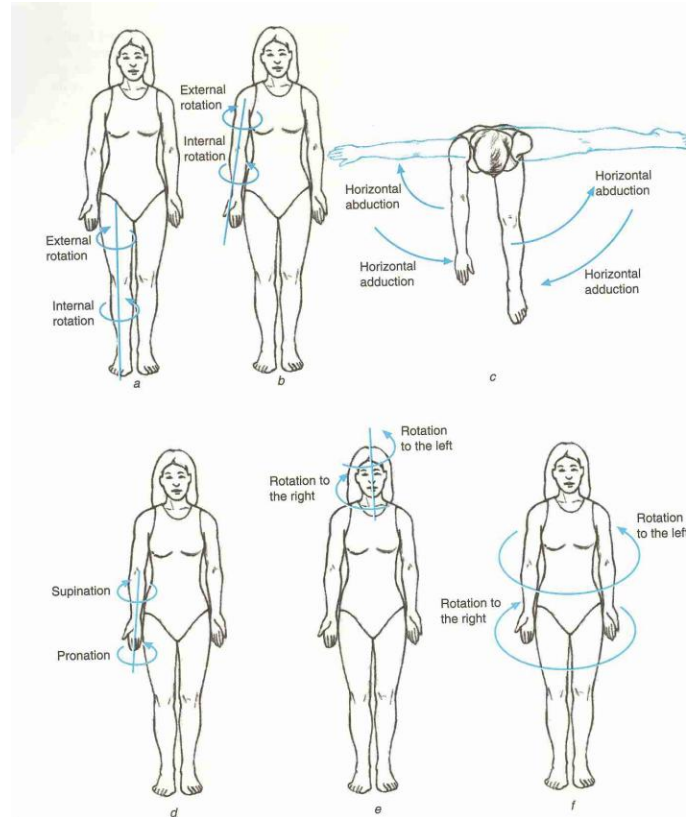


**Figure 2-4: Movements in transverse plane about the vertical axis [98]**

Table 2-1 shows a comparison of the movements occurring in the three mentioned planes and their axes for different activities. It is also important to note that in epileptic seizures the dominant movement is Flexion/Extension. In particular, the tonic seizure type is characterized by excessive flexion or extension of fingers, forced flexion of hand joints, jaw protrusion, shoulder elevation, upper arm abduction, and tonic flexion of the trunk. This hypertonic state continues unchanged even after the patient falls down[99].

**Table 2-1: Anatomical planes and axes and type of motions in which everyday activities are involve**

Plane	Motion	Axis	Examples
Sagittal	Flexion/Extension	Coronal	Walking, Squatting, Overhead press
Frontal	Abduction/Adduction	Sagittal	Star jump, Lateral arm raise, Side bending
Transverse	Internal/External Rotation	Vertical	Throwing, Baseball swing, Golf swing

## 2.2 Model Description

In this section, first the assumptions considered for developing the model are stated and then detailed information for the model anthropometry, segments, joint type and degrees of freedom is presented. Finally a model which is employed for the joint torques is briefly introduced. The information available in this section is essential to perceive the dynamics of the human body and is employed for developing the procedure in Motion Genesis™. In the present model, X-direction is along the sagittal axis, Y-direction is along vertical axis and Z-direction is along coronal axis as shown in Figure 2-1.

### 2.2.1 Modeling Assumptions

It may be pointed out that some simplifying assumptions had to be made in the human body modeling to reduce the complexity of the system to a reasonable number of degrees of freedom since the primary focus of the present work is on the epilepsy detection and prediction of optimal locations for inertial sensor application. The following assumptions are made in the process of developing the human body model:

- The anthropometry data used for the model is for a male model of height 1.741 m and weight of 72.8 kg. However, the model can easily be personalized for a specific patient.
- Effects of gravity are not considered in the current model so that movements of the body are not affected by segment weights.
- As the motor characterization of the epileptic seizure is concerned, it is decided that the skeletal model is an adequate representation of the human body. As a result, the function of neurons as well as the neuromuscular system of the human body is not considered in the present study.
- It is assumed that the effect of the muscles and the muscle activation during epileptic seizure can be approximated by joint moments using nonlinear springs and dampers.
- Since in epileptic seizures the movements in arms, forearms, legs and upper torso are dominant over other parts of the body, neck is not considered to be a separate segment in the model

- As the effect of the epileptic seizure on the human body mechanical response is of interest, the model is not considered in the moving phase so that the resultant acceleration and velocities are solely because of the seizure as well as segment inertia and joint moment interaction. As a result, whole body movement (three degrees of freedom in the x, y and z directions) is not included in the modeling procedure.
- Finally, the myoclonic epileptic seizure model is presumed to be applied in the sagittal plane about the coronal axis.

### 2.2.2 Segments

One of the earliest mathematical models for human body was given by E.P. Hanavan et al in 1964 [96] as shown in Figure 2-5 (a). The model consisted of 15 segments of head, upper torso, lower torso, left hand, right hand, right upper arm, left upper arm, right forearm, left forearm, right upper leg, left upper leg, right lower leg, left lower leg, right foot and left foot. The dimensions and properties of the body segments were calculated using the anthropometric dimensions of the individual subject. Later, R.L. Huston in his book “Principles of Biomechanics” proposed a 17 segment human body model [100] as illustrated in Figure 2-5 (b). The difference between this model and Hanavan’s model was because of considering the mid torso and neck part in Huston’s model.

Other researchers also proposed some modification to these two models, for instance, Hatze [101] modified Hanavan’s model by adding two more segments and considering the fingers in the hands as depicted in Figure 2-6 (a). Selecting a model for human body is more dependent on the phenomena under study, for instance in injury studies, it is useful to initially use the whole-body model to obtain the movement of a crash victim’s chest. Then knowing the chest movement, the detailed movement of the head-neck system can be studied using the head-neck model (Figure 2-7). That is, the output of the whole-body model is used as input for the head-neck model. For the present study, Human model is considered to consist of sixteen rigid bodies representing:

- |                   |                   |                  |
|-------------------|-------------------|------------------|
| 1. head,          | 6. left arm,      | 11. right thigh, |
| 2. upper trunk,   | 7. right forearm, | 12. left thigh,  |
| 3. mid trunk,     | 8. left forearm,  | 13. right shank, |
| 4. lower trunks , | 9. right hand,    | 14. left shank,  |

5. right arm,

10. left hand,

15. right foot,

16. left foot.

Since in epilepsy seizures arms, forearms, legs and upper torso are involved most, there is no need to consider the neck part separately in the model. The model considered in this thesis is shown in Figure 2-6 (b).

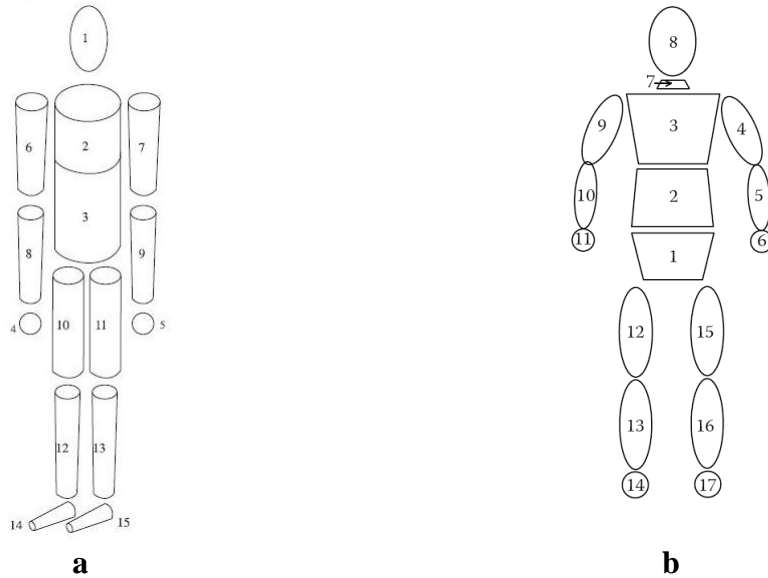


**Figure 2-5 a, b: 15 segment of human body of Hanavan [96] (a), 17 segment of human body of Huston [100] (b)**

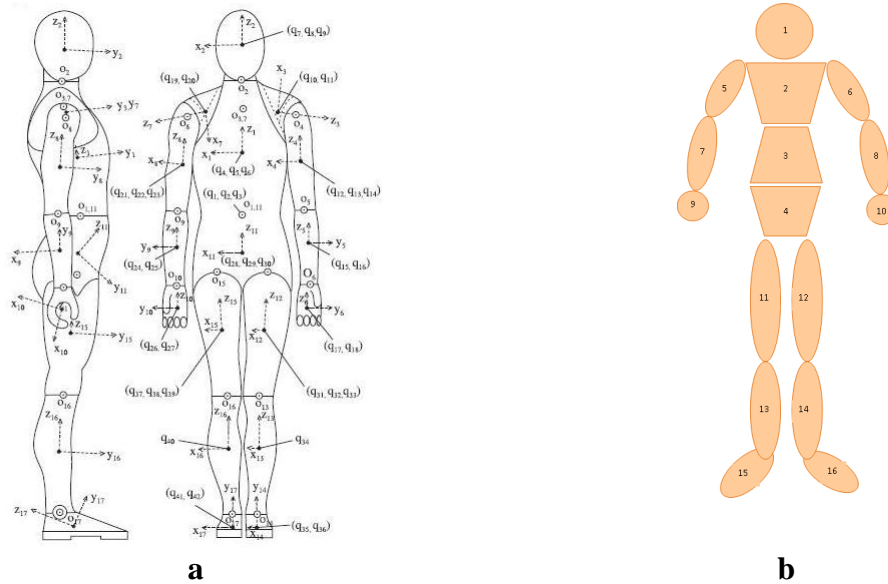


**Figure 2-6 a, b: 17 segment of human body model of Hatze [101] (a), 16 segment of human body model used in this text (b)**

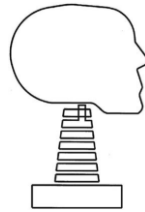


**Figure 2-7: Head/Neck model of Huston [100]**

### 2.2.3 Degrees of Freedom and Segment Connections

In this model, the human body consists of 16 segments interconnected with joints. The total degrees of freedom (DOF) of the model is 32 which is a sum of the individual DOF of each joint. Joints of present model include, the neck joint, upper trunk, two shoulder joint, two elbow joints, two wrist joints, two hip joints, two knee joints, two ankle joints and the stomach joint. The information is summarized in Table 2-2. The knee and ankle joints are considered as hinge joints and consequently each has one degree of freedom whereas upper trunk, hip and stomach joints are considered as ball and socket joints and each has three degree of freedom. The elbow joint is considered as a two degree of freedom joint since it can move both about the coronal and vertical axes.

**Table 2-2: Joints and joint degrees of freedom used in the present model**

Joint	Degree of Freedom	Joint Motion					
		Flexion/Extension	Abduction/Adduction	Sagittal Flexion Right/Left	Internal/External Rotation	Pronation/Supination	Dorsi/Planar Flexion
Neck	1	•					
Upper Trunk	3	•		•	•		
Shoulder (Right & Left)	6	•	•		•		
Elbow (Right & Left)	4	•				•	
Wrist	2	•					

(Right & Left)							
Hip (Right & Left)	6	•	•		•		
Knee (Right & Left)	2	•					
Ankle (Right & Left)	2						•
Stomach (Right & Left)	6	•		•	•		
Whole Body Rotation	3						
Total	32						

## 2.2.4 Model Anthropometry

Anthropological parameter values such as length, mass, position of the center of the mass and moment of inertia of each segment are derived using the data given in reference [6]. The height of the model and the total mass of the model are 1.741 m and 72.8 kg respectively.

**Table 2-3: Model anthropometry data used in the model [6]**

Segment	Mass (Kg)	Length (mm)	$I_{xx}$ (Kg.m <sup>2</sup> )	$I_{yy}$ (Kg.m <sup>2</sup> )	$I_{zz}$ (Kg.m <sup>2</sup> )	Center of Mass Location (mm)
Head	5.07	242.9	0.027	0.020	0.030	59.76
Upper Trunk	11.65	242.1	0.174	0.148	0.070	29.99
Mid Trunk	11.92	215.5	0.129	0.121	0.081	45.02
Lower trunk	8.15	145.7	0.065	0.060	0.053	61.15
Upper Arm	1.98	281.7	0.013	0.004	0.011	57.72
Forearm	1.18	268.9	0.007	0.001	0.006	45.74
Hand	0.45	86.2	0.001	0.001	0.001	79.00
Thigh	10.34	366	0.175	0.036	0.175	40.95
Shank	3.16	430	0.037	0.006	0.035	44.59
Foot (Vertical)	0.9	178.8	0.001	0.004	0.004	44.15

Axis)						
Foot (Sagittal Axis)	-	42.0	-	-	-	21.00
Shoulder Breadth	-	22.46	-	-	-	-
Hip Width	-	83.5	-	-	-	-
Height	1.741					
Weight	72.8					

### 2.2.5 Passive Joint Moments

In the biomechanical model, no active muscle force is considered but the muscle passive behavior is represented. In the present human body dynamic model, the influences of the muscles are realized as moments entered about the joints as shown in Figure 2-8 for the elbow joint. The Ligament moment for the relative rotation of the lower and upper arm is computed as a sum of two exponential terms [102]:

$$T_{lig,j-1} = k_{1j}e^{k_{2j}(q_j-\theta_{1j})} + k_{3j}e^{k_{4j}(q_j-\theta_{2j})}, \quad j = 1,2, \dots 32 \quad \mathbf{2-1}$$

where  $T_{lig,j}$  is the net ligament moment applied about the  $j^{\text{th}}$  joint and  $k_{1j}, k_{2j}, k_{3j}, k_{4j}, \theta_{1j}$  and  $\theta_{2j}$  are constants which determine the profile of the ligament moment-angle relationship. Typical numerical values for these constants are taken from Anderson [102], Davy and Audu [103], [104] and modified by Yamaguchi [105]. In Eq.2-1, the generalized coordinate which represents the angular motion associated with  $j^{\text{th}}$  degree of freedom is denoted by  $q_j$ .

Also to prevent joint angles from reaching values which are physically impossible, penalty areas are applied to simulate the action of the ligaments. The penalty area operates in such a way that it is null during the normal joint rotation but it increases exponentially, from zero to a maximum value, when the two bodies interconnected by that joint reach physically unacceptable positions. The curve for the penalty resisting moment is represented qualitatively in Figure 2-9.



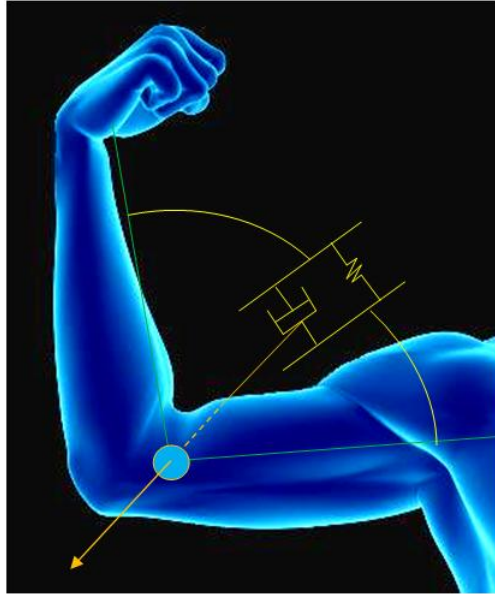


**Figure 2-8: Joint resistance torque modeled with a non-linear torsional spring and damper**

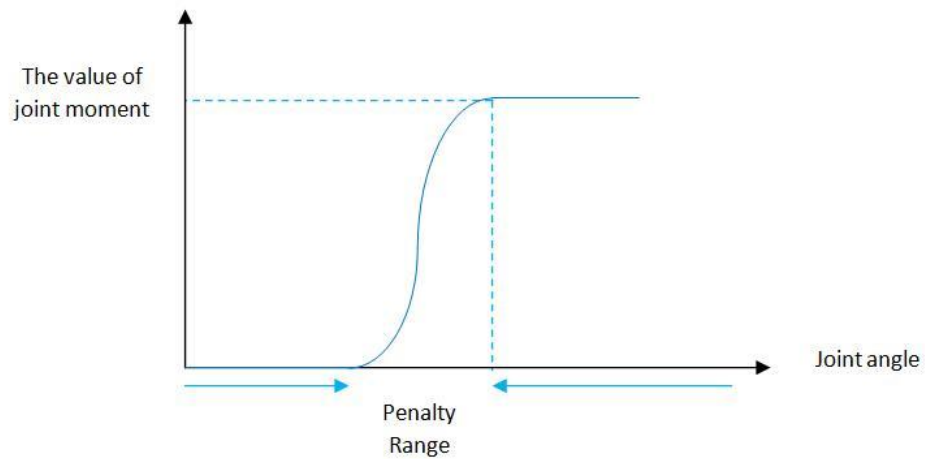


**Figure 2-9: Penalty moment for the elbow joint**

Further, in order to avoid numerical instabilities during a forward integration of the model and for the purpose of increasing the numerical stability of the model, a damping torque is also considered at each joint in the form described in Eq. 2-2:

$$T_{lig,j,2} = -c_j \dot{q}_j. \quad \mathbf{2-2}$$

The constant  $c_j$  denotes the damping coefficient that determines the magnitude of the damping torque and is determined in a way to stabilize the response. Table 2-4 shows a list of the passive parameters and definitions of the joint angles in ankle, knee and hip in terms of the generalized coordinates.

**Table 2-4: Coefficients for passive joint moments**

Joint	Spring coefficients	Damping coefficients	Angle coefficients
Ankle	$k_{1j} = 2.0$ $k_{2j} = 5.0$ $k_{3j} = 9.0$ $k_{4j} = 5.0$	$c_j = 9.43$	$\theta_{1j} = 1.92$ (20° dorsiflexion) $\theta_{2j} = 1.047$ (30° plantarflexion)
Knee	$k_{1j} = 3.1$ $k_{2j} = 5.9$ $k_{3j} = 10.5$ $k_{4j} = 11.8$	$c_j = 3.17$	$\theta_{1j} = 0.00$ (20° full extension) $\theta_{2j} = -1.92$ (110° flexion)
Hip	$k_{1j} = 2.6$ $k_{2j} = 5.8$ $k_{3j} = 8.7$ $k_{4j} = 1.3$	$c_j = 1.09$	$\theta_{1j} = 1.92$ (110° flexion) $\theta_{2j} = 0.1744$ (10° flexion)

Two moment terms,  $T_{lig,j,1}$  &  $T_{lig,j,2}$ , form each joint's moment function. In other words, in this model a viscous torsion damper and a non-linear torsion spring, located in each kinematic joint, describe the joint's moment.

## 2.3 Epileptic Seizure Model

In this section an overview of the epileptic seizure model which is proposed by Nijssen et al [75] is presented. The model proposed is based on the Hill's muscle model and the coefficients of the equation are derived applying curve fitting technique to the experimental acceleration output of the accelerometer obtained during myoclonic seizure. Myoclonic seizures are associated with clearly visible stereotypical patterns in accelerometer signal [53]. In this part, the model is modified to attain an expression for the joint torque during myoclonic seizure which is used in the simulation to study the biomechanics of the seizure and its mechanical expression in terms of velocity, and acceleration.

### 2.3.1 Muscle Contraction

A. V. Hill [106] noticed that muscle has resistance against lengthening but not against shortening. This observation leads to the fact that muscle cannot be modeled by a pure series elastic element. He also noted that the faster a muscle shortens the less total force it produces. To account for the fact that muscle produces less force when it shortens, Hill proposed that a viscous element lies in parallel with the contractile element which accounts for the first observation. In an investigation to find the properties of this viscous element, Hill and his colleagues performed a simple experiment by attaching a muscle to a bar that pivoted around a point (Figure 2-10 (a)). One end of the bar had a catch mechanism that they could release at any time. A basket held a weight on the other end of the bar. They noticed that by putting tension on a spring by pulling it and then suddenly releasing it, the muscle rapidly shortened. The fact that the muscle immediately shortened suggests that something in the muscle acted like a spring. This spring is the series elastic (SE) element shown in Figure 2-11. They further perceived that after an immediate change in muscle length and force, a slow and gradual change in the length was developed (Figure 2-10 (c)), without any change in force (Figure 2-10 (b)). That is, while a part of the muscle's mechanism changed length rapidly in response to the force change, another part did not change as quickly. The parallel elastic element (PE), referred to above, represents this second passive element in the muscle. The muscle's viscosity, the parallel elastic element and the series elastic element compose the passive components of Hill's muscle model as shown in Figure 2-11.

To perform an activity, brain sends an order to the destination muscle. This message is sent via neurons. A neural pulse causes a muscle fibre or groups of muscle fibres, or so called motor unit, to contract. The total force of the muscle is determined by the number of fibres contracting and their state of activity.

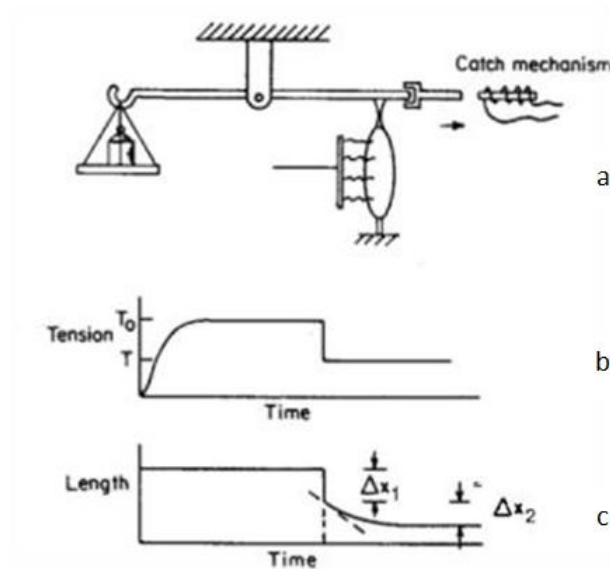


**Figure 2-10: Development of a mathematical model for muscle by Hill [107]**

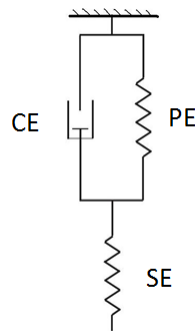


**Figure 2-11: Hill's muscle model**

In their work, Nijsen et al [75] suggested that the overall function of the neuromuscular system during myoclonic seizure can be represented as the synchronized contraction between agonist and antagonist muscle groups stimulated by a pulse input. Their hypothesis was based on the fact that myoclonic seizures involve a short abrupt flexion (<50 ms) in the lower arm and thus in mechanical terms can be demonstrated by an impulse input. The muscles react to this innervations pattern and apply force on the skeletal system. In reference [108], it is stated that the characteristic shape of the motor units in tension are quite similar and the time-response curve follows that of the impulse

response of critically damped second-order system. On the other hand, the general expression for a second-order critically damped impulse response is of the form:

$$F(t) = F_0 \frac{t}{T} e^{-t/T}, \quad \mathbf{2-3}$$

where,  $T$  is the twitch time that is for tension to reach maximum (shown in Figure 2-12), and  $F_0$  is a constant for the given motor unit. Eq. 2-3 is the solution for the following differential equation which is developed by Green [109] based on the Hill's muscle model:

$$[a g(t) + \beta] f \frac{dF_m}{dt} + [K_2 g(t) + K_1] F_m = K_1 K_2 g(t) (x - x_0), \quad \mathbf{2-4}$$

where  $g(t)$  represents the active state of the muscle and  $a, \beta$  are muscle characteristic coefficients and  $K_1, K_2$ , and  $f$  are equal to the slopes of nonlinear springs and dampers at the linearization point of the load-extension curve, the tension-length curve, and the force-velocity curves of the muscle.  $x_0$  is the unstretched length of the muscle and  $x$  is the length of the muscle at time  $t$ . The solution of the above equation is shown in Figure 2-12 [19]. In order to produce a smooth and coordinated movement, two sets of muscles namely agonist and antagonist type are considered to participate. Agonist muscle refer to a muscle that actively contract to produce a desired movement whereas antagonist muscle is a muscle that opposes the action of another as by relaxing while the other one contracts. Nijsen [75] applied Eq. 2-3 for the above mentioned muscles as follows:

$$F_{ag}(t) = F_{sum} \frac{t}{T} e^{-t/\tau_{sum}}, \quad \mathbf{2-5}$$

and

$$F_{ant}(t) = \frac{1}{A} F_{sum} \frac{t}{T} e^{-t/B\tau_{sum}}, \quad \mathbf{2-6}$$

where  $A$  and  $B$  are dimensionless constants approximately equal to unity [2].

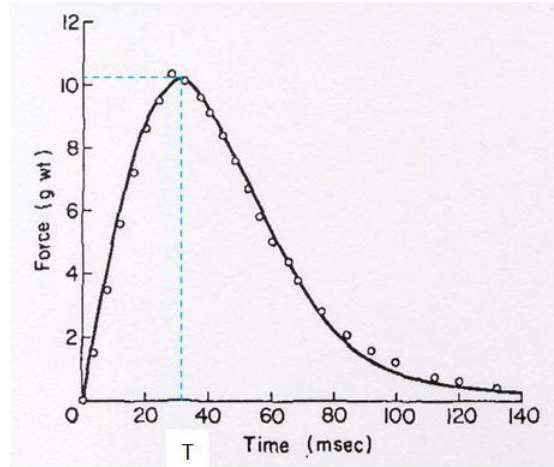


**Figure 2-12: Time- course of the isometric twitch in which  $a = 0.95$ ,  $\beta = 0.08$ ,  $f = 2.5 \frac{gs}{mm}$ ,  $K_1 = 69 \frac{g}{mm}$ ,  $K_2 = 2.0 \frac{g}{mm}$ , and  $x - x_o = 9 mm$  [109].**

### 2.3.2 Mechanical Model of the Arm

In this section, a summary of the mechanical model of the arm and curve fitting of the accelerometry data is presented. Nijssen et al [75] first derived an expression for the acceleration of the arm based on considering the interaction of the agonist and antagonist muscle forces then they fitted their model to the experimental data from patients with myoclonic seizure and calculated the coefficients in the model.

As discussed earlier in section 1.3.2 of chapter 1, in myoclonic seizure the flexion of the elbow can be considered as the most dominant motion and hence modeled as a hinge joint fixed in one end as shown in Figure 2-13. Accelerometers are fixed on the arm close to the wrist and measures acceleration components in the tangential direction ( $A_t$ ). Agonist ( $F_{ag}$ ) and antagonist ( $F_{ant}$ ) muscle forces as well as the joint reaction force ( $F_j$ ) are also illustrated in the figure. The length of the arm is assumed to be  $L$ .

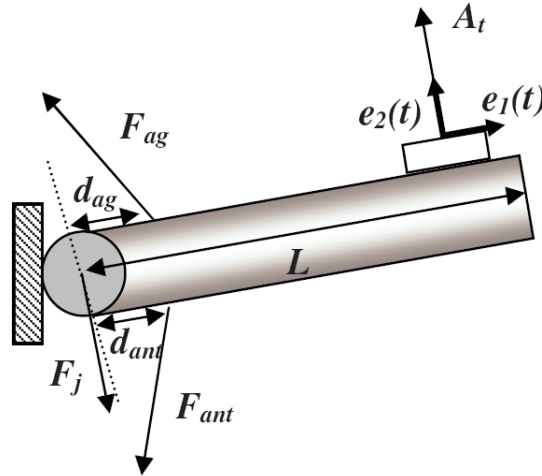


**Figure 2-13: Schematic overview of the biomechanical arm model in [75]**

If  $R$  represents the distance of the elbow to the accelerometer, the time-dependent kinematic relation for the displacement  $x(t)$  in the moving frame of reference  $\{e_1(t), e_2(t)\}$ , is:

$$x(t) = R e_1(t), \quad 2-7$$

The corresponding velocity  $v(t)$  is:

$$v(t) = \omega R e_2(t), \quad 2-8$$

where  $\omega$  represents the angular velocity of the moving frame. The corresponding acceleration  $a(t)$  is:

$$a(t) = \alpha R e_2(t) - \omega^2 R e_1(t), \quad 2-9$$

where  $\alpha(t)$  denotes the angular acceleration of the moving frame. Equation 2-9 shows that during a pure rotation, acceleration  $A_t(t)$  at the position of the accelerometer in the tangential direction  $e_1(t)$  equals  $\alpha R$  whereas the acceleration  $A_n(t)$  in the normal direction  $e_2(t)$  equals  $-\omega^2 R$ .

The moment applied to the arm as a result of the muscle forces is given by:

$$\Sigma M = I\alpha = F_{ag} \cdot d_{ag} - F_{ant} \cdot d_{ant} , \quad \mathbf{2-10}$$

where  $I$  is the mass moment of inertia about a parallel z-axis through the fixed rotating point and  $d_{ag}$ ,  $d_{ant}$  are the distances from the elbow joint to the action point of the agonist and antagonist muscle forces respectively as shown in Figure 2-13. This is clear from Figure 2-13 that the joint reaction force acts on the fulcrum and hence does not contribute to the sum of the moments.

Since the output of interest is  $\alpha$ , Eq. (2-10) is rewritten as

$$\alpha(t) = \frac{F_{ag} \cdot d_{ag} - F_{ant} \cdot d_{ant}}{I} . \quad \mathbf{2-11}$$

For a rigid rod, of length  $L$ , rotating around one end, the moment of inertia is constant and equals to  $\frac{1}{3}mL^2$ , with  $m$  the mass of the lower arm. In their study, Nijsen et al [75] used the full body expressions (full body mass:  $BM$ , full body length:  $BL$ ) for defining of the length and mass of the arm. They also used the average values for  $d_{ag}$  and  $d_{ant}$  and expressed in terms of full body mass ( $BM$ ) and full body length ( $BL$ ). Eq. 2-10 can then be rewritten as:

$$\alpha(t) = \frac{4.5}{BM BL^2} (F_{ag} - F_{ant}) . \quad \mathbf{2-12}$$

The measured output of the accelerometers placed on the arm equals  $\alpha R$ . The distance from elbow to the wrist,  $R$ , can also be expressed in terms of full body length:

$$R = 0.146 BL, \quad \mathbf{2-13}$$

Thus, the acceleration pattern observed during a myoclonic seizure can be presented in the form:

$$A(t) = K \left( t e^{\frac{-t}{\tau_{sum}}} - \frac{t}{A} e^{B \tau_{sum}} \right), \quad \mathbf{2-14}$$

where constant  $K$  is defined as



$$K = \frac{0.66 F_{sum}}{BM BL \tau_{sum}}. \quad 2-15$$

### 2.3.3 Moment Estimation for Myoclonic Epileptic Seizure Model

In this section, based on the model introduced in the previous section, a torque/moment model that represents myoclonic seizure is developed. The average coefficients reported for the accelerometry signal reported in [75] are as follows:

$$K = 42.6 \frac{N}{Kg s}, \tau_{sum} = 0.04s, BM = 74.96 Kg, BL = 1.84 m, \quad 2-16$$

and,

$$F_{max} = F(@ t = \tau_{sum}) = F_{sum} e^{-1}, B = 1.023, A = 1.045. \quad 2-17$$

Using the values given in Eqs. (2-15 - 2-17), following expression for  $K$  can be derived:

$$F_{sum} = \frac{F_{max}}{e^{-1}} = 88e = 239.21 N, \quad 2-18$$

and,

$$K = \frac{0.66 F_{sum}}{BM BL \tau_{sum}} = 28.6. \quad 2-19$$

The values of  $F_{sum}$  and  $K$  are used in Eq. (2-14) to get an expression for the average accelerometry response during myoclonic seizure:

$$A(t) = K \left( t e^{\frac{-t}{\tau_{sum}}} - \frac{t}{A} e^{\frac{-t}{B \tau_{sum}}} \right) = 28.6 t e^{\frac{-t}{0.04}} - 27.368 t e^{\frac{-t}{1.023 \times 0.04}}. \quad 2-20$$

The moment that the arm is subjected to during myoclonic seizure can then be derived as

$$M(t) = I\alpha = I \frac{A(t)}{R}. \quad 2-21$$

Upon employing the expression for  $A(t)$  from Eq. (2-20) and values for  $I$  and  $R$ , the expression for  $M(t)$  takes the form:

$$M(t) = 3.0716 t e^{-25t} - 2.9393 t e^{-24.4499t}. \quad 2-22$$

## 2.4 Dynamic Simulation Results

The resulting computer solution provides the output displacement, angular velocity, angular acceleration, and rotation angle of the human segments as well as the dynamic equations of motion. These equations are then numerically solved using MATLAB™ and the output of MATLAB™ is utilized in the following chapters to simulate the response of the model to epileptic seizure input, optimization of the sensor placements, and finally the torque joint estimation. The method used to derive the equations of motion is based on Kane's method which is explained in detail in Appendix A. An example for deriving the equations of motion for the arm is also presented in Appendix A and solved using both a popular dynamic modeling method, namely Newton-Euler approach and Kane's method, to illustrate the difference between the two approaches and to gain familiarity with the Kane's method which is later used in a software implementation namely, Motion Genesis™. Since the aim of this chapter is to give an idea of how the human body reacts to the seizure input, an epileptic seizure input is chosen and the method explained to deduce the model.

### 2.4.1 Motion Genesis™ Code

A brief description of how Motion Genesis™ formulates equations of motion is provided for the purpose of overall operations of motion development process. As stated earlier, Motion Genesis™ allows the user to perform Kane's method in an organized manner. The included equation manipulation software is designed to assist the user in developing the equations of motion. The user of this software still must be well educated in the formation of equations of motion manually. Familiarity with both Motion Genesis™ and

Kane's method is known to aid effective utilization of the software to produce the required equations of motion.

The process of developing the dynamic equations of motion through Motion Genesis™ is virtually identical to the process used when developing them manually. There may be a slight addition of work at the beginning since the user must describe the configuration of the system before beginning to develop equations. When using Motion Genesis™, one follows a systematic procedure to obtain the equations of motion which is shown as a flowchart in Figure 2-14. This process has also been explained via an example problem in Appendix A.

Once the configuration is set, assigning coordinate systems to each body, kinematics relationships are created. The angular velocities and accelerations are defined and then used with the formulae for a point moving on a moving body and two points stationary on a moving body. This produces relationships for velocities and accelerations for the important points in the system. Once the kinematical equations are set up, forces and torques are defined. Only non-working forces must be manually input. Constraints can also be added to the system at this point, if there are known relationships between parts of the system. Finally, commands are issued to form the equations of motion. Manipulations may be made, other important quantities may be defined (such as momentum or energy expressions), and output statements may also be made so that a simulation can be produced.

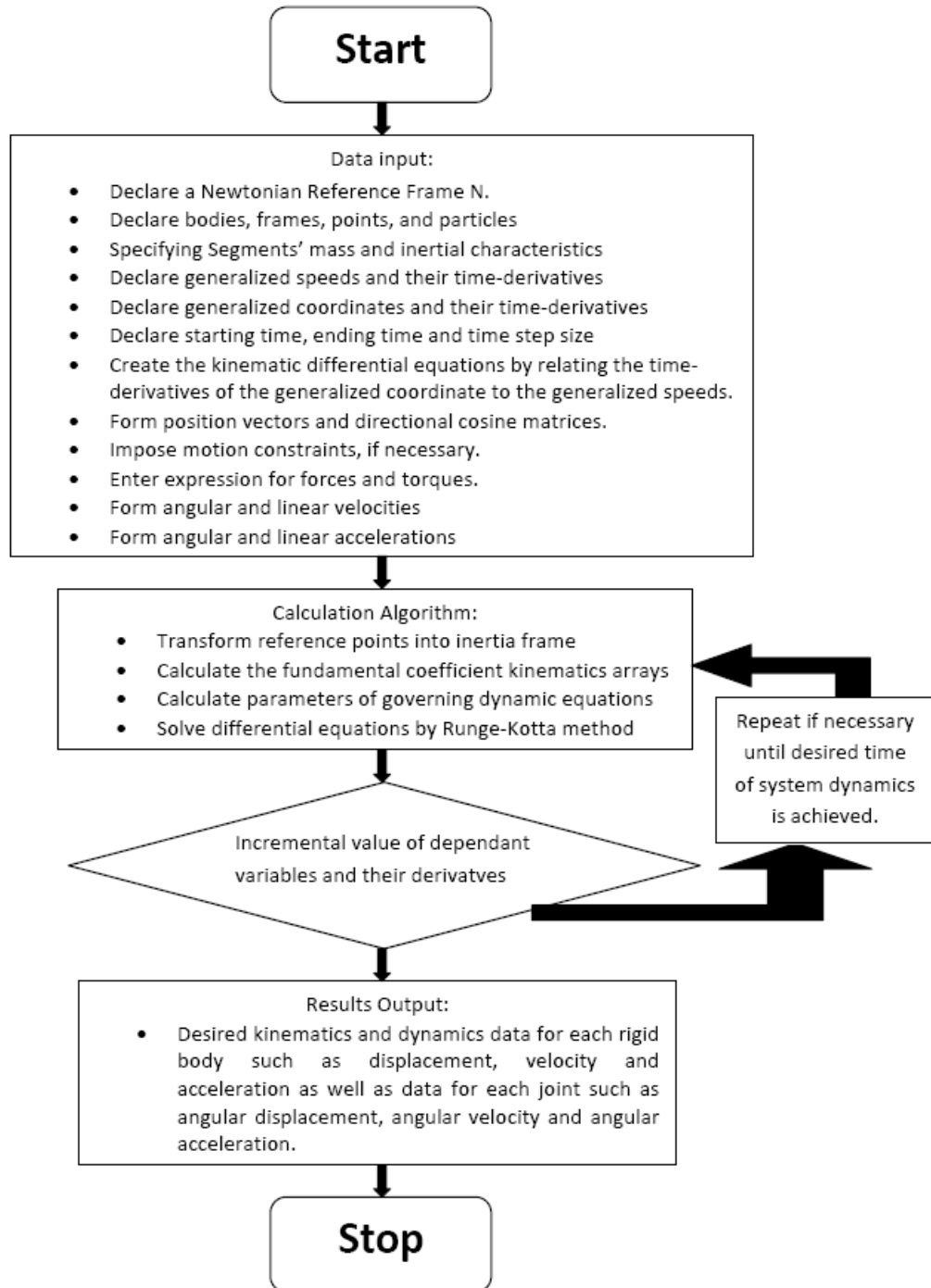


**Figure 2-14: Flowchart of the simulation procedure developed in Motion Genesis™**

## 2.4.2 Simulation Results

Motion Genesis™ creates 32 sets of equations of motion for the 32 degrees of freedom human body model. As mentioned earlier, Motion Genesis™ can generate sets of equations of motion in MATLAB™ or C++ format. The generated code actually integrates Motion Genesis™ equations forward in time using a fourth-order Runge Kutta integration scheme. This process creates data files including kinematics data of the body such as displacement, velocity and acceleration which can be plotted employing a simple script to view the results. For the present human body model, the simulation time is approximately 5 seconds for the chosen time step size of 0.01 seconds. Each simulation took 10 minutes to run in Motion Genesis™ and the generated MATLAB™ code took another 15 minutes to compile. In the following two sections, two sets of output are presented: Joint angular velocities which correspond to Gyroscope outputs and segment accelerations which correspond to the accelerometer outputs. These two quantities are important in the epileptic seizure analysis and are specially used in the following chapter for optimization purposes.

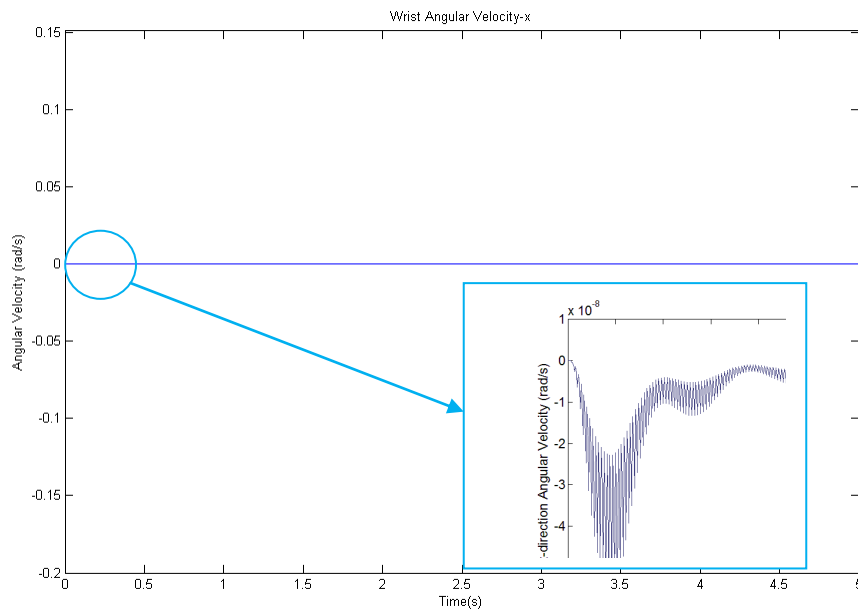
### 2.4.2.1 Joint Angular Velocities

In this section, some of the important joint angular responses during epileptic seizure input are presented. These joints are selected from the upper-body since in practice, myoclonic seizure movements have been found to be dominant in the arms than any other part of the body. The list of joints that is considered here includes elbow, wrist and shoulder.

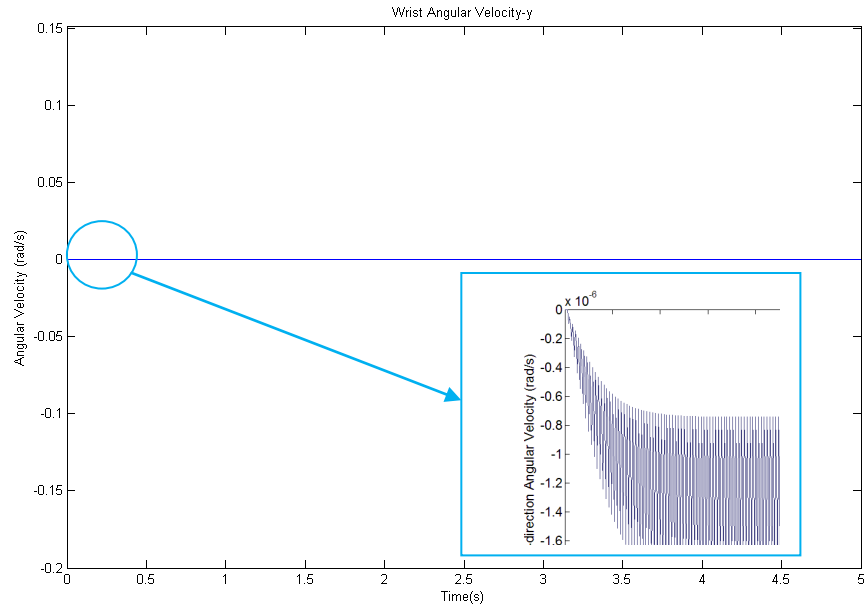
To study of the reaction of the muscular system to the seizure input, the angular velocity response of the human body model is considered to be of interest. The simulated angular velocity output can form an understanding of the human body mechanism and system identification in terms of magnitude, frequency and response. The acquired data can become useful prior to performing the experiments with this class of sensors and can be helpful in predicting the output plots that can be achieved from the gyroscope sensors.

Figure 2-15 to 2-17 display simulated responses to a moment applied on the shoulder joint in the z-direction. As expected, the angular velocity responses in the x and y

directions are relatively small and the responses consist of cross-coupling effects as well as some numerical noise. However, it can be seen from the Figure 2-17 that the response in the z-direction shows a sudden, abrupt impulsive response with exponentially decaying trend of the wrist joint angular velocity which initially in the opposite direction of the applied moment (i.e. in the positive direction of the z axis) but then gets to the same direction as the applied moment. The response can be explained by considering the fact that the moment is applied on the shoulder joint and the movement of the arm and forearm causes the motion of hand which is initially in the opposite direction of the moment applied on the shoulder but eventually as the moment generated motion overcomes the action of springs and dampers, it rotates in the same direction as moment. Based on these plots of the angular velocity components in the three directions tend to go to zero in steady state condition.



**Figure 2-15: Wrist angular velocity in the x-direction**



**Figure 2-16: Wrist angular velocity in the y-direction**

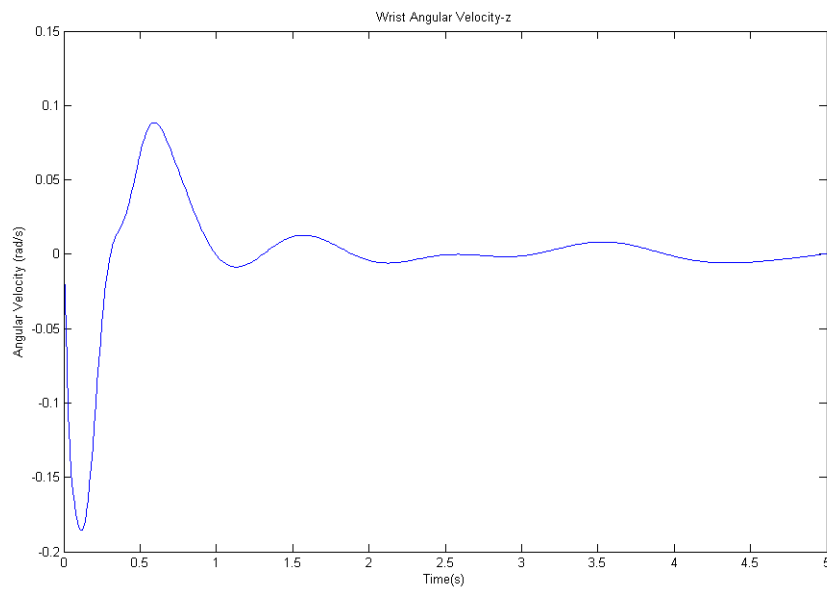


**Figure 2-17: Wrist angular velocity in the z-direction**

It should be also noted that the moment applied in the z-direction creates two significantly small angular velocity components in the x and y directions. These two components are due to the highly nonlinear and complex nature of the human body model and hence can be neglected compared with the z component of the angular velocity. Considering that the components of angular velocity in the x and y directions are negligible, only the z-direction angular velocity plots are presented for the shoulder and elbow joints.

As shown in Figure 2-18 and Figure 2-19, an applied moment to the shoulder joint results in a sudden, abrupt impulsive response of the elbow and shoulder joints which is initially in to the same direction as the applied moment with a zero steady state response.

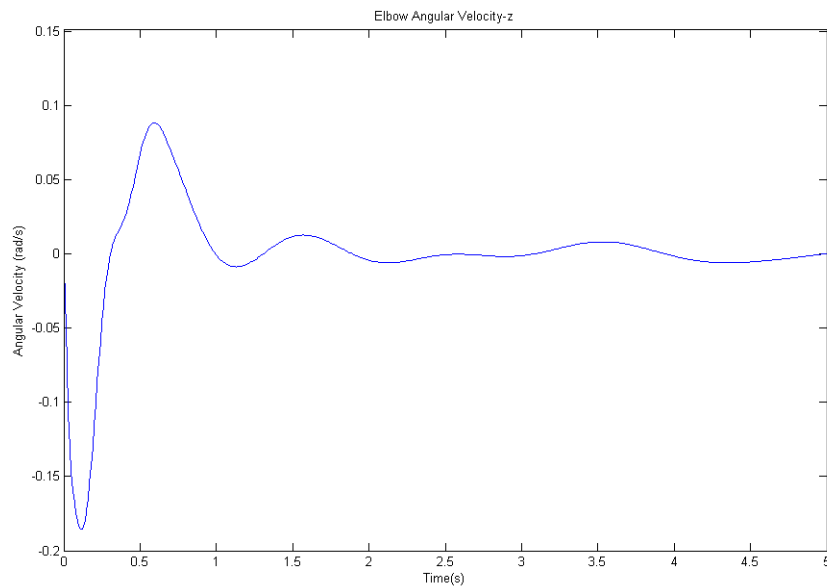


**Figure 2-18: Elbow angular velocity in the z-direction**



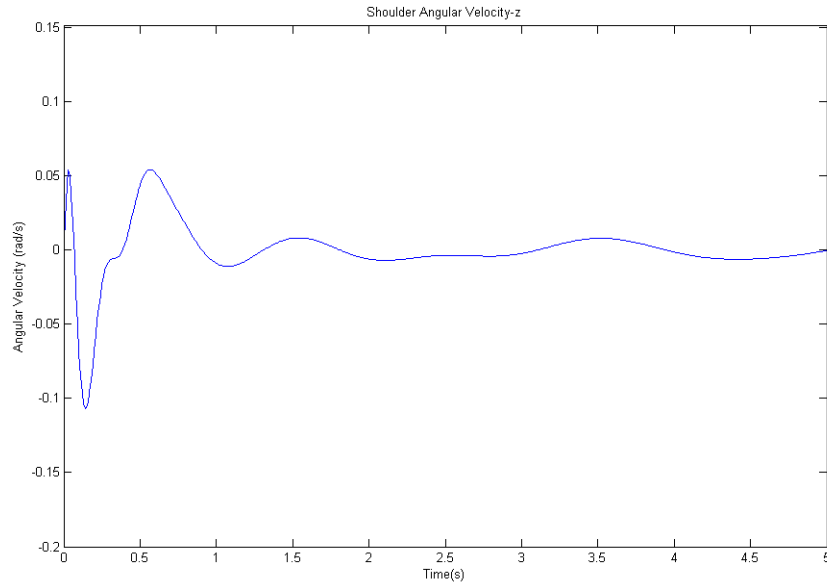


**Figure 2-19: Shoulder angular velocity in the z-direction**

#### 2.4.2.2 Segment Accelerations

In the same manner as previous section, joint acceleration responses during epileptic seizure input are presented. These joints are selected from the upper-body since as established earlier myoclonic seizure movements are dominant in the arms than any other part of the body. The list of joints that is considered here includes elbow, wrist and shoulder.

To study of the reaction of the muscular system to the seizure input, the acceleration response of the human body model is of interest. The simulated acceleration output can form an understanding of the human body mechanism and system identification in terms of magnitude, frequency and response.

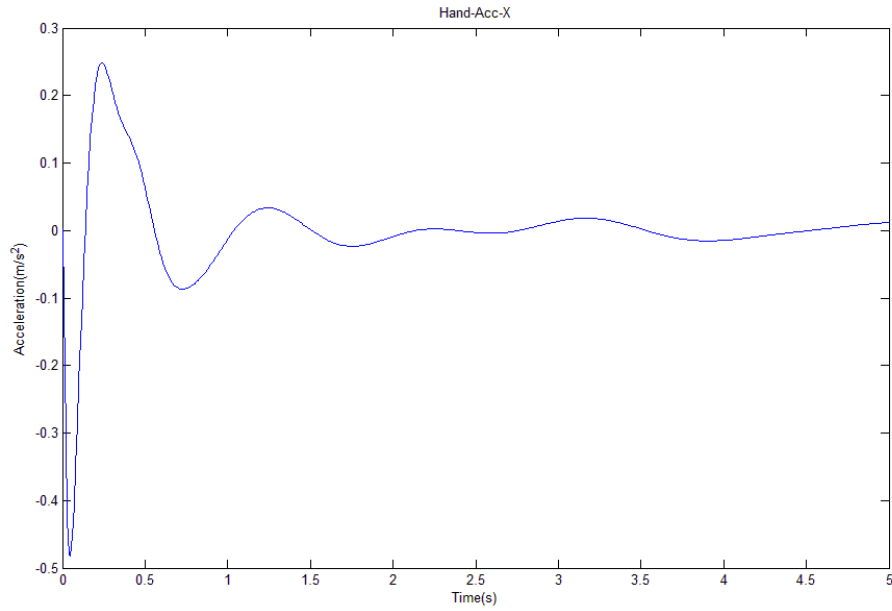


**Figure 2-20: Hand acceleration in the x-direction**

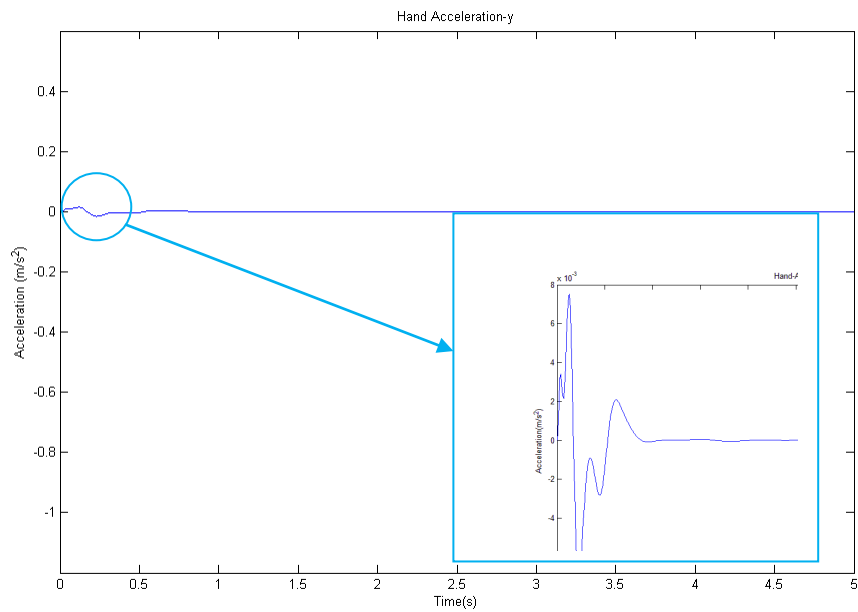


**Figure 2-21: Hand acceleration in the y-direction**

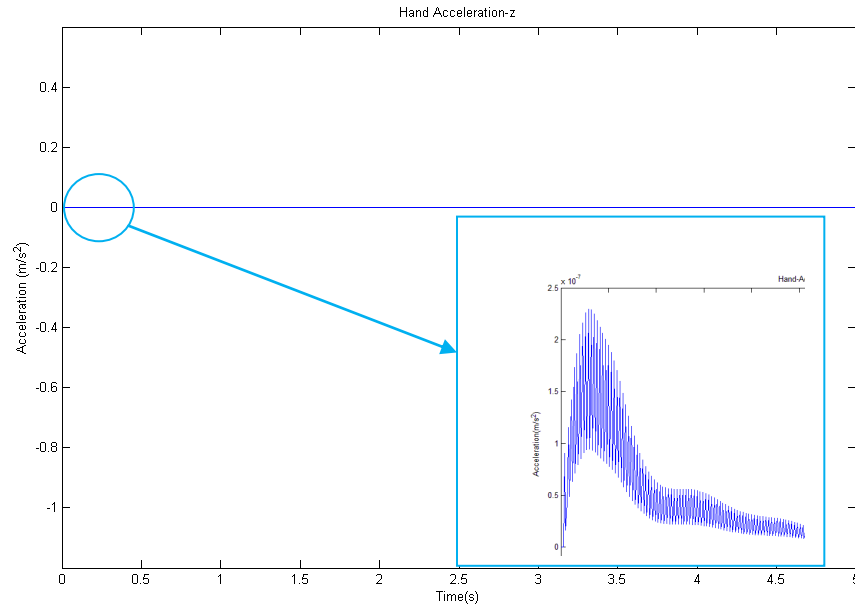


**Figure 2-22: Hand acceleration in the z-direction**

As shown in Figure 2-20 to 2-22, an applied moment to the shoulder joint results in a sudden, abrupt impulsive response with an exponentially decaying response of the hand in the x-direction. The plots also display the expected behavior where all of the three acceleration components in steady-state approach the equilibrium configuration. It may be also noted that the moment applied in the z-direction creates two significantly small acceleration components in the y and z directions. These two components are due to the highly nonlinear and complex nature of the human body model and can be neglected. Considering that the components of acceleration in the y and z directions are negligible, only the x-direction acceleration plots are presented for the forearm and arm segments.

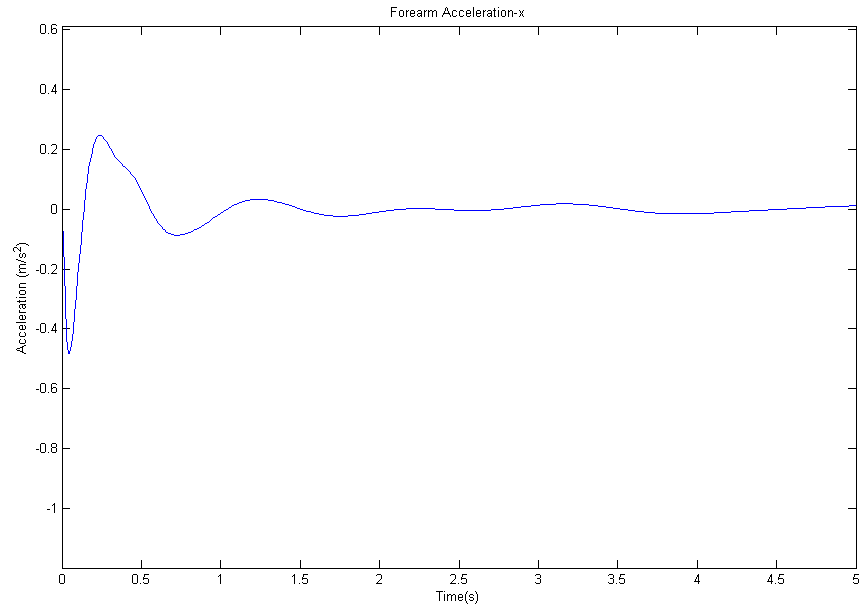


**Figure 2-23: Forearm acceleration in the x-direction**

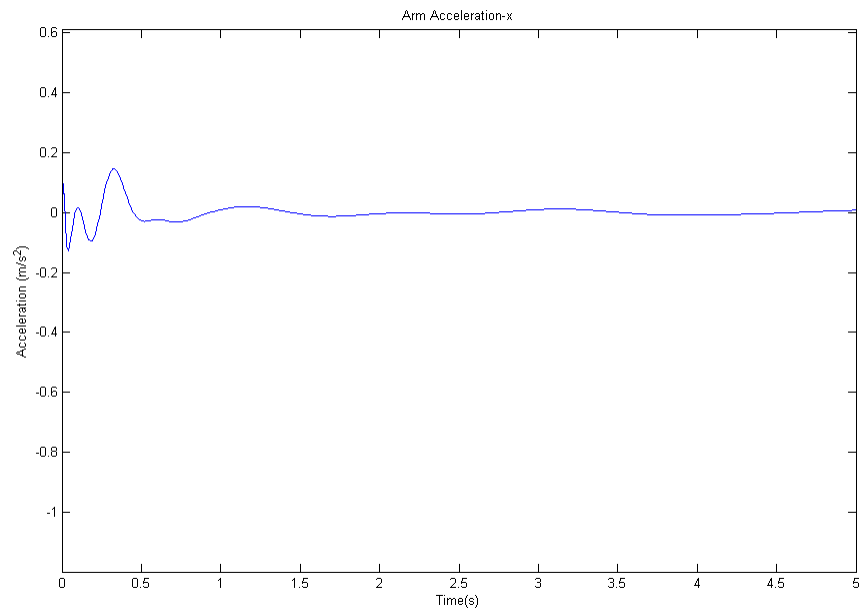


**Figure 2-24: Arm acceleration in the x-direction**

## 2.5 Closure

In this chapter, detailed mathematical model of human body is developed employing a commercially available dynamic analysis software, Motion Genesis™. In the first part of this chapter some preliminary review of the model with the detailed information of the segments, degrees of freedom, Anthropometry data and joint torques is provided and an epileptic seizure torque model as well as the theory that justifies choosing that seizure model is presented. In the final section an overview of the Motion Genesis™ software, coding method in the software and the Kane's method is presented. The procedure developed in this chapter can be considered as a useful tool to understand the dynamics of human body during epileptic seizure and will be utilized in the following chapter to decide on an optimal placement procedure for the inertial sensors.

## Chapter 3

### 3 Optimization of the Sensor Placement

The efficiency of the detection sensory system depends on the information it can retrieve from a seizure episode while the information should be sufficient, but not excessive. Hence, an increased number of sensors alone do not guarantee that the detection system will have a better performance. The relevance of the information brought by an additional sensor must also be taken into account and economical issues must also be taken into account. When designing a sensor system, one must search for those combinations (numbers and placements) of sensors that can provide the highest possible detection level at the lowest possible cost. In this chapter, first an approach based on the proposed method of Latt et.al [110] is developed to relate the angular acceleration of the arm to the outputs of the gyroscopes and accelerometers. Then an optimal placement strategy for inertial sensors that maximizes the resolution of the calculated angular acceleration is proposed. In addition, a sensitivity study is performed to investigate the dependence of the optimal placement outcome to the input values of the model such as arm geometry, mass, damping and spring coefficients. The dependence of the optimal locations on sensor's uncertainty values are also discussed in this part.

#### 3.1 Model Used to Place Inertial Sensors

In this section, assumptions made for optimization purposes are described and the reason for choosing arm to place the sensors is clarified. This part is then concluded by the formulation of uncertainties in calculation of the angular acceleration of the arm.

##### 3.1.1 Model Assumptions

The following assumptions are made in the process of developing the objective function used in the optimization:

- For alarm purposes, myoclonic seizure can act as a threshold:

As in various references such as [64], it is noticed that often seizure is started with myoclonic jerking in one arm and then followed by tonic, clonic or tonic-clonic

contractions that spread towards the other arm, trunk and legs. It is also stated that myoclonic seizures involve an extremely brief muscle contraction happening in less than 100 ms, whereas other types of generalized seizures recur in fractions of second to 20 seconds. On the other hand, sudden death is more likely to happen in tonic-clonic seizures. Considering all of the factors mentioned, myoclonic seizure is decided as a criterion to warn about seizure.

- Arm movements are dominant over other parts of the body in the myoclonic seizure:

From “movement studies” point of view, during a generalized epileptic seizure arms and legs are more affected than any other part of the body. Specifically, the arm movements are dominant over the leg movements and as a result arm movements are dominant over the whole body [75]. According to Nijsen et al [75], video observations confirm that myoclonic seizures appear as short abrupt flexions involving only the Forearm.

- Myoclonic seizure applied about coronal axis:

The epileptic seizure model is assumed to be applied in the sagittal plane about the coronal axis, so that the components of the angular velocity in the sagittal and vertical axis are negligible.

- Homogeneous arm model

A homogeneous shape is considered for arm in the optimization method, i.e. the width of arm is considered to be uniform along the length of the arm. By assuming the homogeneous arm shape, the variables for the optimization objective function are reduced compared to the non-simplified arm model case and that makes the optimization more efficient and processing time faster.

### 3.1.2 Formulation of Arm Acceleration Uncertainties

Following the proposed approach presented in [110], angular acceleration can be calculated using the differences between the acceleration components in multiple locations. The difference of the acceleration components of two accelerometers at locations  $\{i\}$  and  $\{j\}$  can be written in the following form:

$$A_{ij} = A_j - A_i = \omega \times (\omega \times P_{ij}) + \alpha \times P_{ij}, \quad \mathbf{3-1}$$

where  $P_{ij} = [P_{ijx} \ P_{ijy} \ P_{ijz}]^T$ , denotes the position vector from  $\{i\}$  to  $\{j\}$  and  $\omega = [\omega_x \ \omega_y \ \omega_z]^T$ , is the angular velocity vector of the body in three directions and  $\alpha = [\alpha_x \ \alpha_y \ \alpha_z]^T$ , is angular acceleration vector of the body in three directions. Expanding Eq. (3-1) into component-form results in:

$$\begin{bmatrix} a_{ijx} \\ a_{ijy} \\ a_{ijz} \end{bmatrix} = \begin{bmatrix} a_{jx} - a_{ix} \\ a_{jy} - a_{iy} \\ a_{jz} - a_{iz} \end{bmatrix}, \quad \mathbf{3-2}$$

$$= \begin{bmatrix} \omega_x \omega_y P_{ijy} - \omega_y \omega_y P_{ijx} - \omega_z \omega_z P_{ijx} + \omega_z \omega_x P_{ijz} \\ -\omega_x \omega_x P_{ijy} + \omega_x \omega_y P_{ijx} + \omega_y \omega_z P_{ijz} - \omega_z \omega_z P_{ijy} \\ \omega_x \omega_z P_{ijx} - \omega_x \omega_x P_{ijz} - \omega_y \omega_y P_{ijz} + \omega_z \omega_y P_{ijy} \end{bmatrix} + \begin{bmatrix} -\alpha_z P_{ijy} + \alpha_y P_{ijz} \\ \alpha_z P_{ijx} - \alpha_x P_{ijz} \\ \alpha_x P_{ijy} - \alpha_y P_{ijx} \end{bmatrix}.$$

According to the simulation results shown in Figure 3-1 to Figure 3-3, it can be assumed that the components of angular velocity in the x and y directions are negligible compared to the component in the z direction. Therefore, setting the components of the angular velocity in the x and y direction to zero, Eq. (3-2) can be written as

$$\begin{bmatrix} a_{jx} - a_{ix} \\ a_{jy} - a_{iy} \\ a_{jz} - a_{iz} \end{bmatrix} = \begin{bmatrix} -\omega_z \omega_z P_{ijx} + \alpha_y P_{ijz} - \alpha_z P_{ijy} \\ -\omega_z \omega_z P_{ijy} - \alpha_x P_{ijz} + \alpha_z P_{ijx} \\ \alpha_x P_{ijy} - \alpha_y P_{ijx} \end{bmatrix}. \quad \mathbf{3-3}$$



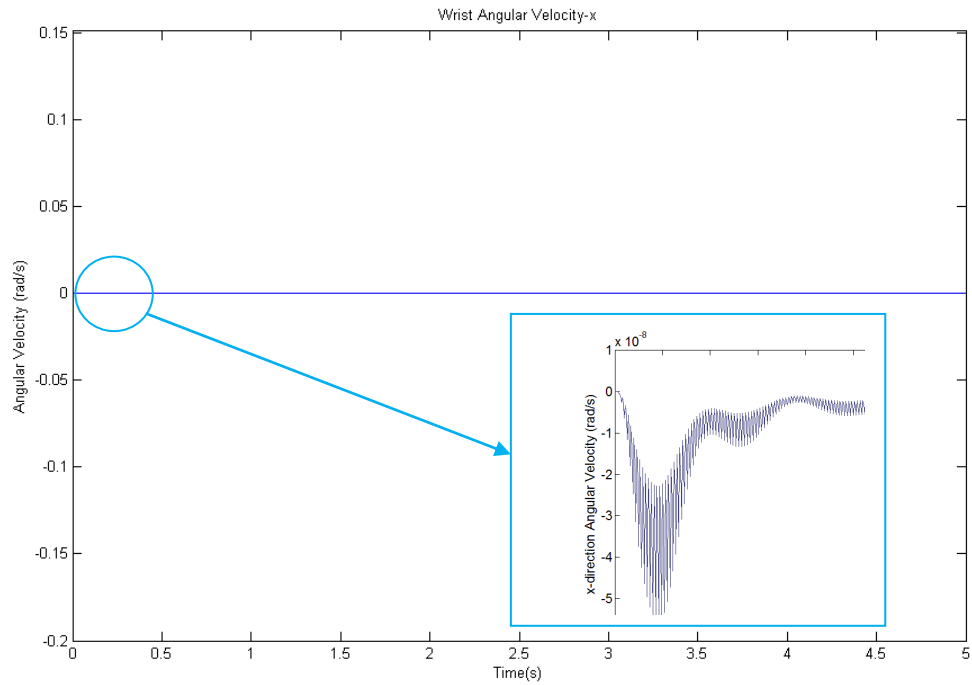


**Figure 3-1: Arm angular velocity components in the x directions**

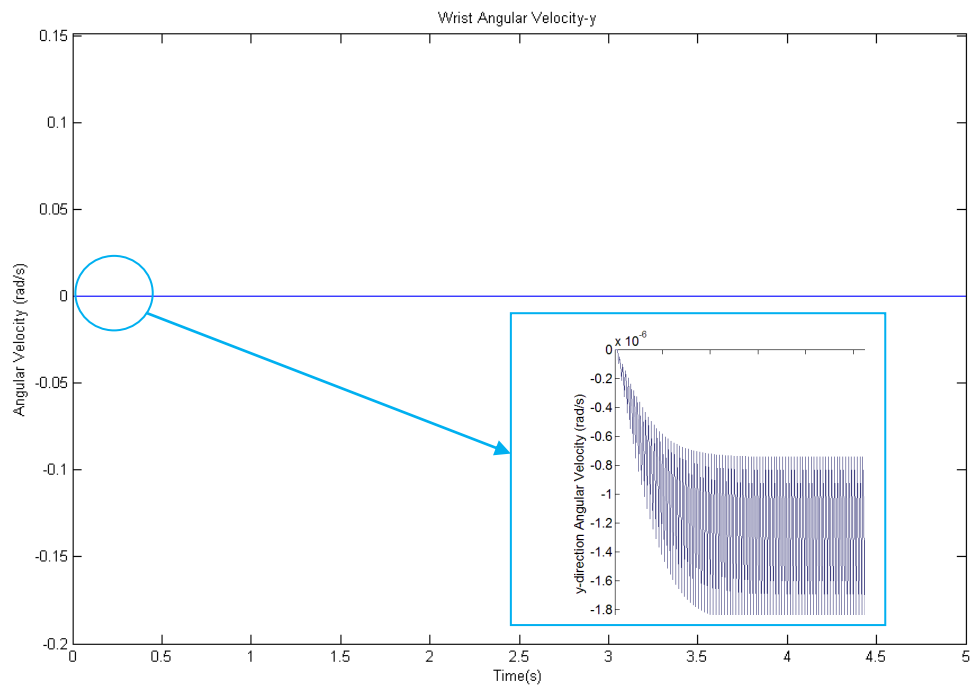


**Figure 3-2: Arm angular velocity components in the y directions**

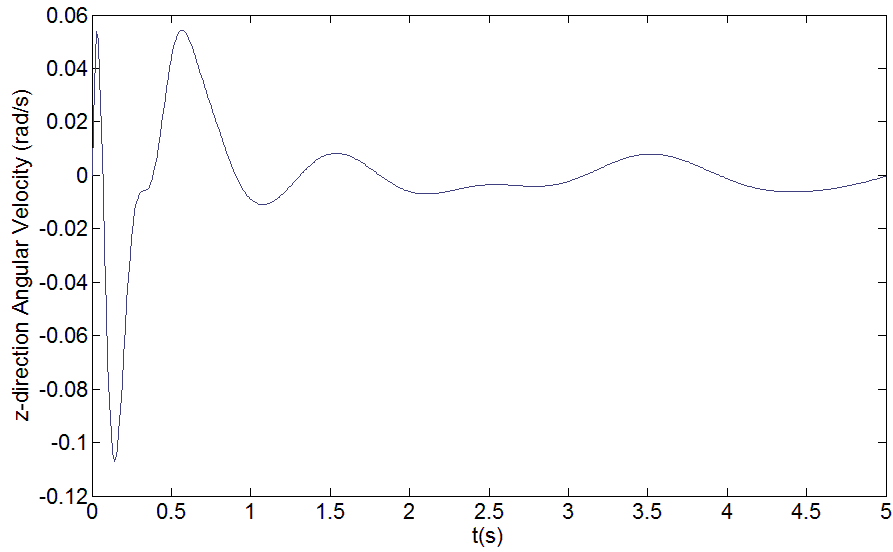


**Figure 3-3: Arm angular velocity components in the z directions**

It is further assumed that the accelerometers will be placed at arbitrary locations on the arm. Constraints in this case are the space limitation as well as placement of all accelerometers at the same y locations as shown in Figure 3-4. Placement of all accelerometers at the same y-location will result in the following equation:

$$\begin{bmatrix} a_{jx} - a_{ix} \\ a_{jy} - a_{iy} \\ a_{jz} - a_{iz} \end{bmatrix} = \begin{bmatrix} -\omega_z \omega_z P_{ijx} + \alpha_y P_{ijz} \\ -\alpha_x P_{ijz} + \alpha_z P_{ijx} \\ -\alpha_y P_{ijx} \end{bmatrix}. \quad \mathbf{3-4}$$

Eq. (3-4) leads to the decision of minimum numbers of sensors to be used on the arm. As it is clear from Eq. (3-4), all the three angular acceleration components cannot be derived from the measurement from just two accelerometers. For this reason at least three accelerometers are needed to calculate the three angular acceleration components via:

$$\begin{bmatrix} a_{3x} - a_{2x} \\ a_{2y} - a_{1y} \\ a_{3z} - a_{1z} \end{bmatrix} = \begin{bmatrix} -\omega_z \omega_z P_{23x} + \alpha_y P_{23z} \\ -\alpha_x P_{12z} + \alpha_z P_{12x} \\ -\alpha_x P_{13z} + \alpha_z P_{13x} \end{bmatrix}. \quad \mathbf{3-5}$$

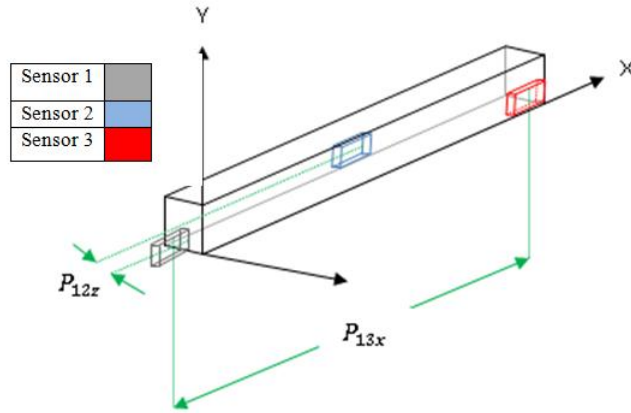


**Figure 3-4: Configuration of accelerometer placement within the space available on the arm**

Solving these three equations, three angular acceleration components  $\alpha_x$ ,  $\alpha_y$  and  $\alpha_z$  are obtained as

$$\alpha_x = \frac{P_{12x}a_{3y} + (P_{13x} - P_{12x})a_{1y} - P_{13x}a_{2y}}{P_{13x}P_{12z} - P_{12x}P_{13z}}, \quad 3-6$$

$$\alpha_y = \frac{a_{3x} - a_{2x} + \omega_z \omega_z P_{23x}}{P_{23z}}, \quad 3-7$$

$$\alpha_z = \frac{P_{12z}a_{3y} + (P_{13z} - P_{12z})a_{1y} - P_{13z}a_{2y}}{P_{13x}P_{12z} - P_{12x}P_{13z}}. \quad 3-8$$

In a general case, consider the results,  $A$ , to be a function of  $n$  measured variables  $x_1, x_2, x_3, \dots, x_n$ ; that is,

$$A = f(x_1, x_2, x_3, \dots, x_n), \quad 3-9$$

Then, small change  $\delta A$  in  $A$  can be related to small changes  $\delta x'_i$ 's in the  $x'_i$ 's through differential equation

$$\delta A = \delta x_1 \frac{\partial A}{\partial x_1} + \delta x_2 \frac{\partial A}{\partial x_2} + \dots + \delta x_n \frac{\partial A}{\partial x_n}, \quad 3-10$$

which can also be written in the following form:

$$\delta A = \sum_{i=1}^n \delta x_i \frac{\partial A}{\partial x_i}, \quad \text{3-11}$$

For a calculated result of  $A$  based on measured  $x_i$ 's,  $\delta x_i$ 's can be substituted by the uncertainties in the variables, and  $\delta A$  can be replaced by the uncertainty in the result. As the overall uncertainty is dependent on the individual uncertainties, an estimate of the overall uncertainty can be given as<sup>1</sup>:

$$\delta A = \left( \sum_{i=1}^n \left[ \delta x_i \frac{\partial A}{\partial x_i} \right]^2 \right)^{1/2}. \quad \text{3-12}$$

It may be noted that Eq. (3-12) propagates the uncertainties of the measured variables to the result with same confidence level. This expression is also known as the root of the sum of the squares (RSS). Employing Eq. (3-12) to the acceleration functions given in Eqs. (3-6) to (3-8), overall uncertainties in the angular acceleration components can be calculated as

$$\sigma_{\alpha_x} = \frac{\sqrt{P_{12x}^2 \sigma_{3y}^2 + (P_{13x} - P_{12x})^2 \sigma_{1y}^2 + P_{13x}^2 \sigma_{2y}^2}}{P_{13x} P_{12z} - P_{12x} P_{13z}}, \quad \text{3-13}$$

$$\sigma_{\alpha_y} = \frac{\sqrt{\sigma_{3x}^2 + \sigma_{2x}^2 + 4\omega_z^2 P_{23x}^2 \sigma_{\omega_z}^2}}{P_{23z}}, \quad \text{3-14}$$

$$\sigma_{\alpha_z} = \frac{\sqrt{P_{12z}^2 \sigma_{3y}^2 + (P_{13z} - P_{12z})^2 \sigma_{1y}^2 + P_{13z}^2 \sigma_{2y}^2}}{P_{13x} P_{12z} - P_{12x} P_{13z}}, \quad \text{3-15}$$

where  $\sigma_{i_{x,y,z}}$ ,  $i = 1,2,3$  are the uncertainty values of the three accelerometers in the x, y and z directions and are obtained from the inertial sensor specification which is used for the experiments[70]. It is clear from Eq. (3-14) that the resultant uncertainty in

---

<sup>1</sup> A detailed explanation on how to derive Eq. (3-12) is given in reference [129]

calculating the angular acceleration also depends on the value of the angular rate  $\omega_z$ . In order to incorporate this effect, peak angular rate value obtained via the simulation is used to calculate the uncertainty in the y-component of the angular acceleration  $\sigma_{\alpha_y}$ .

## 3.2 Constrained Optimization for Sensing Angular Acceleration

There are various optimization methods available in MATLAB™, including Genetic Algorithm (GA), global search, multistart, patternsearch, simulated annealbnd (SA), and gamultiobj. According to the MATLAB™ help, for the “single global solution” option only GA, SA and pattern search are recommended. Considering the fact that pattern search method is slower than the other two optimization techniques, GA and SA are selected for optimization purposes. In this section, a brief overview of the two common global optimization tools is given and the objective function used in the optimization process is introduced. This is then followed by the results of the two optimization techniques which are used to determine an optimal placement of the inertia sensors on the arm.

### 3.2.1 Simulated Annealing Overview

Simulated annealing (SA) is a method for solving unconstrained nonlinear optimization problems. Annealing is a thermal process for obtaining low energy states of a solid in a heat bath. The method models the objective function as a physical process of heating a material and then slowly lowering the temperature to decrease defects, thus minimizing the system energy. The key feature of SA is that it provides a means to escape local minimums by allowing so called “hill-climbing moves” in hopes of finding a global minimum. The search is started with a randomized state. The fitness of the individual population is evaluated during each iteration and is carried out a stochastic selection to constitute the next generation and consequently the new point. The distance of the new generated point from the current point is based on a probability distribution with a scale proportional to the temperature. The algorithm not only accepts all new points that lower the objective function, but also with a certain probability points that raise the objective

function. By accepting points that raise the objective, the algorithm avoids being trapped in local minimums in early iterations and is able to explore globally for better solutions.

### 3.2.2 Genetic Algorithm Overview<sup>2</sup>

GA is a population based stochastic optimization method which mimics Darwin's principle of natural selection and genetic inheritance. The fundamental concepts of GAs were introduced by Holland [111]. In GA, a sequence of populations of candidate solutions to the optimization problem is generated by using a set of genetically inspired stochastic solution transition operators to transform each population of candidate solutions into a generation population. These operations include selection, crossover and mutation. Every solution is assigned a fitness value based on the initial guess, bound limitation and other constraints. Then the selection operator is applied to choose comparatively 'fit' chromosomes to be a part of propagation process. In generation step new individuals are formed through crossover and mutation operators. Crossover operator combines the genetic information between chromosomes to explore the search space, whereas mutation operator is used to maintain adequate diversity in the population of chromosomes to avoid premature convergence. By doing so, it is guaranteed that the technique finds global minimum rather than local minimum.

### 3.2.3 Objective Function

It can be seen from Eqs. (3-13) to (3-15) that parameters  $P_{12x}$ ,  $P_{13x}$ ,  $P_{12z}$ , and  $P_{13z}$  govern the noise level in the three angular acceleration components. In order to get an equivalent measure that incorporates the three variance components an expression which makes use of equal weighting is formulated as

$$\sigma_{\alpha} = \sqrt{\sigma_{\alpha_x}^2 + \sigma_{\alpha_y}^2 + \sigma_{\alpha_z}^2}. \quad 3-16$$

---

<sup>2</sup> A detailed description of GA can be found in Goldberg [128].

Eq. (3-16) forms the basis for calculating the propagation of uncertainty which later is used as the objective function for noise minimization in the proposed optimization problem. For the space available on the arm, the parameters  $P_{12x}$ ,  $P_{13x}$ ,  $P_{12z}$ , and  $P_{13z}$  are replaced with  $ld_1$ ,  $md_1$ ,  $nd_3$  and  $(1 - n)d_3$  respectively, where the fractions  $l$ ,  $m$ , and  $n$  have been introduced to represent the sensor locations on the arm. Hence the variables  $l$ ,  $m$ , and  $n$  are constrained in the range of  $[0, 1]$  while  $d_1$  and  $d_3$  denote, respectively, arm lengths in x and z directions. It may be noted that Eq. (3-16) is a function of four variables (three independent variables and one dependent variable) and is highly nonlinear.

### 3.2.4 Results

Considering the nonlinear objective function given in Eq. (3-16) and the associated constraints, routines within the MATLAB™ global optimization toolbox have been employed to find the minimum noise and eventually optimal sensor placements. For this purpose, the GA from the global optimization toolbox is used and the results are compared with those obtained via the SA available within the same toolbox. It may be noted that in order to guarantee that the resultant minimum produced by the algorithm represents the global minimum, the tolerance parameter is reduced from the default value to a sufficiently low value of  $1e-300$ . Table 3-1 gives a comparison of the two methods as well as the predicted locations of the sensors which yield the minimum noise in calculating the angular acceleration.

**Table 3-1: Optimal Sensor Placement Predictions**

	GA	SA
Iterations	195	4982
Stopping Criteria	Generations: 10000	-
l	0.508	0.508
m	1	1
n	1	1
Function Value	0.01192458	0.01192458

It is proposed that the predicted locations will be considered when implementing a typical sensor cluster for epileptic patient monitoring. To apply optimization result to the

experimental set up, five Motion Node™ unit sensors are considered to be employed, out of which three will be placed on the proposed locations on right arm while other two will be placed on head and the chest to add further useful insight for distinguishing between daily typical normal activity and seizure condition.

### 3.3 Sensitivity Analysis

In this part, sensitivity analysis of the estimated placement configuration due to prescribed uncertainties in the input model-parameters as well uncertainties in the inertial sensor outputs are studied considering the uncertainty range of  $-20\%$  to  $+20\%$  via simulation. This analysis is performed in three steps:

- i. The coefficient of the joint torque and damping are varied in the specified range and the effect of these changes on the angular velocity value is studied. Then using this angular velocity value in the objective function, the optimization process is performed to examine the effect on the optimal placement.
- ii. Arm geometry and mass are changed in the specified range and the new value for angular velocity is calculated. It may be noted that, in this case, the percentage change in the mass moment of inertia values implicitly depend on the assumed changes in geometry and length. Using the angular velocity value as well as arm parameters in the objective function, optimization is then carried out.
- iii. The uncertainty values given for the sensors are changed in the objective function and the results are obtained to decide the sensitivity dependence on the inertial sensor individual uncertainties.

Table 3-2 and Table 3-3 give an overall comparison of different values for joint torque's coefficient and damper's coefficient, mass and length of the body arm and inertial sensor's uncertainty effect on the estimated optimal placement configuration and the noise function value. The results presented for the three sets provides confidence in the proposed optimization process and indicates the validity of the optimal location predictions in the presence of parameter uncertainty in the biomechanical, geometrical as well as sensor noise parameters.



### 3.3.1 Sensitivity to the Joint Torque and Damping Coefficients

The spring and damping coefficients that are used in the model was adopted from [102], however, these values may change for different individuals. Therefore the aim of this part is to investigate the effect of changing these input values on the optimization results. For this purpose, the coefficients of each joint torque and damping are varied between -20% to +20% and the effect of these changes on the angular velocity value is observed. As it is mentioned in section 3-2-2, the objective function is dependant not only on the accelerometer outputs but also on the gyroscope outputs. Considering this fact, new angular velocity value from simulation is substituted in the objective function. Finally GA is used to examine the sensitivity of the results to the mentioned coefficients.

**Table 3-2: Optimization sensitivity to the joint torque and damping coefficients**

case	Deviation from the nominal value (%)	Estimated Optimal Placement			Noise Function Value	Iterations
		l	m	n		
1	-20	0.509	1	1	0.01192333	181
2	-15	0.509	1	1	0.01192333	132
3	-10	0.508	1	1	0.01192122	171
4	-5	0.508	1	1	0.01192122	204
5	0	0.508	1	1	0.01192122	51
6	+5	0.507	1	1	0.01191896	175
7	+10	0.506	1	1	0.01191839	125
8	+15	0.507	1	1	0.01191896	177
9	+20	0.506	1	1	0.01191839	144

It is clear from Table 3-2 that changing joint damping and spring coefficients result in the change of the number for iterations that is needed to achieve the optimal location but has no effect on the optimal locations (less than 0.004%). However, the change in the iterations results in a longer processing time (average processing time is 6 minutes). The change of the noise function value due to the derivation from the nominal input values is also negligible.

### 3.3.2 Sensitivity to the Arm Geometry and Mass

Other coefficients that change from a person to another are mass and geometrical values. As mentioned in chapter 2, these values are used from data associated with a male

cadaver of height 1.741 m and mass of 72.8 kg; however, these values may change for different individuals. Therefore, for analysis purposes, these values are varied between -20% to +20% and consequently the angular velocity value is also changed. As the objective function is dependant not only on the accelerometer and gyroscope outputs but also the dimension of the arm model; new angular velocity value from simulation as well as new geometrical values are substituted in the objective function. Finally, optimization using GA method is performed to examine the sensitivity of the results to the arm geometry and mass.

**Table 3-3: Optimization sensitivity to the arm geometry and mass**

case	Deviation from the nominal value (%)	Estimated Optimal Placement			Noise Function Value	Iterations
		l	m	n		
1	-20	0.506	1	1	0.01036512	156
2	-15	0.506	1	1	0.01036002	134
3	-10	0.508	1	1	0.01325123	51
4	-5	0.508	1	1	0.01325110	51
5	0	0.508	1	1	0.01192365	51
6	+5	0.507	1	1	0.01135492	51
7	+10	0.507	1	1	0.01135685	51
8	+15	0.506	1	1	0.01036462	134
9	+20	0.506	1	1	0.01036945	156

It is clear from Table 3-3 that changing anthropometric data result in the change of the iteration number needed to achieve the optimal location but has no effect on the optimal locations (less than 0.004%). However, the change in the iterations makes the rendering time little bit longer (average processing time is 6 minutes). The change of the noise function value due to the derivation from the nominal input values is also negligible.

### 3.3.3 Sensitivity to the Inertial Sensor's Uncertainty

For the present work, uncertainty values given in the Motion Node™ catalogue are used in Eq. (3-16). It is obvious that these values are dependent on the inertial unit and may change for other products. In order to quantify the effect of changes in the uncertainties on the output optimal locations, sensitivity analysis of the output to the input sensor uncertainties is performed. Therefore in the present analysis these values are varied

between -20% to +20% and the effect of input changes on the objective function as well as optimization results is investigated.

**Table 3-4: Optimization sensitivity to the inertial sensor's uncertainty**

case	Deviation from the nominal value (%)	Estimated Optimal Placement			Noise Function Value	Iterations
		l	m	n		
1	-20	0.508	1	1	0.01411236	51
2	-15	0.508	1	1	0.01311562	51
3	-10	0.508	1	1	0.01073562	51
4	-5	0.508	1	1	0.01073264	51
5	0	0.508	1	1	0.01192458	51
6	+5	0.508	1	1	0.01252648	51
7	+10	0.508	1	1	0.01192856	51
8	+15	0.508	1	1	0.01252635	51
9	+20	0.508	1	1	0.01423565	51

Table 3-4 summarizes the results. It is clear that changes in the uncertainty values of the inertial sensors in the range of -20% to +20% have no effect on the optimal locations and iterations number. The change of the noise function value due to the derivation from the nominal input values is also found to be negligible.

### 3.4 Closure

Achieving high resolution in the sensing applications is an important factor to increase the reliability of the system. In particular, the practical requirement for wearable sensory monitoring device is that it should preferably have a small, light-weight sensor embodiment that can provide maximum information content by assuring a high resolution results as well as the maximum comfort for the patient. Having this goal in mind, an objective function based on the angular acceleration calculation is developed. Applying two common optimization methods, GA and SA, the procedure is further extended to determine the optimal placement for the inertial sensors. Finally a sensitivity analysis is done to examine the dependence of the optimal locations on the input values. It is envisaged that the outcome of this chapter will be applied when these sensors are used for the epileptic seizure in order to achieve highest possible resolution sensing.

## Chapter 4

### 4 Seizure Detection via Inertial Measurement based Torque Estimation

The simulation procedure developed in chapter 2 is a powerful tool to enable researchers to gain insight into the governing mechanical equations of human motion and elucidate limitations associated with experimentally derived measures. The algorithms currently employed for seizure detection are time consuming and often can only be implemented via off-line procedures. It is also widely reported in the literature that the detection algorithms often do not have an acceptable correlation with the motor phenomena that occurs during seizure and, as a consequence, may be very difficult for clinical staff to understand. Our central premise in this chapter is then to formulate the process which can be physically interpreted and as a result easily related to the type of body motion that occurs during a seizure episode. For this purpose, a technique for joint torque estimation using inertial sensors is proposed.

The outline of the chapter is as follows; first, the principle of the joint angle estimation is described, followed by a description of the estimation of the angular acceleration using inertial sensors. Then, incorporating the two expressions derived for the angles and angular acceleration, a procedure for estimation of joint torque is developed.

#### 4.1 Joint Torque Estimation

As discussed earlier, response prediction via dynamical equations of human body motion can be used for developing a procedure for joint torque estimation. In this section, first, a method to estimate joint angle using the accelerometer and magnetometer is developed and then the angular acceleration terms of segments are calculated using accelerometer outputs. These values together with the output response of the gyroscopes (angular rates) are used in the dynamical equations of motion to estimate the joint torques. This method is of particular interest for the study and analysis of human movement, as it can be used to compare estimates of the torque required to perform normal activities such as walking and running with those of involuntary movements such as Epileptic seizure or Parkinson

Disease tremor. This estimation procedure utilizes the dynamic equation of motion generated in chapter 2 via a modified version of the generated C++ code from Motion Genesis™. It may be noted that procedures developed here may find applications in classifying movement patterns based on inertial sensor data.

#### 4.1.1 Joint Angle Estimation Using Accelerometers and Magnetometers

Tracking a human body's joint angle empowers the clinical studies for post-operative analysis and prediction of an unhealthy as well as healthy subjects' possibility of injury. To this end, joint angles of a human jumping and landing are estimated in a daily environment where professional medical facilities are not available. Joint angle estimation along with the inertial data of the human body movement can form a strong tool for activity detection. In this section, an attempt is made to address the problem by finding the joint angle changes during an epileptic seizure.

Current approach to estimate the joint angles rely on the complimentary features of both accelerometers/gyroscopes and compute the best estimate. Indeed, other portable sensors, such as magnetometers, may be included in the integration in order to improve the overall quality. However, the provided estimates may be corrupted by different types of errors such as the induced error of angular rate signal integration. To overcome these problems, a method of angle estimation without integration of the angular rate signal is proposed. This method has been originally proposed by Kun et al [112] and is composed of inertial sensor difference based and virtual sensor difference based algorithms. Virtual sensors are sensors that are not physical and are imagined in order to relate the acceleration of the arm to the acceleration of the forearm at their intersection point which is the elbow joint in the present case. Hence, the difference of the two accelerometer terms of the virtual sensors is thought to be solely due to the rotation of the coordinate systems. Considering this fact, the rotation matrix can be defined for relating the two accelerometer terms and this can eventually lead to the joint angle estimation. As shown in Figure 4-1, three accelerometers are attached to the forearm, out of which two are in the same plane in accordance with the configuration proposed in chapter 3. The equivalent acceleration measured by the accelerometer including the gravitational component is given by

$$A_{ix,y,z} = g - \ddot{R}_{i,x,y,z} - \omega \times (\omega \times P_{i,x,y,z}) + \alpha \times P_{i,x,y,z}, \quad 4-1$$

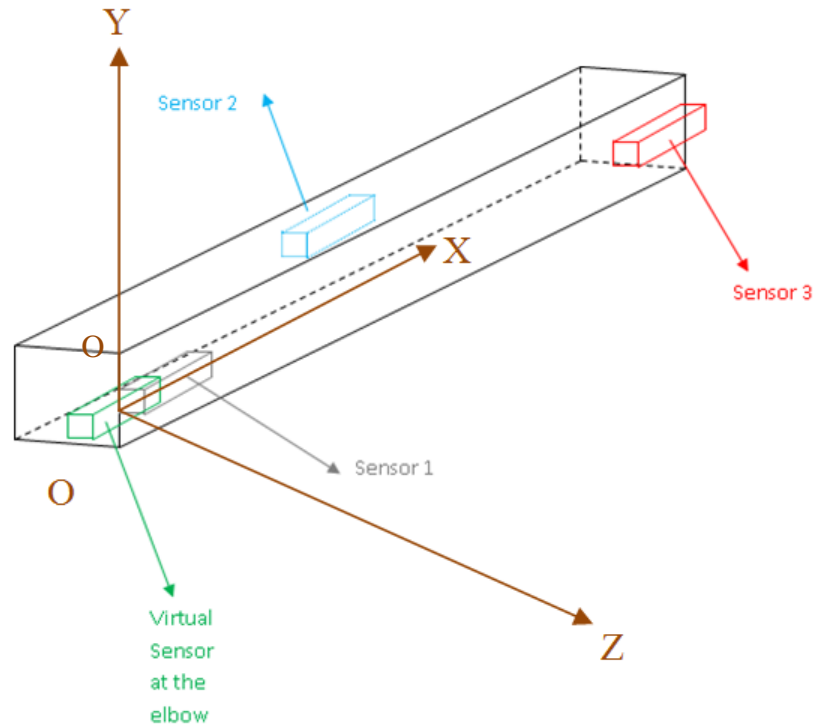


**Figure 4-1: The elbow virtual sensor and three forearm physical sensors**

where  $A_i$  is the equivalent acceleration at point  $i$  where the  $i$ th sensor is located,  $g$  is the gravitational acceleration,  $R_i$  is the position vector associated with point  $i$  relative to the global coordinate system ( $O$ - $XYZ$ ) and  $P_i$  is the rotational radii about the origin of the forearm at point  $O$  which corresponds to the elbow location in the forearm. Based on the proposed configuration, following equations are derived for the acceleration of each sensor:

$$A_{0x,y,z} = g - \ddot{R}_{0x,y,z}, \quad 4-2$$

$$A_{1x,y,z} = g - \ddot{R}_{1x,y,z} - \omega \times (\omega \times P_{1x,y,z}) + \alpha \times P_{1x,y,z}, \quad 4-3$$

$$A_{3x,y,z} = g - \ddot{R}_{3x,y,z} - \omega \times (\omega \times P_{3x,y,z}) + \alpha \times P_{3x,y,z}. \quad 4-4$$

In Eq. 4-2 to Eq. 4-4,  $A_{0x,y,z}$  represents the virtual sensor acceleration while  $A_{1x,y,z}$  and  $A_{3x,y,z}$  denote the accelerations of the two sensors placed in the same plane of the forearm.

Using equations 4-2 to 4-4, the vector of acceleration at the rotation joint can be obtained as follows:

$$A_{0x,y,z} = \frac{P_{3x,y,z}A_{1x,y,z} - P_{1x,y,z}A_{3x,y,z}}{P_{3x,y,z} - P_{1x,y,z}}. \quad 4-5$$

To analyze the elbow joint rotation angles, an algorithm based on the difference between double virtual sensors implanted in the elbow joint, called virtual-sensor difference based, is employed. The forearm and the arm segments are assumed as rigid segments connected with a 3-DOF joint. Three physical sensors in locations determined by the optimization technique in chapter 3 and a virtual sensor in ‘green’ are fixed on the forearm as shown in Figure 4-1. In the same manner, three physical sensors and a virtual sensor are attached on the arm. The corresponding axes of the two physical sensors in the same plane and the virtual sensor in each segment are in the same direction. Hence, the accelerations of the two virtual sensors can be calculated from the accelerations measured by the pair of physical sensors associated with each group, respectively, using the physical-sensor-difference based algorithm as explained earlier in this section.

It is clear from the fundamentals of dynamics, when a multi segment rigid body is moving in space each point on that body has a unique acceleration; hence, the two virtual sensors in the elbow joint must have equal accelerations in the same coordinate frame. As shown in Figure 4-2, two virtual sensors are placed on the elbow joint at the same position and plane but with different orientation; one in the longitudinal direction of the arm and another in the longitudinal direction of the forearm. On the same position and plane at the elbow joint, the two virtual sensors attached in different orientations measure two groups of accelerations. The difference between the acceleration vectors represents the angular change associated with the joint connecting the two segments, which can

illustrate the rotation angles of the elbow joint. The relationship between the two accelerations measured by the two virtual sensors can then be formulated as

$$A_{forearm} = RA_{arm}, \quad 4-6$$

where  $R$  is the rotation matrix between the two virtual sensors, which also represents the rotation matrix between the forearm and arm segments.

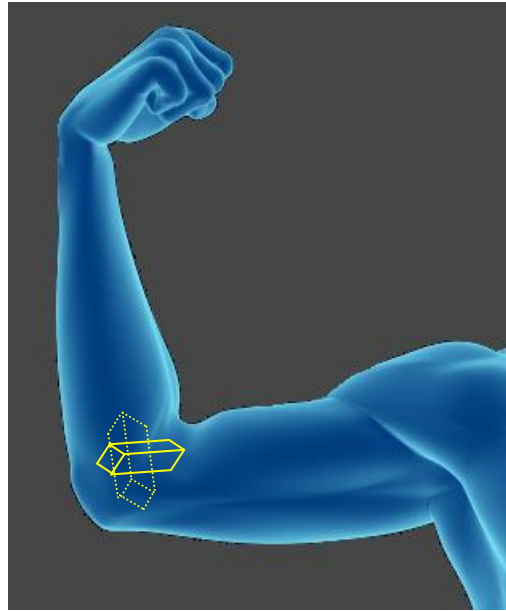


**Figure 4-2: Analysis of the elbow joint angle using the double virtual sensors considered to be on the elbow**

It may be noted that for calculating the rotation angles, at least two vectors relating the two planes are required. For this purpose, two magnetometers in conjunction with the accelerometers are used to measure the magnetic field data attached on the forearm and arm, with the corresponding axes in the same directions as those of the accelerometers. Following the same procedure for calculating the rotational angles from accelerations using the virtual accelerometers in the elbow joint, two virtual magnetometers attached with different orientations in the elbow joint must physically have a unique magnetic field data. The orientation difference between the vectors of magnetic field data represents the elbow joint angular change and hence can be employed in order to



calculate the joint angles. The relationship between the measured magnetic field data is then governed by

$$M_{forearm} = RM_{arm}, \quad 4-7$$

Hence, based on physical-sensor-difference-based algorithm and virtual-sensor-difference-based algorithm, the rotational angles of the elbow joint can be calculated from 4-5 to 4-7, and then the rotation matrix  $R$  can be obtained. Once the rotation matrix  $R$  is obtained the angles can be computed from the following expression

$$R = R_{\theta_x}R_{\theta_y}R_{\theta_z} = \quad 4-8$$

$$\begin{bmatrix} \cos \theta_z & -\sin \theta_z & 0 \\ \sin \theta_z & \cos \theta_z & 0 \\ 0 & 0 & 1 \end{bmatrix} \begin{bmatrix} 1 & 0 & 0 \\ 0 & \cos \theta_x & -\sin \theta_x \\ 0 & \sin \theta_x & \cos \theta_x \end{bmatrix} \begin{bmatrix} \cos \theta_y & 0 & -\sin \theta_y \\ 0 & 1 & 0 \\ \sin \theta_y & 0 & \cos \theta_y \end{bmatrix},$$

In the same manner, two physical sensors can be placed on the chest so that the angles of the shoulder can be decided.

#### 4.1.2 Angular Rate Estimation using Accelerometers

As discussed in the previous section, the primary goal of the estimation of the joint angles and angular accelerations without integration or differentiation of the angular rate signal is to avoid the associated errors. To do so, following the method presented in chapter 3, components of forearm angular accelerations are presented as follows:

$$\alpha_x = \frac{P_{12x}a_{3y} + (P_{13x} - P_{12x})a_{1y} - P_{13x}a_{2y}}{P_{13x}P_{12z} - P_{12x}P_{13z}}, \quad 4-9$$

$$\alpha_y = \frac{a_{3x} - a_{2x} + \omega_z \omega_z P_{23x}}{P_{23z}}, \quad 4-10$$

$$\alpha_z = \frac{P_{12z}a_{3y} + (P_{13z} - P_{12z})a_{1y} - P_{13z}a_{2y}}{P_{13x}P_{12z} - P_{12x}P_{13z}}, \quad 4-11$$

and Eqs. 4-9 to 4-11 are used in conjunction with the estimated joint angles in the following section to estimate the joint torques.

### 4.1.3 The Procedure for Joint Torque Estimation

Epileptic seizure occurs mainly due to the malfunctioning in the neuromuscular system. As the focus of the present study is on the mechanical behavior of the human body during seizure, formulating the seizure episode in mechanical terms such as torque, force, etc. is envisaged to be advantageous. The torque estimation of the epileptic seizure and comparison between involuntary movement's torque value and normal activities torque value can form a new detection technique which is easily related to the movement that occur during these activities. The torque measured about the joint is shown to be algebraically related to the joint angles and angular acceleration according to the relationship which is derived via Motion Genesis™. This procedure is modified to be numerically solved in the symbolic math toolbox of MATLAB™, MuPAD. The angles as well as the angular accelerations that are computed via the method described in sections 4.1.1 and 4.1.2 form the inputs needed in the procedure for joint torque estimation.

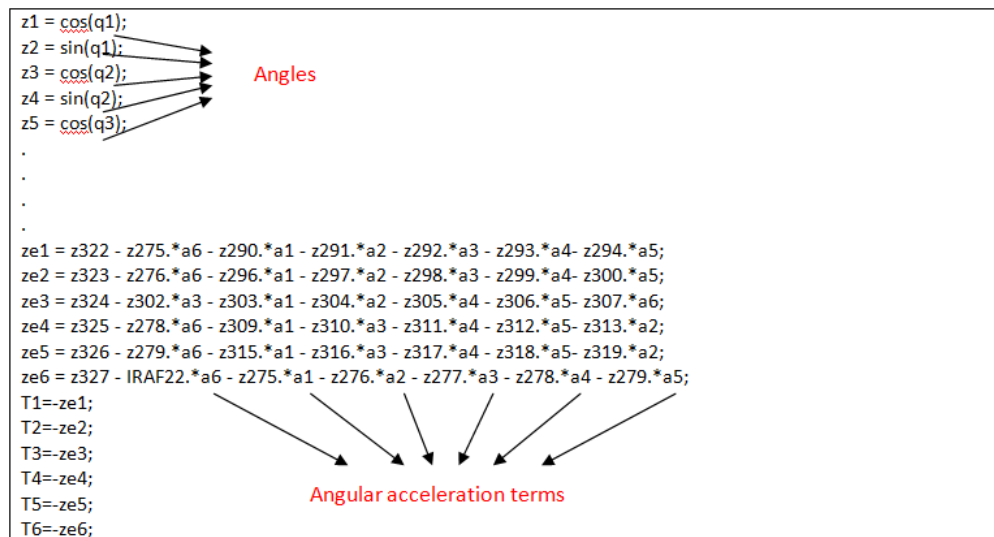


**Figure 4-3: Kane's equation of motion to calculate the joint torques**

As shown in the modified MATLAB™ code in Figure 4-3, for the system of forearm and arm which totally have 6 degrees of freedom, six dynamical equations are derived from Kane's method ( $ze1$  to  $ze6$ ). To calculate the torque of each degree of freedom, torque component associated with each equation is replaced by the variables ' $ze1$  to  $ze6$ ' and the equation is calculated based on the known values. Then, to make each equation equal to

zero, the torque value is considered to be equal to the negative value of the correspondent equation. In other words, these equations are directly related to the joint torques, hence this procedure allows computation of the six joint torque components ( $T1$  to  $T6$ ). In the symbolic code provided in Figure 4-3,  $a1$  to  $a6$  are the angular accelerations of the arm and forearm in the three directions and  $q1$  to  $q6$  are the angular change of the forearm and arm in the three directions. Complete procedure used in MATLAB™ to derive an expression for joint torques is presented in Appendix B.

In order to verify this method, a torque component in the coronal axis is applied to the elbow joint and the resultant angles and angular acceleration components are calculated using the proposed method. Then using the angles and angular acceleration values from the simulated response outlined in section 4.4, the estimated torque values are computed. As shown in Figure 4-4, it is clear that the estimated torque values closely match the actual torque applied and in terms of the magnitude and nature of the torque (e.g. impulse, sinusoidal ...) it can provide valuable information for the purpose of detection as well as quantification of the epileptic seizure.

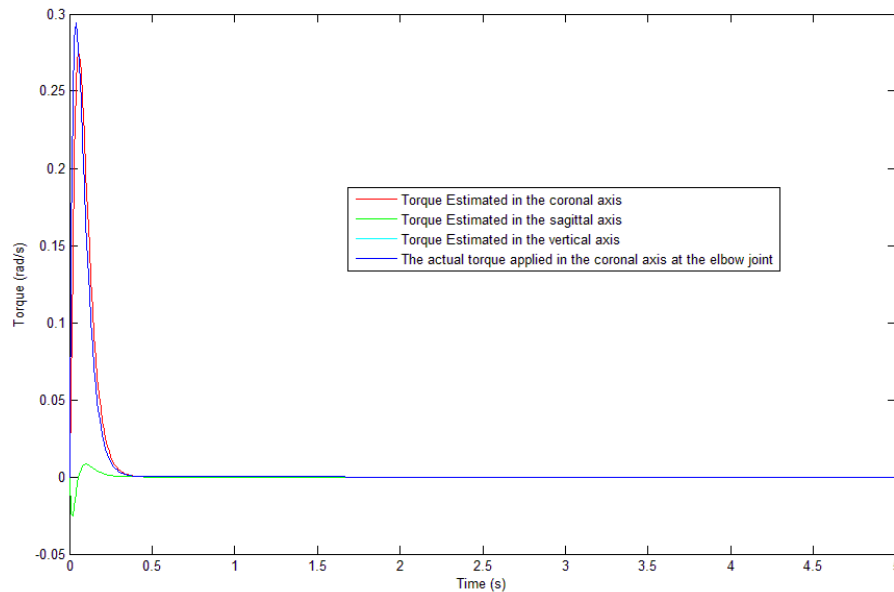


**Figure 4-4: The actual and estimated torques at the elbow**

Even though the method estimates a significantly low torque values in the sagittal and vertical axes, these components are both negligible compared to the actual torque which is estimated by the proposed method. This error originates from the fact that the applied torque along the coronal axis produces some vibration and oscillation at the elbow along other two axes and consequently results in an estimation of two torque components in vertical and sagittal axes directions.

Based on the results achieved in this section, it is concluded that the joint torque estimation procedure using the inertial sensor outputs can prove to be a useful tool for distinguishing an epileptic seizure from normal activities. A monitoring system based on the proposed detection algorithm can also be useful in notifying the relatives or the hospital staff when critical situations arise. However, detection algorithm needs further experimental validation which can be achieved by acquiring data from different types of epileptic seizure and quantifying them in terms of magnitude and frequency using the available methods. Then sets of normal activity should be studied so that the difference between voluntary and involuntary movements can be perceived.

## 4.2 Closure

The primary aim of this chapter is to propose a torque estimation method at the elbow and shoulder joints of the epileptic patient during the seizure episode by using inertial sensors and avoiding the integration of the raw data in order to reduce the error. This detection technique if further developed can be a threshold for the warning system as well as the trigger for an absorption device which can be designed to suppress the vibration of the body during epileptic seizure.

## Chapter 5

### 5 Motion Based Identification for Epilepsy

In chapter 4, an approach based on the torque estimation from the inertial sensor data was introduced for the purpose of detection and analysis of certain classes of epileptic seizures. Even though torque estimation based detection is a useful tool for this purpose, it can be greatly affected by the propagated error due to inexact placement of the sensors as well as joint angular change estimations. Further, the presented approach requires the placement of three sensors on the arm as well as forearm. This configuration may become difficult for some patients as the length of upper arm especially in female patients and children is not sufficiently long for the placement of three sensors. On the other hand, less number of sensors attached on the body seems to be more favorable considering the comfort level of the patient. Hence, development of alternate approach using less number of sensors and preferably one in the arm and one in the leg is attempted via experimentation. In this section, a method based on the nonlinear response is presented for analyzing the inertial measurement data. The proposed detection method presented in this chapter is primarily based on the system identification and hence expected to provide a more reliable algorithm for detection purposes.

#### 5.1 Inertial Sensory Detection System

For the present investigation, initially the Xsens™ MVN BIOMECH suit was considered. However, the Motion Node™ inertial unit developed by ‘GLI Interactive’ was found to have similar specs to those offered by Xsens for almost half the cost and hence the motion Node system was chosen for the present experimental analysis. The overall principle of the inertial system is shown in Figure 5-1. The Motion Node™ system consists of 5 inertial sensor packages with one Motion Node™ Bus. Each package is an inertial measurement unit and contains tri-axial gyroscopes, tri-axial accelerometers and tri-axial magnetometers (35×35×15 mm, 10 g). The sensors are attached on the body segments using AIRCAST™ Pneumatic Armband. The armband is of universal fit type and it guarantees minimal skin motion artifact. It also provides less restriction and its

breathable material enhances comfort and wearability which is highly important in the project to guarantee patient comfort. Straps can be also worn over normal clothing. The sensor modules are connected in a chain to the Motion Node™ Bus, meaning that only one cable leads to each segment. The Motion Node™ Bus synchronizes all sensor sampling, powers the sensors and makes the wireless communication with the stationary unit which can be either PC or laptop.

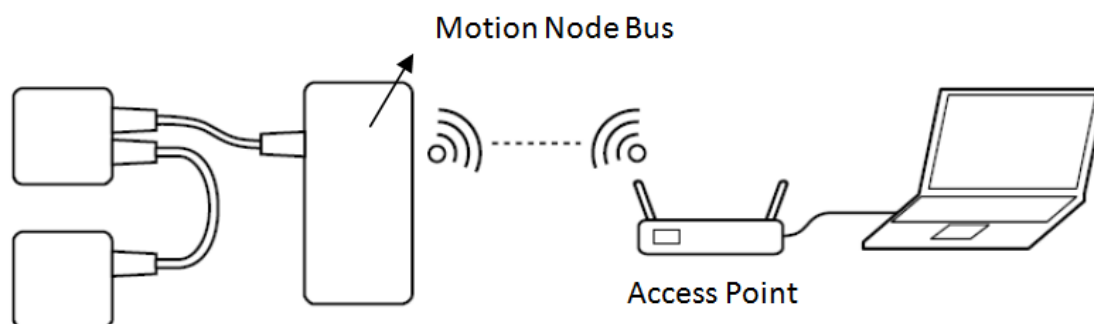


**Figure 5-1: Principle of seizure detection inertial sensory system**

The Motion Node™ system operates on a set of selections called the configuration. To record data from a Motion Node™ device it must first be a member of the current configuration set. The current configuration is displayed as the main table in the user interface provided along with the inertial sensor. Configuration consists of setting the range of acceleration ( $g$  level) as well as the date and time of the data recording and also calibration information. Unless the sensor parameters are manually changed, each Motion Node™ is set to sample at 100Hz with an accelerometer range of 2 g. After adding the configuration, one is ready to record data from the Motion Node™. The Motion Node™ Monitor is a utility application that detects device arrival and removal. The monitor can automatically configure and start reading from Motion Node™ devices as they are plugged in. After adding the unit sensors, called Nodes, to the configuration; the Motion Node™ system organizes a session of recorded data into an entity called a take. Each take consists of the take definition file, the associated configuration, and the binary data stream files from each configured Motion Node™.

The Motion Node™ software automatically calibrates the sensor-based ‘Take’ which is a recorded binary data stream. Using the procedure developed and coded in the software, the best calibration and as a result, the most accurate measurements are obtained by Motion Node™. The software also consists of the sensor fusion algorithms implemented on the sensor responses ensuring highly accurate output. The sensor fusion involves with correcting the information taken from an inertial sensor against other information taken from another inertial sensor. The calibration process only requires a couple of minutes. To view the data in real time rather than off line, one can use Motion Node™ Viewer which is a graphical application that displays all real time outputs of the Motion Node™ system. The viewer displays the orientation of the sensor as a three dimensional box and the sensor data as a set of rolling plots.

It may be noted that after recording sufficient data in the ‘Take’ file, the take should be stopped in order to save the data as the definition file. After this step, one may wish to export the data to an external program. The Motion Node™ system provides export to the standard common file formats such as FBX, COLLADA, BVH, and CSV which can be read and analyzed in programs such as MATLAB™, Lab View or Excel. By default, the exported file name is take stream.csv in the Motion Node™ data folder. The CSV stream format contains 25 fields which are included in Table 5-1.

**Table 5-1: Motion Node™ data output**

CSV Column No.	Output	Unit
1	Time	seconds
2	Gq [w, x, y, z], global quaternion	
3	Lq [w, x, y, z], local quaternion	
4	r [x, y, z], local Euler angle rotation	radians
5	l [x, y, z], global linear acceleration	specified in g
6	a [x, y, z], accelerometer measurement	specified in g
7	m [x, y, z], magnetometer measurement	μT
8	g [x, y, z], gyroscope measurement	degree/second
9	temp, temperature measurement	degrees Celsius

The Battery life for 5 sensors is approximately 7 hours which seems to be quite satisfactory for the purpose of patient monitoring even during night. The total weight of the system, including batteries, is approximately 1.9 kg. For evaluation and analysis, inertial sensory data are recorded from an epileptic patient who suffers from clonic seizures. The patient is monitored with the setup described in previous section, with five triaxial sensors placed on the left forearm and left leg. The sampling frequency of the inertial signals set to be 100 Hz. Then considering the video and EEG signals, the inertial sensor outputs are divided into four classes including:

- no movement,
- seizure waveform,
- normal movement,
- and unclear movements.

#### 5.1.1 Subjects and Attachment Locations

The experimental data presented in this section consists of two parts: normal activity data and epilepsy data. In order to characterize normal activity, an M.Sc. student was asked to perform normal movements such as rising from the chair, sitting, jumping, walking and finally rhythmic movement imitation. The recording was performed in the Dynamics and Sensing Systems laboratory, mechanical engineering department. The subject was asked to perform each activity for a period of approximately two minutes. In the case of the epileptic seizure, measurement was taken from a patient who predominantly suffered from clonic seizure. The recording for the patient took place at the University Hospital, London Health Science Center, Ontario. The overall recording took almost 3 hours from the time that the sensors were attached to the patient to the time of occurrence of a seizure episode.

The Motion Node™ sensory system has a very quick and easy set up which can be performed in less than 15 minutes by a non-technical person. As shown in Figure 5-2, five sensors on the left arm and leg of the patient as well as the student are attached. Three sensors on the forearm are placed according to the configuration proposed in chapter 3. The sensors on the leg are attached in the approximate location of the knee and



ankle joints. The battery was placed in one of the front pant pockets while the bus was placed in the back pocket of pant pocket of the subject.

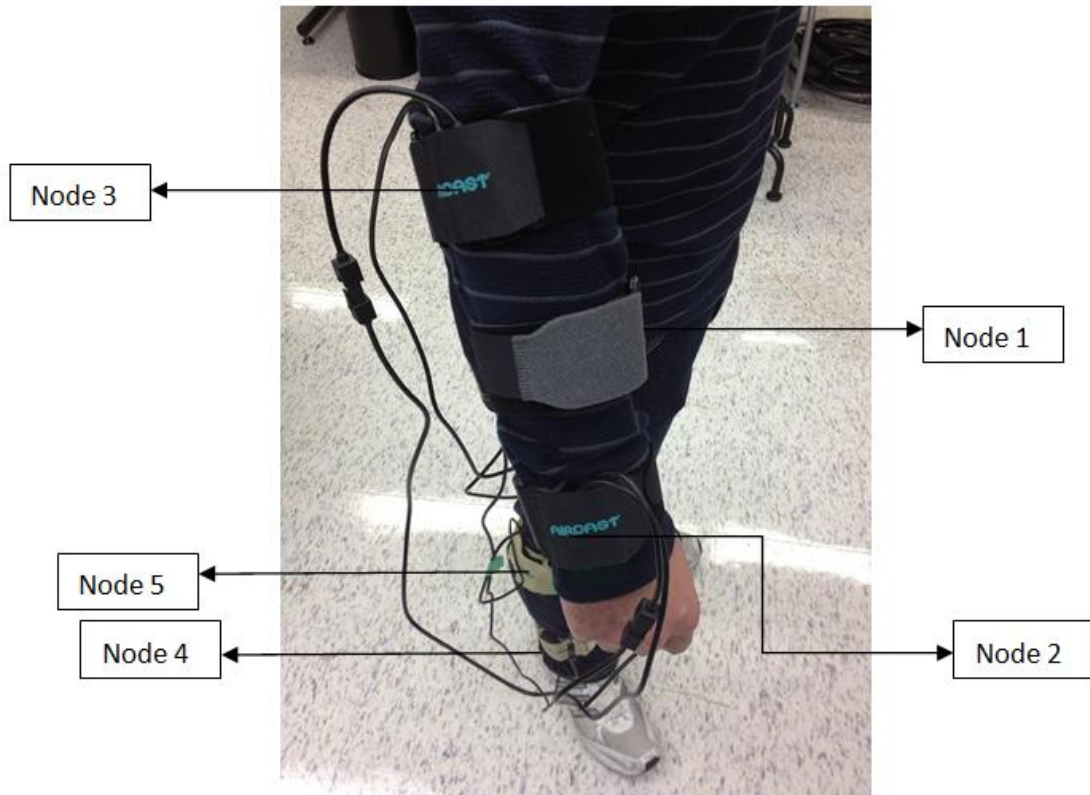


**Figure 5-2: Sensors attachment on the body**

### 5.1.2 Synchronized Inertial and EEG

In order to compare the inertial sensor outputs with the EEG signals associated with the epileptic patient movements, a monitoring study with both EEG and inertial sensors attached to a patient is performed at the epilepsy unit of the London Health Sciences center. The XLTEK™ EEG system manufactured by Natus Medical Inc. is employed for this purpose. In order to correlate the movements of the patient to the inertial sensor outputs, video recording is also carried out. The notebook with the Motion Node™ sensory system data acquisition interface was also located in the monitoring room close to the patient so that the physical movement of the patient and the EEG/Video can be observed and correlated with the inertial sensor system measurements. The time synchronization between the clock of the notebook and the prolonged Video-EEG system

clock was set manually and documented by the researcher. In the above monitoring process the EEG electrode attachment process took approximately 20 minutes to set up while the attachment of Motion Node™ sensory system took approximately 10 minutes to set up. In order to avoid any conflict with the proprietary XLTEK™ EEG data acquisition system, a standalone laptop was used for running the Motion Node™ inertial measurement data acquisition system. It should be noted that since the EEG measurement performed by proprietary XLTEK™ EEG data acquisition system has a closed architecture and does not permit transfer of data in any standard form, the EEG data is not presented in this section. However, during the inertial measurement data acquisition and especially at the time of epileptic seizure the EEG signal was monitored for any unusual activity by the researcher.

## 5.2 Inertial Measurement Results and Discussion

In this section, the inertial sensor outputs obtained during the experiments described in section 5.1 are presented for each Node. In all cases two sets of outputs have been available for the analysis: accelerometer and gyroscope outputs. For each inertial sensor, three measurement components in the three directions are available, and to avoid the analysis of large sets of data; the magnitude of each sensor is calculated and plotted against time. For the seizure plot, it was decided that the first 50 seconds give useful information. This time range is also used for other activities for the purpose of data analysis and comparison.

Five types of normal activities are investigated in this study:

- rising from a chair and sitting back six times,
- sitting on the chair with no other movement,
- walking around a loop of almost 80 m at a moderate speed,
- initially sitting and then standing and jumping six times which is simply referred to as jumping motion,
- rhythmic movement which involves the tremor-like movement in the forearm while sitting in the chair.

These five normal activities have been chosen for the purpose of obtaining an evaluation of the largest acceleration and angular velocity which the body can reach. These maximum values are considered valuable for the purpose of normalization of the plotted

data and for motion classifications. It is also important to note that since each Motion Node™ sensory unit has 15 outputs and also for the sake of simplicity, only the magnitude of the accelerometers and gyroscopes are considered for getting an initial insight into the relative magnitudes of motion for activities considered in the present study. It may be noted that this process was justified by observing the component signals in the time as well as in the frequency domain to ensure that important spectral as well as time-peak characterization are presented. X, Y, and Z directions of the sensor unit are defined as shown in Figure 5-3. Figure 5-4 and Figure 5-5, respectively, show time-scale representation of accelerometer and gyroscope signal patterns observed during typical epileptic seizure together with the correspondent magnitudes. It may be noted that as shown in Figure 5-4, the component of the earth's gravity is not removed from the accelerometer results and as a result the equilibrium state in all of the plots is found to be in the neighborhood of 1g.

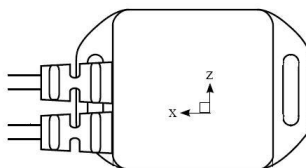


**Figure 5-3: X, Y, and Z definition for each Motion Node™ sensor [1]**

It must also be noted that since analysis considering all of the inertial measurement components may become cumbersome, the magnitude of the inertial sensors are considered for the purpose of data analysis. The magnitude of the gyroscope outputs are, in particular, used for Poincaré map, Pseudo-Phase-Space and Lyapunov exponent calculation in the following sections. However, one must exercise caution as magnitude vector may cause lose of some frequency content, FFT analysis is performed on the filtered data of the individual components, to see if any useful information can be obtained from the acceleration and angular rate spectrum.

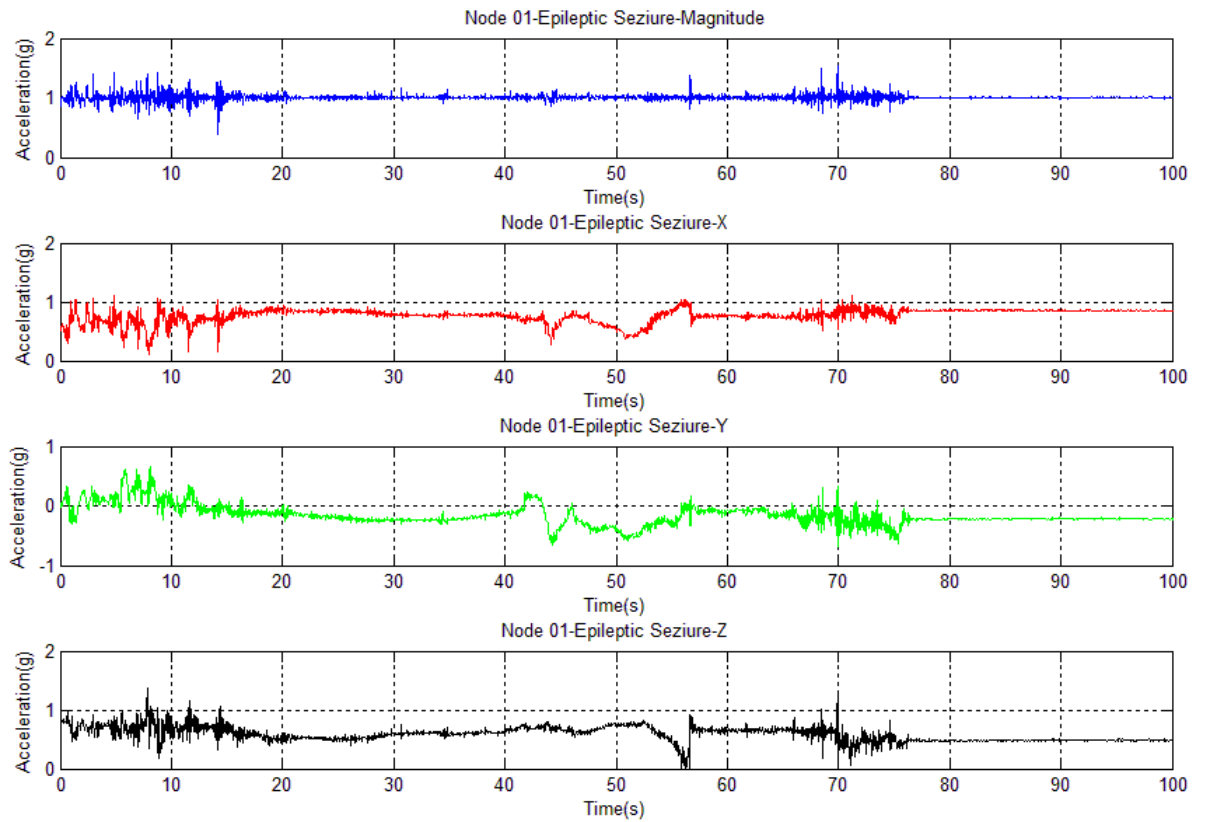


**Figure 5-4: Magnitude of the acceleration and components in X, Y, and Z directions for the sensor unit placed on the forearm for seizure measurement**

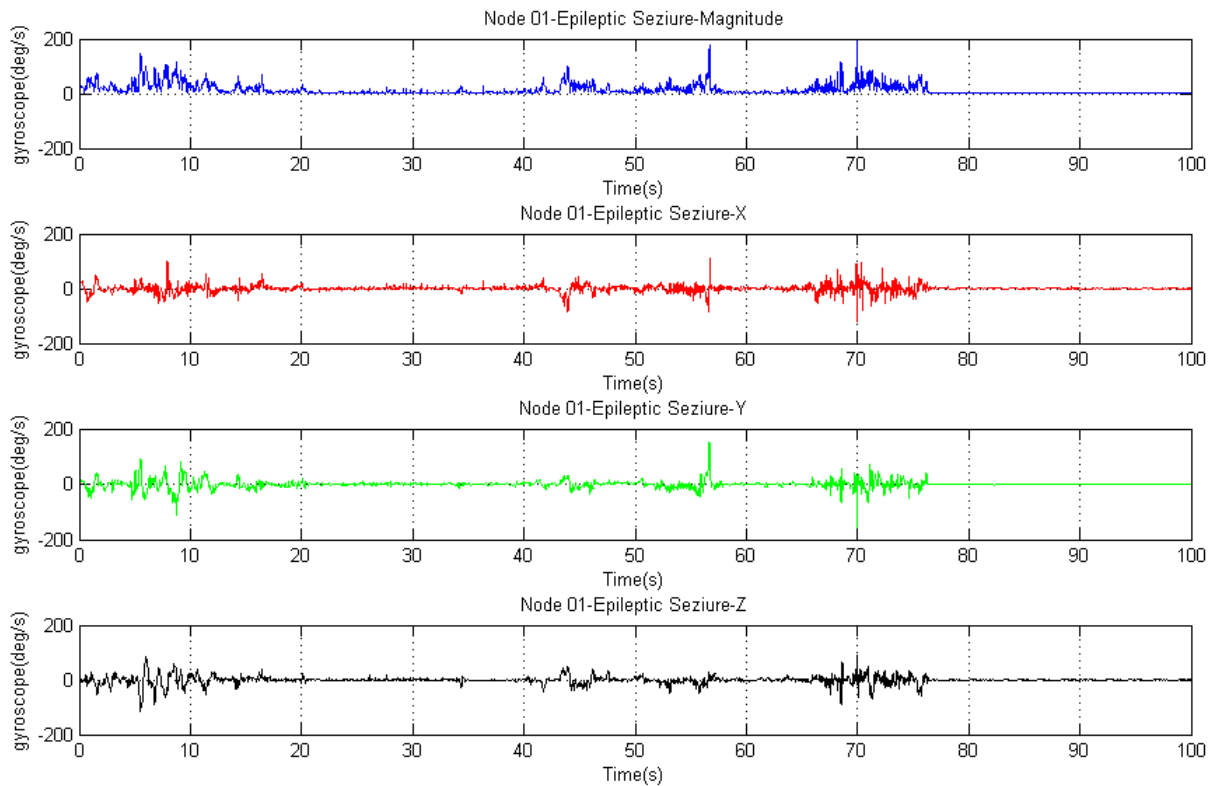


**Figure 5-5: Magnitude of the angular rate and components in X, Y, and Z directions for the sensor unit placed on the forearm for seizure measurement**

Only two sets of sensor outputs for different activities are presented since the output of sensors on the forearm as well as the sensors placed on the leg have been found to be similar. Reader is referred to appendix C for complete sets of plots obtained for other sensors. For the purpose of obtaining the plots of the responses, a time range of 50 seconds is considered for all of the sensors. These plots are then compared on the basis of magnitude as well as the frequency response.

### 5.2.1 Node 01 on the Forearm

In this section, the acceleration and gyroscope output of the sensor placed on the middle of the forearm are presented and a preliminary discussion on the magnitude and frequency of each activity is given. For each activity, the magnitude values are plotted against time. As mentioned earlier in chapter 2, some types of epileptic seizure reveal

themselves as abrupt movements of different parts of body with a dominant movement in the arm. For the purpose of studying the arm movement during seizure and other normal activities which may not necessarily have dominant motion of the arm, such as standing or walking, the plots of arm movement is presented.

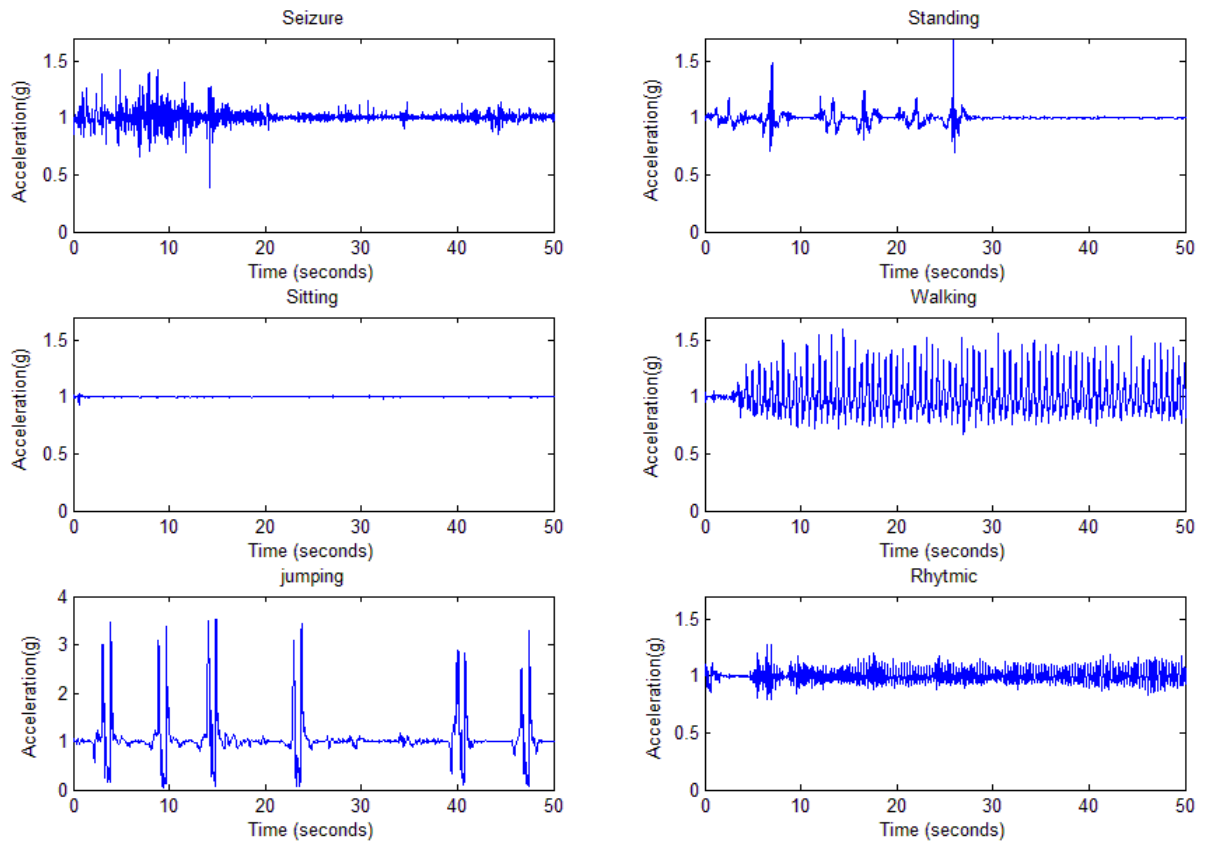


**Figure 5-6: Acceleration magnitude of the Node 1 attached to the forearm**

According to Figure 5-6 and Figure 5-7, arm movement during seizure can be expressed as a high frequency, abrupt motion. In terms of magnitude, seizure activity can be classified as a medium activity. Based on the signal levels falling in a certain range, medium range normal activities such as standing and walking can be recognized. Sitting is classified as the no-movement activity and the jumping motion is classified as the high movement activity. Rhythmic motion, however, is similar to the seizure in terms of the frequency. It is also important to note that, using the accelerometer and gyroscope together can strengthen the detection technique, for instance considering the standing

motion, accelerometer output may not be distinguished from the accelerometer output associated with seizure, however, the gyroscope outputs are clearly identified in terms of frequency. For normal movements that are more rhythmical and contain sharper peaks, it was observed that high acceleration values up to 1.5g are recorded and observed from the plot. Further, these observations suggest that sharp peaks due to normal movement such as jumping differ from peaks induced by Tonic seizures, i.e. they possess a pulse-like broader frequency pattern.

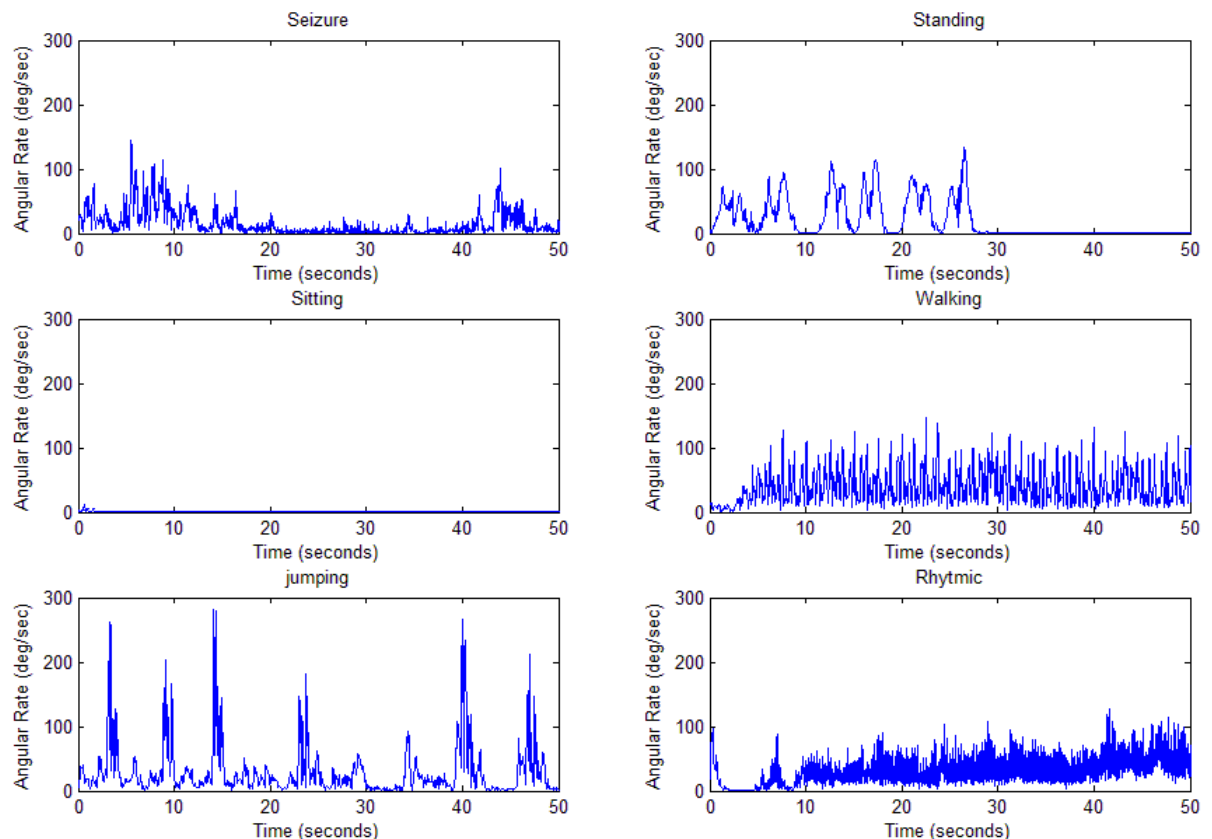


**Figure 5-7: Gyroscope magnitude of the Node 1 attached to the forearm**

### 5.2.2 Node 05 on the Leg

The acceleration and gyroscope output of the sensor placed on the leg can be useful to distinguish normal activities such as walking, jumping, standing from involuntary movement such as seizure. This is especially important in the cases that epileptic seizure causes abrupt and sudden fall from bed. Considering the fact that placing a sensor on the

leg can add another useful piece of information for life-threatening situation in general and seizure detection in particular, output of Node 05 which is placed on the leg is presented here and a preliminary discussion on the magnitude and frequency of each activity is given. For each activity, the absolute value is plotted as mentioned earlier in this chapter.

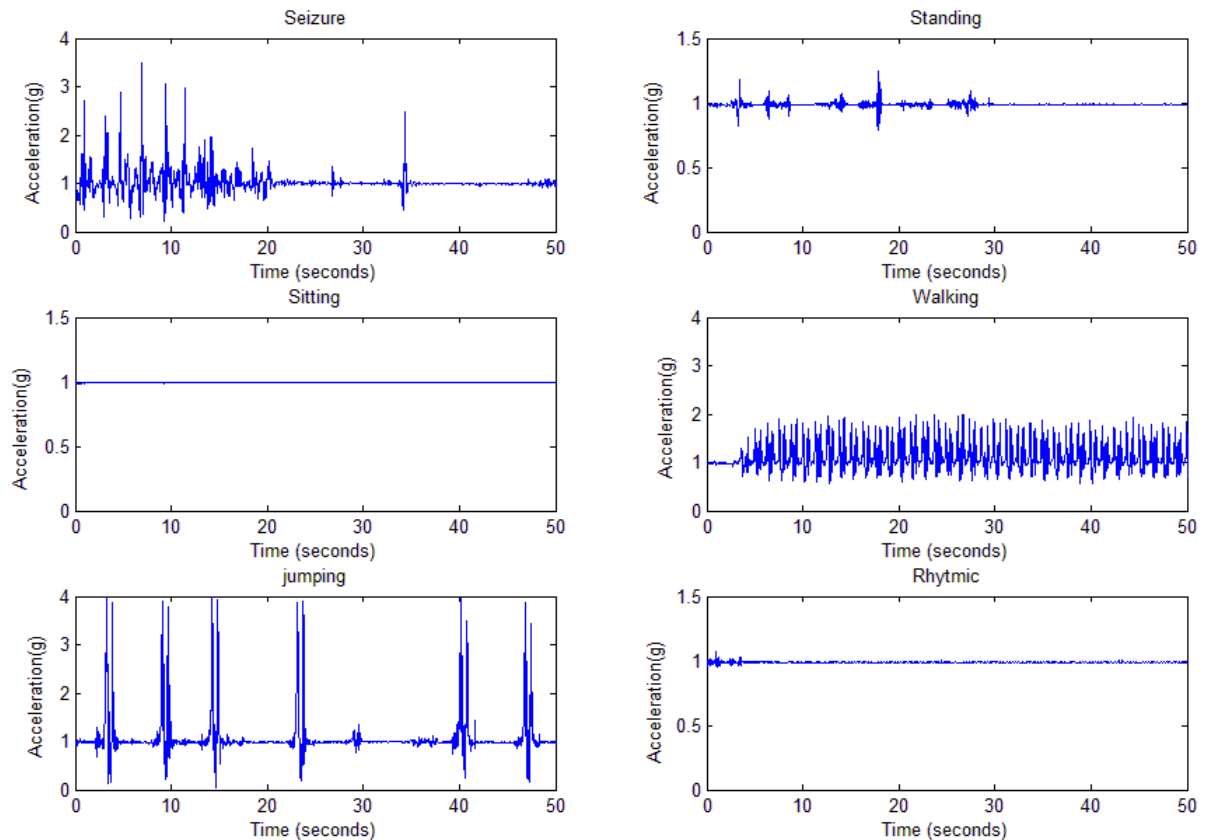


**Figure 5-8: Acceleration magnitude of the Node 5 attached to the leg**

According to Figure 5-8 and Figure 5-9, leg movement during seizure can be expressed as a high frequency, abrupt motion. In terms of magnitude, seizure activity in the leg can be classified as a high activity. High activities are activities in which the magnitude is larger than a certain range. According to the experimental results, such activities include jumping and seizure. Sitting and rhythmic movements are classified as the no-movement activity whereas walking and sit-rising motions are classified as the medium activity movements. It is important to note that, using the accelerometer and gyroscope together



can strengthen the detection technique. For instance considering the sit-rising motion, gyroscopic output may not be clearly distinguished from that associated with seizure but the accelerometer outputs are able to clearly identify in terms of frequency and magnitude. For normal movements that are more rhythmical and contain sharper peaks, it was observed that high acceleration values up to 2g in the leg occur as seen from plots. Further, these observations suggest that sharp peaks due to normal movement such as jumping differ from peaks induced by Tonic seizures, i.e. they possess a pulse-like broader frequency pattern.

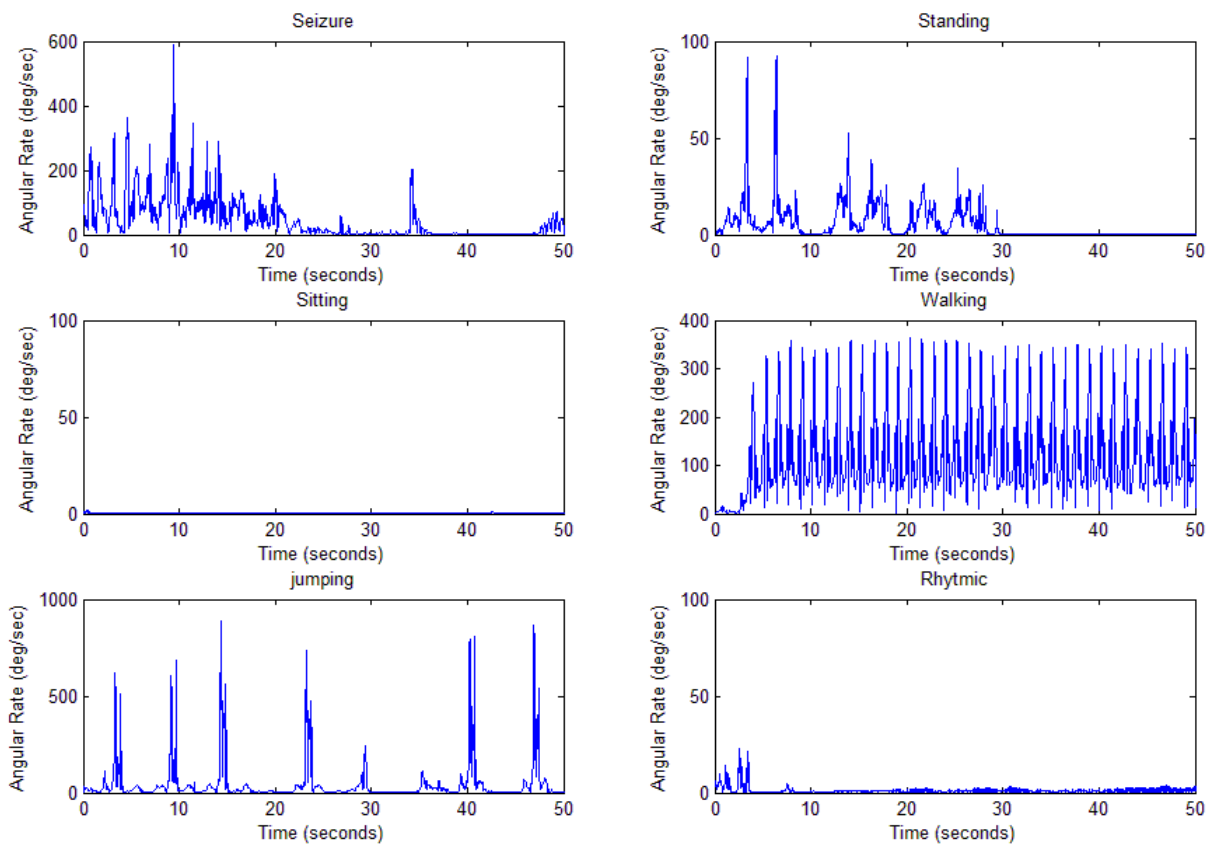


**Figure 5-9: Gyroscope magnitude of the Node 5 attached to the leg**

### 5.3 Data Analysis

The analysis of potentially nonlinear behavior in biomechanics and biomedical fields for the purpose of system identification has attracted great interest in recent years [84]. Although no universally accepted mathematical definition of the terms such as decaying

response or growing response especially in spectrums that exhibit chaotic behavior. This non-periodic behavior is normally defined as aperiodic long-term behavior in a deterministic system that exhibits sensitive dependence on initial conditions [85]. Aperiodic long-term behavior means that trajectories do not converge to a fixed point, but instead exhibit irregular unpredictable behavior. When referring to a system as “Deterministic”, it is understood that this unpredictable, aperiodic behavior derives from the inherent nonlinearities in the system itself and are not caused by noise or other stochastic sources in the system. Lyapunov exponents provide a direct measure of separation of the trajectories that start arbitrarily near each other by quantifying the exponential rates at which neighboring orbits on an attractor diverge (or converge) as the system evolves in time. An  $n$ -dimensional system which is defined by  $n$  first-order differential equations of motion, will have  $n$  Lyapunov exponents, each representing the rate of growth or decay of small perturbations along each of the principal axes in that system’s state space. These exponents are typically ordered from largest to smallest for analysis purposes. The magnitude of the largest Lyapunov exponent specifies the maximum average exponential rate of divergence of trajectories on an attractor and thus the maximum amount of instability along any direction. Therefore, largest Lyapunov exponent is often also used as a measure of the local instability of a given system.

When one observes apparently aperiodic and unpredictable behavior from biological system experimental measurements, it is of great interest to determine if that aperiodicity is simply because of some source of noise or uncertainty in the system or the measuring apparatus, or is indeed because of some underlying non-linear deterministic process.

### 5.3.1 Fast Fourier Transform Analysis of the Data

Frequency response analysis of the data can be useful in order to determine the dominant frequency in typical periodic activities. For the detection system, it is considered advantageous if the dominant frequency of the incident to be detected is different from other activities. In order to study the frequency response of the measurements, Fast Fourier Transform (FFT) analysis is performed in this section. As observed from typical output signals, a DC offset is always found to be present. In order to remove this offset, the data is passed through a high pass filter prior to performing the FFT analysis. Filter

design as well as the FFT analysis are both performed employing the MATLAB™ Signal Processing Toolbox. In order to design the filter, considering the fact that the sampling frequency is 100 Hz, a digital high pass Butterworth filter with the cutoff frequency of 1 Hz and the order of 20 has been selected. In addition, to ensure that the high pass filter does not affect the useful range of spectrum (ie. 1 – 50 Hz), the raw data spectrum as well as filtered result is compared and shown in Figure 5-10 and Figure 5-11.

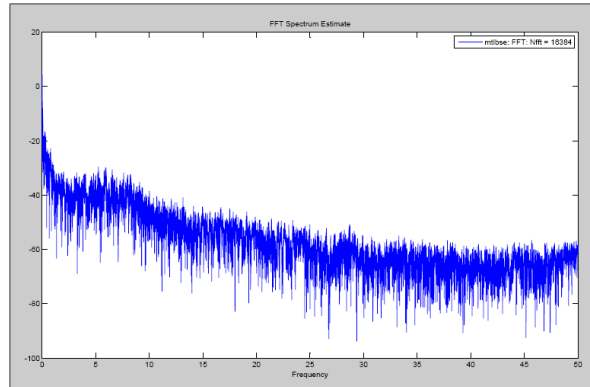


**Figure 5-10: FFT spectrum of Node 01 (accelerometer output in the y-direction) on the forearm for seizure without high pass filter**

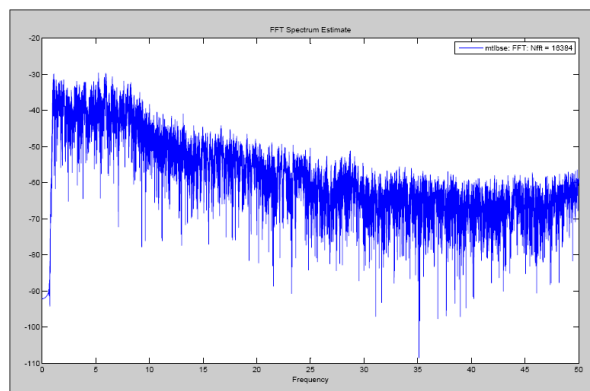


**Figure 5-11: FFT spectrum of Node 01 (accelerometer output in the y-direction) on the forearm for seizure with high pass filter**

In order to calculate and compare the dominant frequency for the normal periodic activity such as rhythmic movement of the wrist in the vertical axis with the epileptic seizure, accelerometer's z-component FFT analysis of Node 1 attached to the arm is performed as shown in Figure 5-12. It may be noted from this figure that no clear dominant frequency is evident for detecting seizure. There are, however, appears to be some peaks present in the initial frequency range (less than 10 Hz). Two peaks are especially highlighted in the figure. The area between these frequencies corresponds to the DC offset, as previously described. It is decided that the seizure movement is highly nonlinear, composed of multiple signals with different frequencies, hence it is not possible to assign a unique dominant frequency value to this activity and alternate approaches must be employed to extract useful information that pertains to seizure activity.

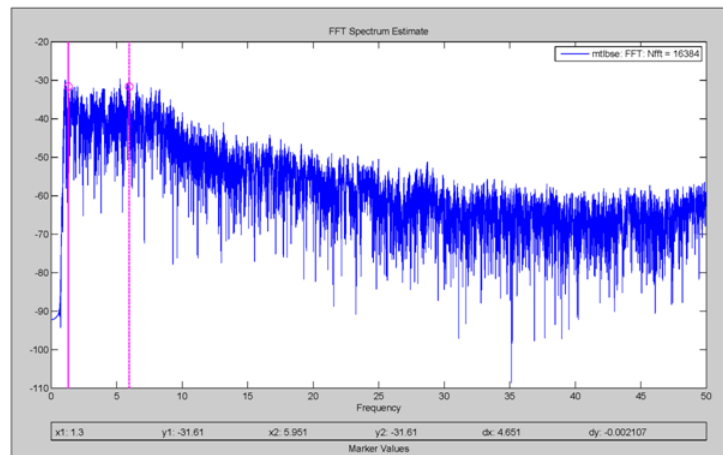


**Figure 5-12: FFT spectrum of Node 01 (accelerometer output in the z-direction) on the forearm for seizure**

In order to investigate the possible differences in the frequency response of the accelerometer and gyroscope, the FFT analysis is also performed for the Node 01's y-direction gyroscope output, as shown in Figure 5-13. It is clear that both the accelerometer and gyroscope sensors depict similar frequency response behavior and hence only one set of the sensors can be considered for the FFT analysis.

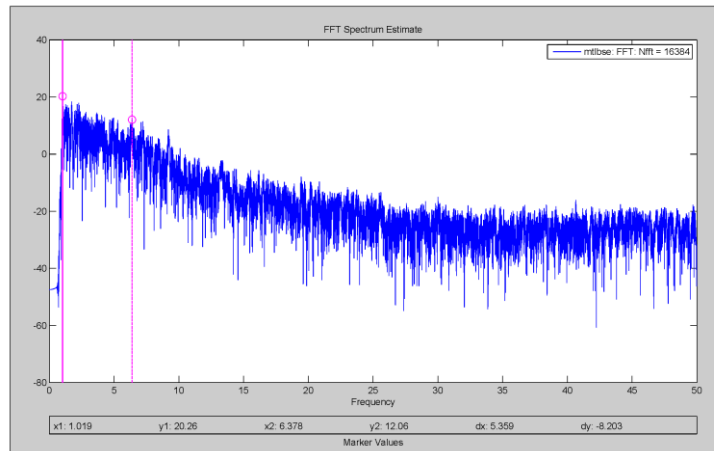


**Figure 5-13: FFT spectrum of Node 01 (gyroscope output in the y-direction) on the forearm for seizure**

For the rhythmic movement of the wrist and arm, however, a clear dominant frequency of about 3 Hz is recognized in Figure 5-14. The result of Figure 5-14 confirms the applicability of the FFT analysis of inertial measurements, as initially the subject undergoing seizure was asked to perform the rhythmic movement with an approximate frequency of 3 Hz or 3 cycles per second. This confirms that usefulness of this class of sensors for picking up rhythmic activity around 3 Hz which happens to be in the range when typical clonic seizures take place. It should be noted that the FFT analysis of the gyroscope output as shown in Figure 5-15, also confirms the dominant frequency recognized in the FFT plot of the accelerometer output.

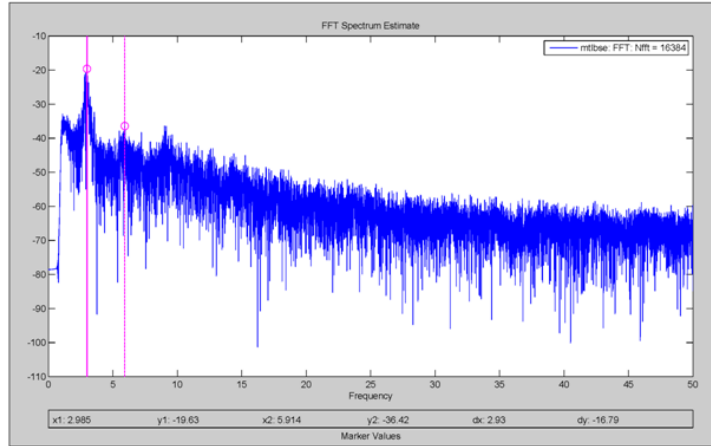


**Figure 5-14: FFT spectrum of Node 01 (accelerometer output in the z-direction) on the forearm for rhythmic motion**

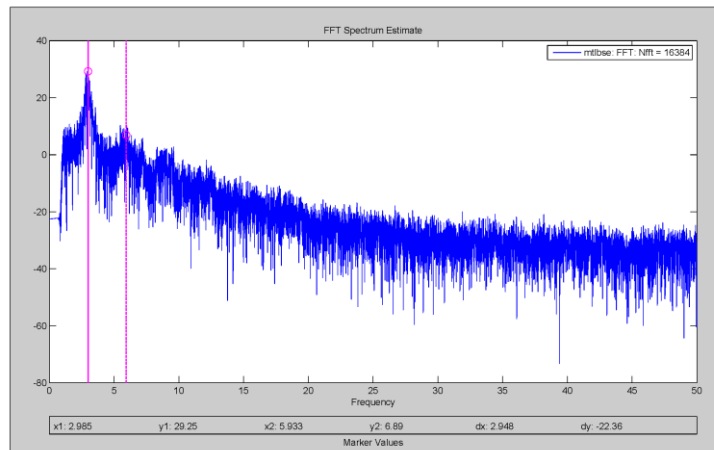


**Figure 5-15: FFT spectrum of Node 01 (gyroscope output in the y-direction in the z-direction) on the forearm for rhythmic motion**

In order to compare the dominant frequency for the normal periodic activity such as walking with the epileptic seizure, the FFT analysis of the sensor Node attached to the leg (Node 5) is carried out. As shown in Figure 5-16, there is no clear dominant frequency for the seizure. There are, however, some peaks in the initial frequency range (less than 5 Hz). These peak values may be attributed to the left-over signals that contribute towards the DC offset, as previously described. It is decided that the seizure movement is highly

nonlinear, composed of multiple signals with different frequencies, hence assigning a unique dominant frequency value to this activity becomes impossible. For the walking activity, however, dominant frequencies of about 3 Hz are evident based on Figure 5-17 and hence confirming the usefulness of the inertial measurements.

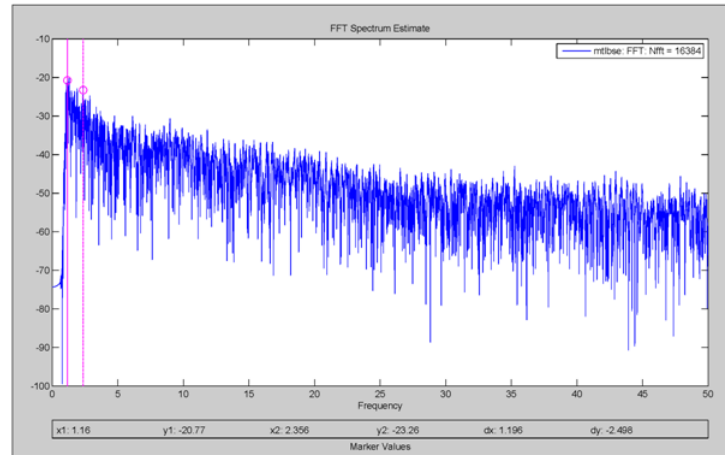


**Figure 5-16: FFT spectrum of Node 05 (accelerometer output in the z-direction) on the leg for seizure**

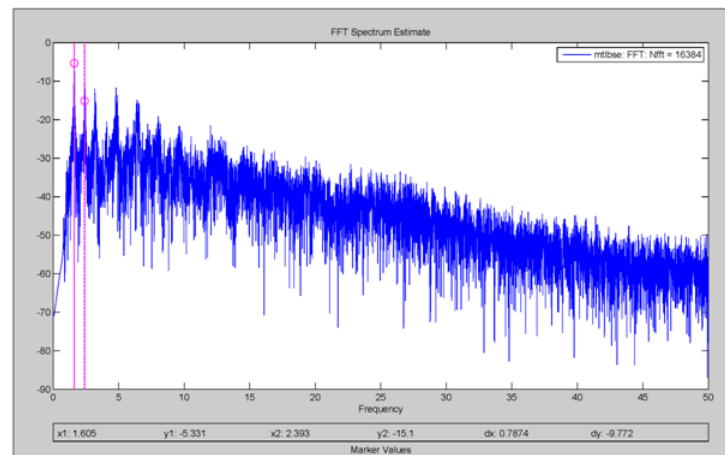


**Figure 5-17: FFT spectrum of Node 05 (accelerometer output in the z-direction) on the leg for walking**

According to the spectrum plots presented in this section, it is concluded that the FFT analysis can only at best provide sufficient information for regular highly rhythmic motion, but found to be unsuccessful in distinguishing seizure and normal activities. In

order to address these shortcomings, it was decided to try some approaches that are employed for nonlinear response analysis. In particular, methods of Lyapunov exponent and Poincaré maps have been considered in the present research.

### 5.3.2 Pseudo-Phase-Space Method

A useful technique which has been used when only one variable is measured is the time-delayed pseudo phase-plane method. The pseudo phase space method, also called the embedding space method, is a plot of signal vs. the signal from the same source, but shifted in time by an increasing time  $T$ . It is argued that the pseudo-phase space method reveals the relationship between  $X$ ,  $\dot{X}$  and  $\ddot{X}$ . The visualization of the experimental data in pseudo-phase space gives some qualitative information about the physical motion in the system. Figure 5-18 and Figure 5-19 show the projection of the gyroscopic components in pseudo-phase space domain for different motions.

Some guidelines need to be followed when plotting the pseudo phase-space map:

- Number of data points: The number of data points is an important parameter which has been subject of debate. A sufficient number of points are needed to ensure accuracy. A number of authors have shown that 4000 to 10,000 points are generally sufficient. In the present study, 5000 points are used to obtain the Pseudo-Phase-Space plots.
- Delay time. Various rules are given in the literature regarding the choice of the delay time. Van den Bleek and Schouten [113] chose the time delay as simply the time interval between successive points in the time series. When selecting a time delay, the goal is to find a delay large enough so that the resulting individual coordinates are relatively independent, but not too large that they are completely independent statistically; in our case, the time delay is chosen to be 0.04 seconds.

By following the above mentioned guidelines, the Pseudo-Phase-Space plots for the  $z$ -direction component of the acceleration output for Nodes 1 and 5 are developed as shown in Figure 5-18 and Figure 5-19, respectively.



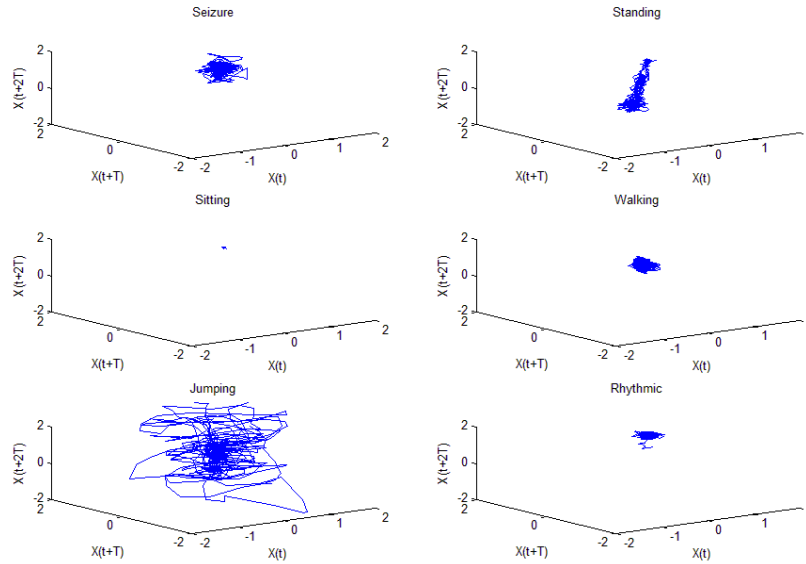


**Figure 5-18: Pseudo-Phase-Space method for Node01 (accelerometer output in the z-direction) on the forearm**

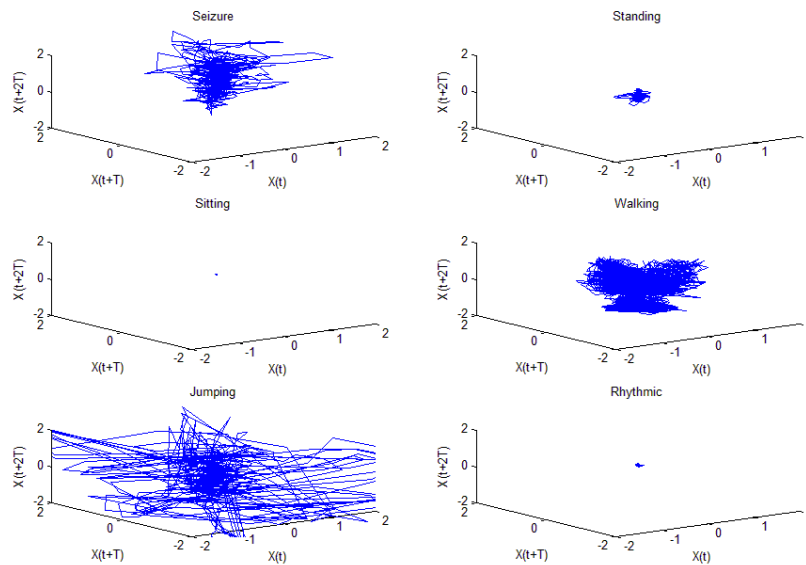


**Figure 5-19: Pseudo-Phase-Space method for Node05 (accelerometer output in the z-direction) on the leg**

As illustrated in Figure 5-18 and Figure 5-19, except for the relative magnitudes there is no more information that can be extracted from the Pseudo-Phase-Space method. As expected, plots show a wide range, chaotic like curves for high activity movements such as jumping whereas for a low activity (i.e. sitting) it shows almost a dot meaning highly centered sets of curves.

### 5.3.3 Lyapunov Exponent

Lyapunov exponent calculations have been applied to a wide range of biological and biomedical phenomena. Researchers have used Lyapunov exponents to analyze mathematical models of individual neurons and neural networks [88], examine experimental molecular and cellular dynamics including gas transport through blood cells [89], study the dynamics of blood flow [90], investigate human hand writing [91] and understand the control of oscillatory limb movements [92].

One of the biggest areas of focus has been in understanding heart rate variability and analyzing functional brain activity through ECG and EEG, respectively [93]. An extensive recent review by Stam [94] summarizes the findings of nonlinear analyses of these signals in healthy subjects during a wide variety of cognitive states and in a wide range of patients with various pathologies, ranging from seizures to degenerative diseases like Alzheimer's or Parkinson's disease and even to psychiatric disorders. Although the evidence seems to point toward a view of brain activity as being far more complex and less stationary than can be reasonably modeled by any low-dimensional deterministic model such as a chaotic model, both reviews remain optimistic about the future applications of nonlinear analyses in understanding brain function. Particularly, Stam [94] suggests that the most promising potential clinical applications appear to be in identifying and predicting epileptic seizures and sleep disorders.

As a result of the inherent computational difficulties in estimating the full Lyapunov spectrum and because estimating the maximum Lyapunov exponent is often of greatest interest in diagnosing the growing or decaying response of a nonlinear system, many algorithms have been proposed to compute just the maximum Lyapunov exponent. Perhaps the most well-known of these algorithms is from Wolf et al [95]. This algorithm

monitors the long-term evolution of a single pair of initially nearby orbits. Given some initial point in state space and its nearest neighbor, the initial Euclidean distance between the two points is denoted. After some appropriately short time interval, the initial length will have evolved to length. When this length becomes too large, a new nearest neighbor point to the original reference trajectory is selected that minimizes both the replacement length and the orientation change between the reference and neighboring points. This procedure is repeated until the original reference trajectory has traversed the entire dataset. If  $d_o$  is a measure of the initial distance between the two starting points, and  $d$  is a measure of the distance at a small but later time; the maximum Lyapunov exponent is estimated from:

$$\lambda = \frac{1}{t_N - t_0} \sum_{k=1}^N \log_2 \left[ \frac{d(t_k)}{d_o(t_{k-1})} \right], \quad \mathbf{5-1}$$

where  $N$  is the number of replacement steps. In calculation of Lyapunov exponent, the choice of the finite evolution time and  $N$  has a great influence on the answer. As the number of replacement steps allowed will depend on the number of samples in the original dataset,  $N$ , this will also significantly affect the outcome.

The top Lyapunov exponent predicted via Eq. 5-1 can indicate whether the system undergoes growing or decaying type of nonlinear response. It is known that negative sets of values for the exponent, i.e.  $\lambda < 0$  implies stable, dissipative behavior. Also, the positive set of values, i.e.  $\lambda > 0$  implies that the system undergoes predominately an exponentially growing magnitude and the system is typically unstable or chaotic.

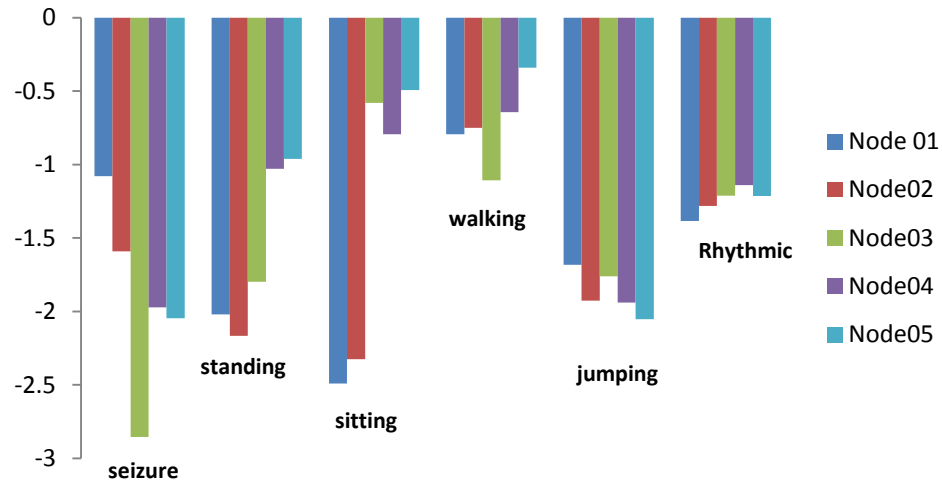


**Figure 5-20: Lyapunov exponent for different activities**

Even though it was originally envisaged that normal activities such as walking, standing, and jumping should reveal non-periodic behavior but according to the Lyapunov exponent calculated in the previous section these activities as well as seizure movement fall in periodic stable category. As mentioned earlier, when the Lyapunov exponent computed properly, positive values provide a definitive diagnosis of non-periodic/chaotic dynamics. However, Lyapunov exponents are also difficult to estimate reliably from experimental data because of the existence of noise. When using Lyapunov exponent as an indicator of the chaotic behavior of a system, one should always be very skeptical about accepting or rejecting any claims of ‘periodicity of a system’ only based on the Lyapunov exponent, regardless of the algorithm used. Such claims should always be backed up by significant additional evidence and algorithms. In general then, although this algorithm has been very popular because it is relatively easy to implement, it is also shown to be very sensitive to noise and rather unreliable for short or non-stationary time series.

### 5.3.4 Poincaré Map

Nonlinear analysis of the time series data is a newly presented approach for the study of complex systems. According to nonlinear systems theory, the degree of non-periodicity/chaos can be presented both graphically and numerically (i.e. Lyapunov

exponent). When studying highly complex systems, an established graphical procedure to reduce the system's multidimensional continuous trajectory in state space to a discontinuous low dimensional projection known as Poincaré map can be useful. Poincaré maps that are generally extracted from experimental data are found to be useful for analyzing the dynamic systems by showing periodicity and are obtained by representing pairs of consecutive time series differences in the coordinate or by plotting one quantity against the differentiation of that quantity. These Poincaré maps can sometimes be used to distinguish between various qualitative states of motion such as periodic, quasi periodic, or chaotic. Finally, if the Poincaré map does not consist of either a finite set of points or a closed orbit, the motion may be chaotic. Poincaré technique is commonly applied in the field of cardiology and more recently, the technique is used for the indication of the sudden cardiac death risks [86].

In the present research, a novel seizure detection method based on Poincaré chaos is proposed. The Poincaré chaos can detect the time seizure onset, and the artificial intelligent reasoning can decide the end of seizure. As the Poincaré maps for the sensors on the forearm as well as the sensors placed on the leg are similar, only two sets of sensor outputs for different activities are presented as shown in Figure 5-21 and Figure 5-22. In these figures the y-direction component of the gyroscope output vs. correspondent angle in the same direction are plotted. Reader is referred to appendix C for the complete sets of plots obtained for other sensors.

As shown in Figure 5-21 and Figure 5-22, epileptic seizure is depicted as scattered, wide range of points in both arm and leg Poincaré maps. Standing and sitting activities can be easily detected in terms of the magnitude and the distribution of points. Walking motion is shown to represent major concentrated areas separated from each other. It is also shown that the rate of change in the angular rate is more than the rate of change in angle for walking activity, whereas for seizure, standing, and jumping activities the rate of change in the angle is more than the rate of change in angular velocity. For the rhythmic motion of the arm, the plot shows a more centralized, circular pattern which can be used for distinguishing this activity from the seizure. These findings lead to consideration of an approach which is based on the moment of inertia and radius of gyration measures.

This proposed approach relies on emphasizing spread of the data points that represent larger magnitudes compared to those of lower magnitudes. In order to implement this idea, the second moment of inertia in the x and y directions of Poincaré plots as well as the radius of gyration associated with the XY plane are calculated. These values can be used for extracting the degree of centralization and the propagation of the points.

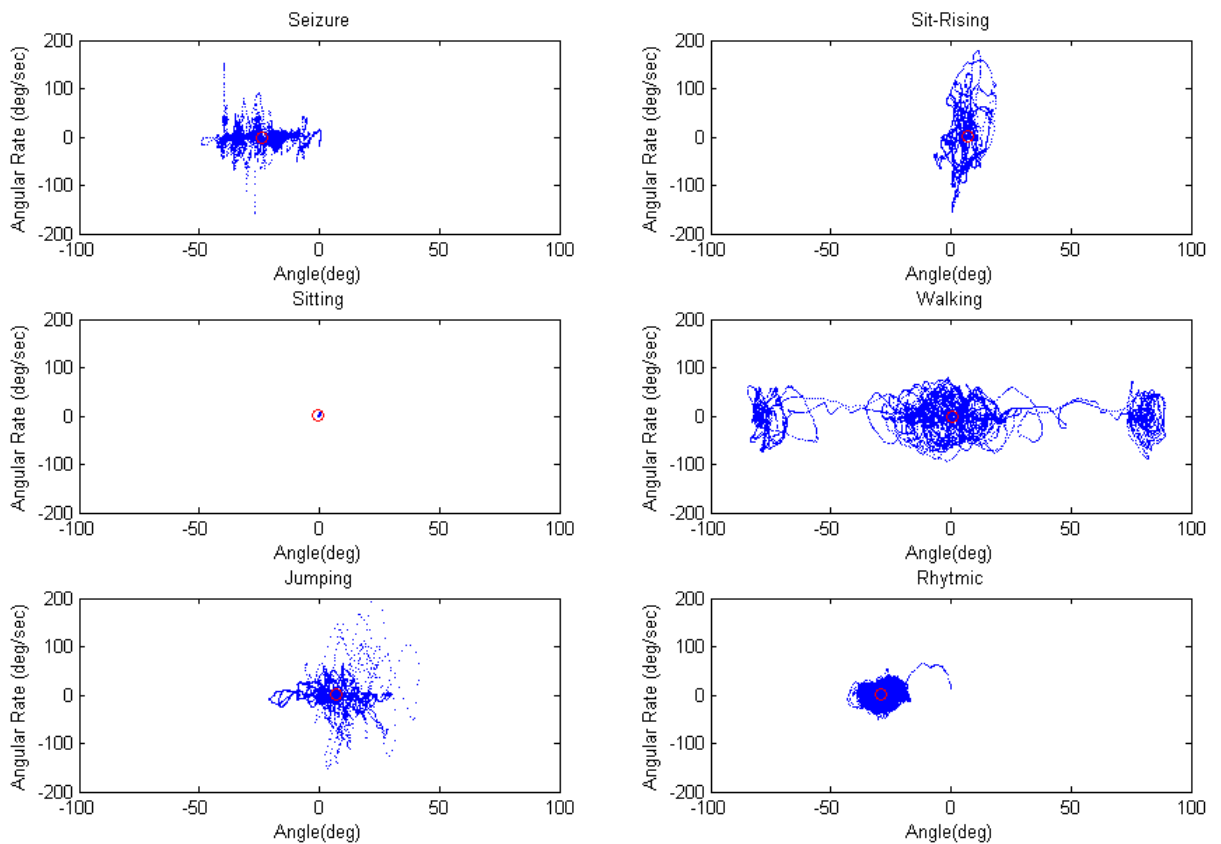


**Figure 5-21: Poincaré map for the Node 01 on the arm  
(angular rate vs. angle in the y-direction)**

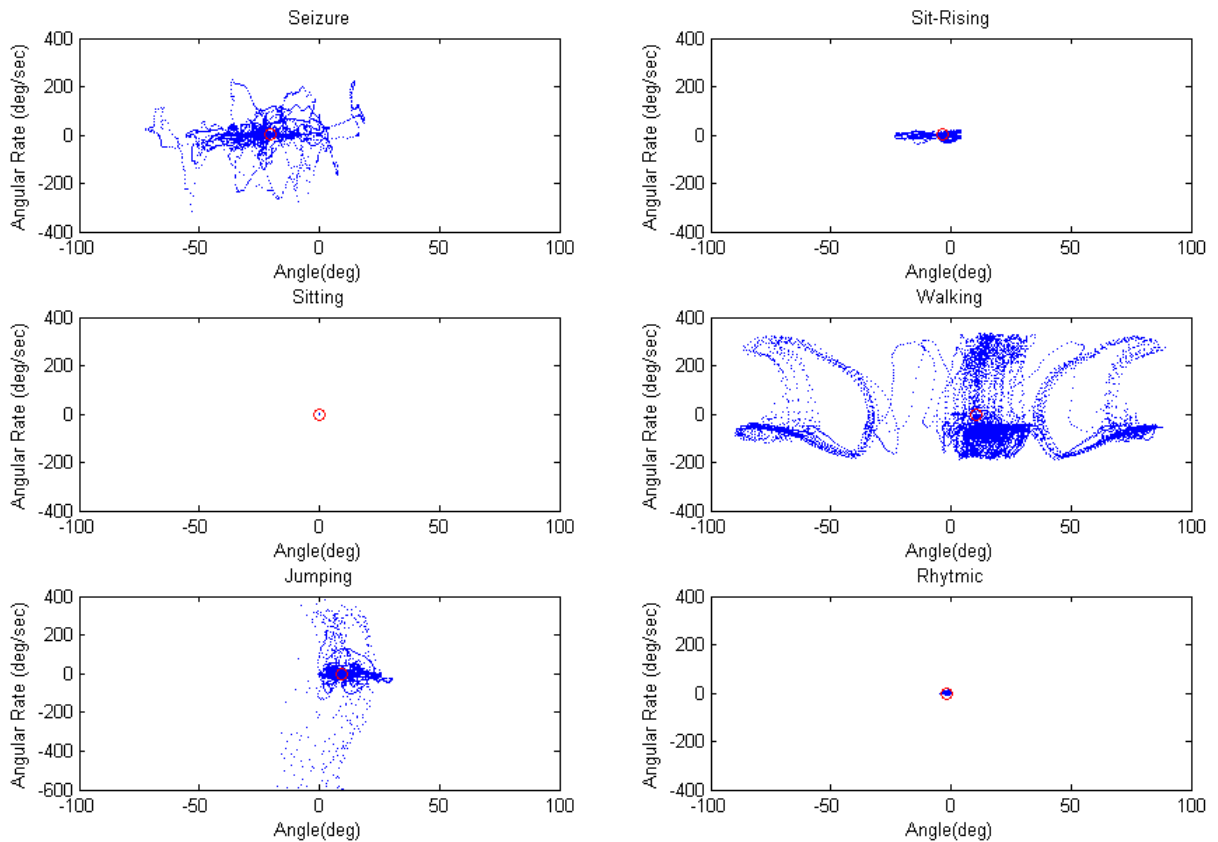


**Figure 5-22: Poincaré map for the Node 05 on the leg (angular rate vs. angle in the y-direction)**

### 5.3.5 Moment of Inertia Based Approach

Methods based on Pseudo-Phase-Space. Lyapunov Exponent and Poincaré map are all capable of providing a preliminary detection algorithm. However, for establishing a reliable and robust detection method that can make the predictions more accurate, a modified form of Poincaré map is proposed. According to the plots presented in the previous sections, it is also perceived that the difference between the normal and involuntary movements can be given in terms of the level of scattering or concentration in one point as well as the ratio of the y-axis (angular rate) to the x-axis (angle) spread. These criteria can be assessed in terms of the inertia measure of the system. Hence, an approach utilizing the idea of second moment of inertia ratios and radius of gyration is proposed for this purpose. This method can be thought of as a modified form of the

Poincaré to accommodate the range of motion and rates as well as spread ranges presented in a suitable space. In other words, the ratio of the second moment of inertias in the x and y directions,  $J_{2yy}/J_{2xx}$ , can be thought of representing the scattering or concentration of the Poincaré map points indicating x or y preference while the radius of gyration can be thought of as a measure of scattering level about the imaginary center of mass of the sampled data. In this section, an approach based on assigning equal weights to each sample point of the Poincaré map is presented. After assigning the aforementioned quantities to each sample, the following two quantities are calculated from the Poincaré maps of angle vs angular rate axes: ratio of the second moment of inertia in the x and y directions ( $J_{2yy}/J_{2xx}$ ), and the radius of gyration.

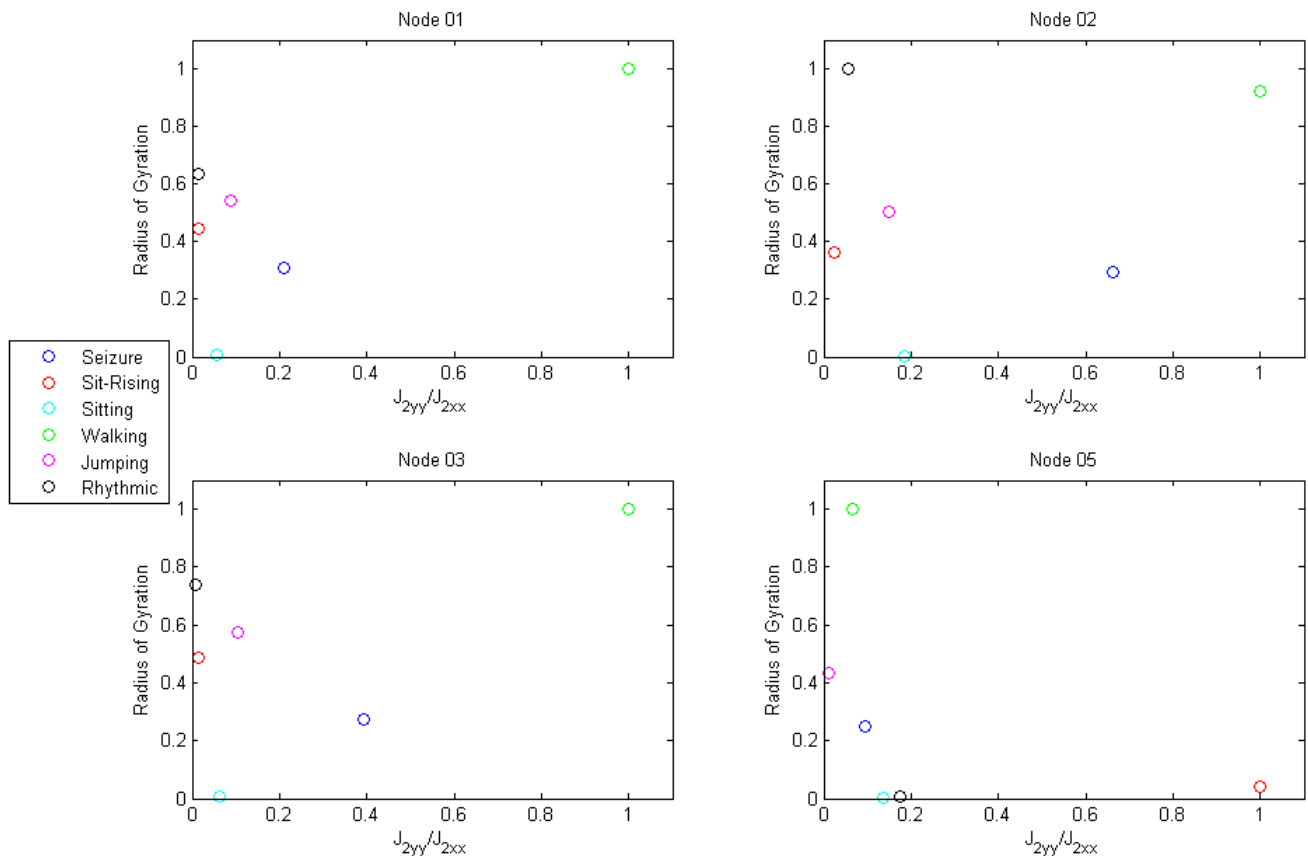


**Figure 5-23: Moment of Inertia based approach**

As shown in Figure 5-23, walking activity depicts largest radius of gyration among all the activities. This is because the walking activity involved exhibits the largest range of



angular changes. In addition, jumping movement has the largest moment of inertia ratio since the angular rate in the jumping activity has the largest change. Finally, seizure movement can be classified as an activity with the average value of radius of gyration which represents a moderate angular change whereas standing shows a low angular change. It is then concluded that the proposed moment of inertia based approach can be useful in providing a suitable sets of data in which the activities are well separated and hence can be instrumented in future activity classification based seizure detection.

### 5.3.6 Discussion

In general, considering the preliminary results, three fundamental advantages of the proposed approach may be stated when compared to conventional EEG and Video-EEG systems. The system can be easily set up just by fastening three sensor Nodes to the forearm for the patients with dominant movements in the arms or three sensors in the leg for the patients with dominant movements of the lower body. The system can perform unobtrusive, long-term monitoring of the patient's motion parameters during daily activities and thus provides objective real-life data less likely to be influenced by artificial lab conditions. The algorithm proposed in the present chapter is not computationally-intensive and can be implemented on wearable systems and even the sensor Nodes themselves. This renders live measurements and feedback to the patient or the caretaker when necessary. By performing further experiments, it is envisaged that regions similar to Figure 5-24 may be generated. It is envisaged that experimental data for each activity cluster can be used for further validation of the proposed method and for developing useful criteria for seizure detection.

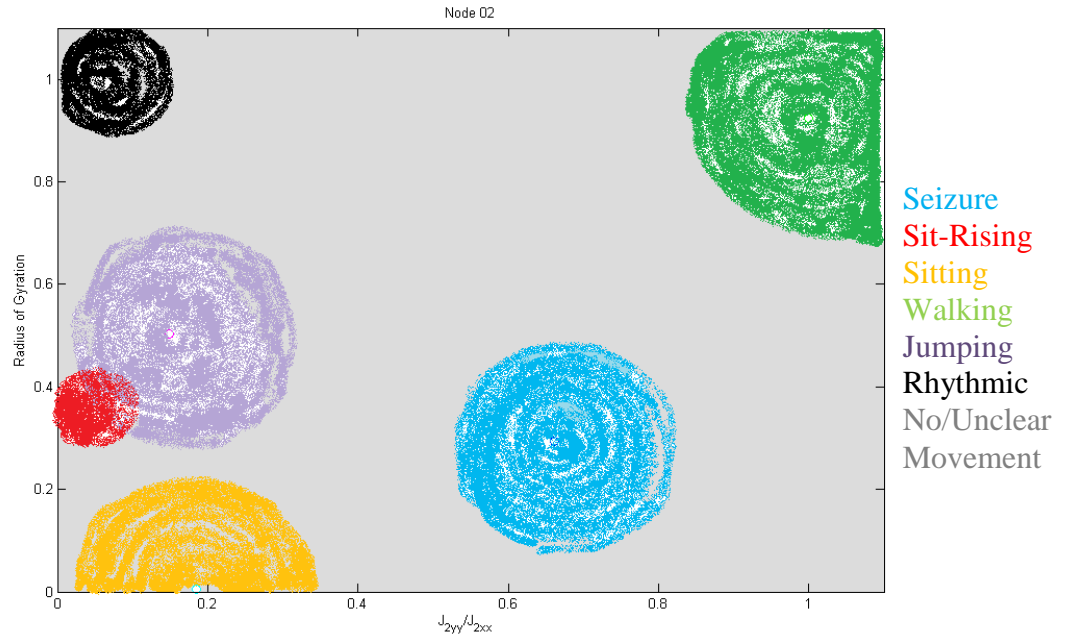


**Figure 5-24: Proposed method for the detection**

### 5.3.7 Limitations

The present study has been performed in the monitoring room of the hospital and thus is to some extent also subject to movement changes because of the patient being initially uncomfortable with the instrument attached to her as well as the supervision. Further during the seizure event, patient's mother and the nurse presented in the monitoring room attempted to hold the patient's arms and legs to keep her calm. Hence, it may be noted that the reason the data derived 10 seconds after the seizure event cannot be considered reliable. Finally, the video recording was not consistent throughout the whole recording time and stopped functioning several times in the middle of recording, thus some video data may have been missed.

The measurements for the normal activities are performed with a healthy master's student subject, albeit with possible difference in normal movements expected for epileptic patients. Also due to the differences in height, weight, age and in general the physical condition of body between the healthy and epileptic subjects, it is anticipated that the some variability in movement response may occur. Therefore this study needs to be

repeated with more healthy subjects and especially with epileptic patients in order to conclude a prevailing characterization of normal vs. seizure-type movements.

## 5.4 Closure

The main propose of the present chapter was to develop activity classification based method for distinguishing epileptic seizure from normal activities. In order to attain this goal, a set of inertial measurement data was obtained from a healthy and epileptic patient subjects. Frequency response of different activities recoded via inertial sensors is then considered for determination of the dominant frequency. According to the Fourier spectrum, it was decided that seizure may be classified as non-rhythmic motion and hence a novel nonlinear response based on Poincaré map was proposed and validated via experimental data. The proposed method ascertained a distinguishable, well separated activity clusters and is considered to be suitable for activity classification based seizure detection.

## Chapter 6

### 6 Conclusion and Recommendations for Future Work

#### 6.1 Summary of Research

The present thesis is concerned with the use of inertial sensory system to monitor and detect the seizure of the patients suffering from epilepsy. In an effort to address this concern and propose a method for epileptic seizure detection, a mathematical model that represents the human body dynamics during the epileptic seizure is developed. The model is consisted of 16 segments representing different parts of human body and has 32 degrees of freedom in total. The equations of motion are derived employing a software implementation, Motion Genesis™ which is based on Kane's dynamic formulation. In addition, an epileptic seizure accelerometry model is adopted and modified for the purpose of numerical simulations. This model is then utilized for proposing an optimal placement strategy for inertial sensors to achieve the highest possible resolution in determination of angular acceleration during epileptic seizure episodes. In addition, employing the model developed for human body, a joint torque estimation procedure is developed within the symbolic math toolbox environment of MATLAB™ and proposed as a possible detection scheme. The proposed method has been able to avoid direct integration or differentiation process of raw data and is expected to minimize errors associated with these processes.

Further, employing an inertial measurement unit, Motion Node™, acceleration as well as angular rate data is obtained experimentally from an epileptic seizure patient as well as a healthy subject and a preliminary comparison study on the dominant frequency of each activity is performed based on the Fourier Spectrum approach. Further, in order to provide a quantified characterization of different activities, a preliminary attempt to characterize experimental data via nonlinear system based algorithms such as Lyapunov exponent, Poincaré map and Pseudo-Phase-Space method was made. Following the nonlinear-based analysis of experimental data, a method based on quantification of Poincaré map results in terms of mechanical quantities such as second moment of inertia

and radius of gyration was proposed. This method has been shown to yield promising results for activity recognition and classification.

## 6.2 Thesis Contributions

The original contributions of this thesis are summarized as follows:

- Employing commercially available dynamic analysis software, detailed mathematical model of human body is developed. The procedure developed is shown to be useful for understanding the dynamics of human body during epileptic seizures. The predicted responses have formed the basis for optimal placement/number and the type of inertial sensors that can be used for detection purposes.
- In order to achieve high sensing resolution as well as to minimize the number of sensors, an objective function based on the angular acceleration evaluation is developed. A sensitivity analysis is performed to examine the dependence of the predicted optimal locations on the significant model parameters. This outcome is envisaged to help future experimental studies that utilize these sensors for seizure detection.
- Torque estimated at the elbow joint via inertial sensor measurements has been proposed as a possible measure for seizure characterization. This method has inherent advantage of avoiding direct integration/differentiation of raw data.
- A preliminary study for activity characterization via experimental inertial sensory data has been performed on the basis of nonlinear response analysis. In particular, a method based on quantification of Poincaré map has been proposed. This method has been shown to be promising for activity recognition as well as classification.

## 6.3 Recommendations for Future Work

The research performed in this thesis has lead to the following suggestions for a number of future research directions:

The biomechanical model developed in this thesis is a simplified model of human body by considering solely passive components of muscles. Hence, development of an active muscle based human body model which is capable of depicting the movements of human body during epileptic seizure more realistically, may prove to be useful.

The epileptic seizure model used in this thesis is a biomechanical model of the myoclonic seizure. Hence, it may be useful to extend the model to other types of epileptic seizures such as tonic-clonic, clonic and tonic.

The proposed modified Poincaré map approach requires further investigation and validation prior to implementation. This needs to be achieved through experiments considering a variety of epileptic seizure patients as well as healthy subjects.

## References

- [1] H. Witte, L. Iasemidis and B. Litt, "Special issue on epileptic seizure prediction," *IEEE Transactions on Biomedical Engineering*, vol. 50, p. 537–539, 2003.
- [2] C. L. Bottasso and B. I. Prilutsky, "A Numerical Procedure for Inferring from Experimental Data the Optimization Cost Functions Using a Multi-body Model of the Neuro-Musculoskeletal System," *Multi-body System Dynamics*, vol. 16, pp. 123-154., 2006.
- [3] M. P. T. Silva and J. A. C. Ambrósio, "Kinematic Data Consistency in the Inverse Dynamics Analysis of Biomechanical Systems," *Multi-body System Dynamics*, vol. 8, pp. 219-239, 2002.
- [4] M. G. Pandy, "Computer Modeling and Simulation of Human Movement," *Annual Review of Biomedical Engineering*, vol. 3, pp. 245-273, 2001.
- [5] F. C. Anderson and M. G. Pandy, "A Dynamics Optimization Solution for Vertical Jumping in Three Dimensions," *Computer Methods in Biomechanics and Biomedical Engineering*, vol. 2, pp. 201-231, 1999.
- [6] A. Nagano, S. Yoshioka, T. Komura, R. Himeno and S. Fukashiro, "A three dimensional linked segment model of the whole human body," *International Journal of Sport and Health science*, vol. 3, pp. 311-325, 2005.
- [7] Y. Bei and B. Fregly, "Multibody Dynamic Simulation of Knee Contact Mechanics," *Medical Engineering & Physics*, vol. 26, pp. 777-789, 2004.
- [8] k. Sasaki and R. R. Neptune, "Differences in Muscle Function during Walking and Running at the Same Speed," *Journal of Biomechanics*, vol. 39, pp. 2005-2013, 2006.
- [9] S. C. Huang and R. L. Huston, "A Model for Human Vibrations Studies and for Predicting Response to Jolting and Jarring," *Journal of Mechanics in Medicine and Biology*, vol. 2, no. 1, pp. 37-52, 2002.
- [10] Gallenstein, J. and Huston, R.L., "Analysis of swimming motions," *Human Factors*, vol. 15, no. 1, pp. 91-98, 1973.
- [11] M. P. T. Silva, J. A. C. Ambrósio and M. S. Pererira, "Biomechanical Model with Joint

- Resistance for Impact Simulation," *Multibody System Dynamics*, vol. 1, pp. 65-84, 1997.
- [12] D. A. Winter, *Biomechanics and Motor Control of Human Movement*, Hoboken, NJ: Wiley, 2005.
- [13] M. Schwartz and A. Rozumalski, "A new method for estimation joint parameters from motion data," *Journal of Biomechanics*, vol. 38, no. 1, pp. 107-116, 2005.
- [14] T. Kane, "Dynamics of nonholonomic systems," *Journal of Applied Mechanics*, vol. 28, p. 574, 1961.
- [15] T. Kane and C. Wang, "On the derivation of equations of motion," *J. Soc. Ind. App. Math*, vol. 13, p. 487, 1965.
- [16] <http://www.mae.ufl.edu/~fregly/eml5215.htm>, . [Online].
- [17] P. G. Smith and T. R. Kane, "On the dynamics of a human body in free fall," *Journal of Applied Mechanics*, vol. 35, pp. 167-168, 1968.
- [18] M. P. Scher and T. R. Kane, "Alteration of the State of Motion of a Human Being in Free Fall," NASA, NASA-CR-108938, SU-TR-198 , 1969.
- [19] M. P. Scher and T. R. Kane, "Pitch and Yaw Motions of a Human Being in Free Fall," NASA, NASA-CR-97902, SU-TR-190 , 1968.
- [20] D. R. Lemmon, M. YiWu and R. L. Huston, "SUPERCRAH- A Three-dimensional, Crash Victim Simulation Program," *Advance. In Bioengineering-ASME*, vol. 28, 1994.
- [21] H. Gastaut, *Dictionary of epilepsy*, Geneva, Switzerland: World Health Organization, 1973.
- [22] <http://www.epilepsy.ca/en-CA/Epilepsy-Canada.html>, . [Online].
- [23] R. McLachlan, "Julius Caesar's Late Onset Epilepsy: A Case of Historic Proportions," *Can. J. Neurol. Sci.*, vol. 37, pp. 557-561, 2010.
- [24] [http://en.wikipedia.org/wiki/List\\_of\\_people\\_with\\_epilepsy](http://en.wikipedia.org/wiki/List_of_people_with_epilepsy), . [Online].
- [25] <http://www.epilepsy.com/node/986825>, . [Online].
- [26] H. O. Luders and S. Noachtar, "Epileptic Seizures, Pathophysiology and Clinical Semiology," 2000.
- [27] o. C. a. T. o. t. I. L. A. E. Commission, "Proposal for revised clinical and electroencephalographic classification of epileptic seizures," *Epilepsia*, vol. 22, pp. 489-



501, 1981.

- [28] J. Engel Jr., "A proposed diagnostic scheme for people with epileptic seizures and with epilepsy: Report of the ILAE task force on classification and terminology," *Epilepsia*, vol. 42, pp. 796-803, 2001.
- [29] P. Brown and C. .. D. Marsden, "Rhythmic cortical and muscle discharge in cortical myoclonus," *Brain*, vol. 119, pp. 1307-1316, 1996.
- [30] M. Hallett, "Myoclonus: Relation to epilepsy," *Epilepsia*, vol. 26, no. 1, pp. S67-s77, 1998.
- [31] H. Luders, J. Acharya, C. Baumgartner, S. Benbadis, A. Bleasel, R. Burgess, D. Dinner, A. Ebner, N. Foldvary, E. Geller, H. Hamer, H. Holthausen, P. Kotagal, H. Morris, H. Meencke, S. Noachtar, F. Rosenow, A. Sakamoto, B. Steinhoff and I. Tuxhorn, "Semiological seizure classification," *Epilepsia*, vol. 39, no. 9, pp. 1006-1013, 1998.
- [32] H. Hamer, H. Lüders, S. Knake, B. Fritsch, W. Oertel and R. F., "Electrophysiology of focal clonic seizures in humans: a study using subdural and depth electrodes," *Brain*, vol. 126, pp. 547-555, 2003.
- [33] <http://www.nlm.nih.gov/medlineplus/ency/imagepages/19076.htm>, . [Online].
- [34] C. Bazil and T. Pedley, *Epilepsy*, 12th ed., T. P. e. M. N. Epilepsy. In LP Rowland, Ed., Philadelphia: Lippincott Williams and Wilkins., 2010, p. 927–948.
- [35] D. Raskovic, T. Martin and E. Jovanov, "Medical monitoring applications for wearable computing," *The Computer Journal*, vol. 47, no. 4, pp. 495-504, 2004.
- [36] T. Martin, E. Jovanov and D. Raskovic, "Issues in wearable computing for medical monitoring applications: A case study of a wearable ECG monitoring device," in *Proc. of the 4th Int. Symp. Wearable Computers*, Atlanta, Georgia, USA, 2000.
- [37] <http://sites.pcmd.ac.uk/time/methods.php?cat=eeg>, . [Online].
- [38] M. Schepers, M. Koopman and H. Veltink, "Ambulatory assessment of ankle and foot dynamics," *IEEE Trans. Biomed. Eng.*, vol. 54, p. 895–900, 2007.
- [39] K. Tong and M. Granat, "A practical gait analysis system using gyroscopes," *Medical Engineering and Physics*, vol. 21, p. 87–94, 1999.
- [40] G. Cooper, I. Sheret, L. McMillian, K. Siliverdis, N. Sha, D. Hodgins and D. Howard, "Inertial sensor-based knee flexion/extension angle estimation," *Journal of Biomechanics*, vol. 42, pp. 2678-2685, 2009.

- [41] S. Asokanathan and T. Wang, "Instabilities in a MEMS Gyroscope subjected to Angular Rate Fluctuations," *Journal of Vibration and Control*, vol. 15, no. 2, pp. 299-320, 2009.
- [42] A. Salarian, H. Russmann, F. J. G. Vingerhoets, P. R. Burkhar, Y. Blanc, C. Dehollain and K. Aminian, "An ambulatory system to quantify bradykinesia and tremor in Parkinson's disease," in *Fourth Annual IEEE Conference on Information Technology Applications in Biomedicine*, Birmingham, United Kingdom, 2003.
- [43] P. Veltink, E. Engberink, B. Van Hilten, R. Dunnewold and C. Jacobi, "Towards a new method for kinematic quantification of bradykinesia in patients with Parkinson's disease using tri-axial accelerometry," in *17th Annual Conference IEEE EMBS*, , 1995.
- [44] A. Chwaleba, J. Jakubowski and K. Kwiatos, "The measuring set and signal processing method for the characterization of human hand tremor," *CADSM*, p. 18–22, 2003.
- [45] D. Giansanti, "Investigation of fall-risk using a wearable device with accelerometers and rate gyroscopes," *Phys. Meas.*, vol. 27, pp. 1081-1090, 2006.
- [46] T. Choudhury, G. Borriello, S. Consolvo, D. Haehnel, B. Harrison, B. Hemingway, P. Hightower, K. Klasnja, K. Koscher, A. LaMarca, J. Landay, L. LeGrand, J. Lester, A. Rahimi, A. Rea and D. Wyatt, "Themobile sensing platform: An embedded system for activity recognition," *Appears in IEEE Pervasive Magazine - Special Issue on Activity-Based Computing*, vol. 7, no. 2, pp. 32-41, April 2008.
- [47] S. Morris and J. Paradiso, "Shoe-integrated sensor system for wirelessgait analysis and real-time feedback," Houston, TX, USA , 2002.
- [48] A. Yang, S. Iyengar, S. Sastry, R. Bajcsy, P. Kuryloski and R. Jafari, "Distributed segmentation and classification of human actions using awearable sensor network," in *Proceedings of the CVPR Workshop on Human Communicative Behavior Analysis*, Alaska, USA, 2008.
- [49] N. Oliver and F. Flores-Mangas, "Healthgear: a real-time wearablesystem for monitoring and analyzing physiological signals," in *International workshop on Wearable and Implantable Body Sensor Networks*, Boston, USA, 2006.
- [50] P. Bonato, "Wearable sensors/systems and their impact on biomedical engineering," *IEEE Engineering in Medicine and Biology Magazine*, vol. 22, no. 3, pp. 18-20, 2003.
- [51] E. Foxlin, "nertial head-tracker sensor fusion by a complementary separate-bias Kalman filter," *Proceedings of VRAIS '96*, pp. 185-194, 1996.

- [52] E. Bachmann, "Inertial and magnetic tracking of limb segment orientation for inserting humans into synthetic environments," PhD Thesis, Naval Postgraduate, Monterey, CA, 2000.
- [53] T. Nijsen, J. Arends, P. Griep and P. Cluitmans, "The potential value of three-dimensional accelerometry for detection of motor seizures in severe epilepsy," *Epilepsy. Behav.*, vol. 7, no. 1, p. 74–84, 2005.
- [54] G. Becq, S. Bonnet, L. Minotti, R. Guillemaud and P. Kahane, "Classification of epileptic motor manifestations using attitude sensors," *Computers in Biology and Medicine*, vol. 41, p. 46–55, 2011.
- [55] D. Roetenberg, H. Luinge and P. Slycke, "Xsens MVN: Full 6DOF Human Motion Tracking Using Miniature Inertial Sensors," 2009. [Online]. Available: [www.xsens.com/images/stories/PDF/MVN\\_white\\_paper.pdf](http://www.xsens.com/images/stories/PDF/MVN_white_paper.pdf).
- [56] R. Zhu and Z. Zhou, "A Real-Time Articulated Human Motion Tracking Using Tri-Axis Inertial/Magnetic Sensors Package," *IEEE Transactions on Neural Systems and Rehabilitation Engineering*, vol. 2, pp. 295-302, 2004.
- [57] G. Becq, S. Bonnet, L. Minotti, M. Antonakios, R. Guillemaud and P. Kahane, "Collection and exploratory analysis of attitude sensor data in an epilepsy monitoring unit," in *29th annual international conference of IEEE EMBS*, Lyon, France, 2007.
- [58] P. Jallon, S. Bonnet, M. Antonakios and R. Guillemaud, "Detection system of motor epileptic seizures through motion analysis with 3D accelerometers," in *EMBC 2009*, Minneapolis, USA, 2009.
- [59] I. Conradsen, S. Beniczky, P. Wolf, T. Kjaerd, T. Samsa and H. Sorensena, "Automatic multi-modal intelligent seizure acquisition (MISA) system for detection of motor seizures from electromyographic data and motion data," *computer methods and programs in biomedicine*, vol. 107, pp. 97-110, 2012.
- [60] P. Jallon, "A Bayesian approach for epileptic seizures detection with 3D accelerometers sensors," in *32nd Annual International Conference of the IEEE EMBS*, Buenos Aires, Argentina, 2010.
- [61] B. Huyghe and J. Vanfleteren, "Design of Flexible, Low Power and Wireless Sensor Nodes for Human Posture Tracking Aiding Epileptic Seizure Detection," in *IEEE SENSORS 2009 Conference*, Canterbury, New Zealand, 2009.
- [62] S. Bonnet, P. Jallon, A. Bourgerette, M. Antonakios, V. Rat, R. Guillemaud and Y. Caritu, "An Ethernet motion-sensor based alarm system for epilepsy monitoring," *IRBM*, vol. 32,

- no. 2, pp. 155-157, 2011.
- [63] T. Nijsen, P. Cluitmans, J. Arends and P. Griep, "Detection of subtle nocturnal motor activity from 3-D accelerometry recordings in epilepsy patients," *IEEE Trans Biomed Eng*, vol. 54, pp. 2073-2081, 2007.
- [64] T. Nijsen, R. Aarts, P. Cluitmans and P. Griep, "Time-Frequency Analysis of Accelerometry Data for Detection of Myoclonic Seizures," *IEEE Transactions on Information Technology in Biomedicine*, vol. 14, no. 5, 2010.
- [65] E. Schulc, I. Unterberger, S. Saboor, J. Hilbe, M. Ertl, E. Ammenwerth and C. T. E. Them, "Measurement and quantification of generalized tonic-clonic seizures in epilepsy patients by means of accelerometry--an explorative study," *Epilepsy Res*, vol. 95, pp. 173-83, 2011.
- [66] I. Conradsen, S. Beniczky, P. Wolf, D. Terney, T. Sams and H. Sorensen, "Multi-modal intelligent seizure acquisition (MISA): A new approach towards seizure detection based on full body motion measures," in *Proceedings of the 31st annual international confer*, 2009.
- [67] <http://www.analog.com/en/mems-sensors/products/index.html>, . [Online].
- [68] <http://www.xsens.com/en/mvn-biomech>, . [Online].
- [69] <http://www.xsens.com/en/general/mtx>, . [Online].
- [70] <http://www.motionnode.com/bus.html>, . [Online].
- [71] <https://www.djoglobal.com/products/aircast/pneumatic-armband>, . [Online].
- [72] <http://www.airbracestore.com/shop-by-body-part/arm-elbow/pneumatic-armband>, . [Online].
- [73] L. Atallah, B. Lo, R. King and G. Yang, "Sensor placement for activity detection using wearable accelerometers," in *BSN, Biopolis*, Biopolis, Singapore, 2010.
- [74] L. Bao and S. Intille, "Activity Recognition from User-Annotated Acceleration Data," *Pervasive Computing, Linz/Vienna*, pp. 1-17, 2004.
- [75] T. Nijsen, R. Aarts, J. Arends and P. Cluitmans, "Model for arm movements during myoclonic seizures," in *Proc. 29th Annu. Int. Conf. IEEE EMBS*, Lyon, France, 2007.
- [76] K. Cuppens, L. Lagae, B. Ceulemans, S. Van Huffel and B. Vanrumste, "Detection of nocturnal frontal lobe seizures in pediatric patients by means of accelerometers: a first study," in *Proceedings of the 31st annual international conference of the IEEE EMBS*,

Minnesota, USA, 2009.

- [77] J.-Y. Yang, J.-S. Wang and Y.-P. Chen, "Using acceleration measurements for activity recognition: An effective learning algorithm for constructing neural classifiers," *Pattern Recognition Letters*, vol. 29, no. 16, pp. 2213-2220, 2008.
- [78] T. Hester, D. Sherrill, M. Hamel, K. Perreault, P. Boissy and P. Bonato, "Identification of tasks performed by stroke patients using a mobility assistive device," in *Engineering in Medicine and Biology Society, EMBS '06. 28th Annual International Conf*, New York City, USA, 2006.
- [79] A. F. N. L. a. B. C. M. Mathie, "Detection of daily physical activities using a triaxial accelerometers," *Med. Biol. Eng. Comput.*, vol. 41, no. 3, pp. 296-301, 2003.
- [80] B. L. L. Atallah, O. Aziz, M. ElHelw, A. Darzi and G. Yang, "Realtime pervasive monitoring for postoperative care," *Proceeding of BSN07/IFMBE*, vol. 1, p. 122-127, 2007.
- [81] D. Karantonis, M. Narayanan, M. Mathie, N. Lovell and B. Celler, "Implementation of a real-time human movement classifier using a triaxial accelerometer for ambulatory monitoring," *IEEE Transactions on Information Technology in Biomedicine*, vol. 10, pp. 156-167, 2006.
- [82] N. L. Keijsers, M. W. Horstink, J. J. Van Hilten, J. I. Hoff and C. Gielen, "Detection and assessment of the severity of levodopa-induced dyskinesia in patients with Parkinson's disease by neural networks," *Mov. Disord.*, vol. 15, p. 1104-1111.
- [83] D. Buck, G. Baker, A. Jacoby, D. Smith and D. Chadwick, "Patients' Experiences of Injury as a Result of Epilepsy," *Epilepsia*, vol. 38, no. 4, pp. 439-444, 1997.
- [84] P. Holmes, "Ninety plus years of nonlinear dynamics: less is more and more is different," *Intl. J. Bifurc. Chaos*, vol. 15, no. 9, p. 2703-2716, 2005.
- [85] S. Strogatz, *Nonlinear Dynamics and Chaos: With Applications to Physics, Biology, Chemistry, and Engineering*, New York : Addison-Wesley, 1994.
- [86] M. Woo, W. Stevenson, D. Moser, R. Trelease and R. Harper, "Patterns of beat-to-beat heart rate variability in advanced heart failure," *American Heart Journal*, vol. 123, no. 3, pp. 704-710, 1992.
- [87] W. Freeman, "Simulation of chaotic EEG patterns with a dynamic model of the olfactory system," *Biological Cybernetics*, vol. 56, pp. 139-150, 1987.
- [88] E. Rossoni, Y. Chen, M. Ding and J. Feng, "Stability of synchronous oscillations in a system

- of Hodgkin-Huxley neurons with delayed diffusive and pulsed coupling," *Phys. Rev. E*, vol. 71, 2005.
- [89] B. Havsteen, "Evidence of quasi-linear gas transport through sperm whale myoglobin," *Eur. Biophys. J.*, vol. 31, no. 7, pp. 549-553, 2002.
- [90] M. Bracic and A. Stefanovska, "Nonlinear dynamics of the blood flow studied by Lyapunov exponents," *Bull. Mathemat. Biol*, vol. 60, no. 3:4, pp. 17-433, 1998.
- [91] M. Longstaff and R. Heath, "A nonlinear analysis of the temporal characteristics of handwriting," *Human Mov. Sci.*, vol. 18, no. 4, pp. 485-524, 1999.
- [92] L. Goodman, M. Riley, S. Mitra and M. Turvey, "Advantages of rhythmic movements at resonance: minimal active degrees of freedom, minimal noise, and maximal predictability," *J. Motor Behav.*, vol. 32, no. 1, pp. 3-8, 2000.
- [93] J. Perkiomaki, T. Makikallio and H. Huikuri, *Clin. Experiment.Hypertens.*, vol. 27, no. 2:3, pp. 149-158, Fractal and complexity measures of heart rate variability 2005.
- [94] C. Stam, "Nonlinear dynamical analysis of EEG and MEG: review of an emerging field," *Clin. Neurophysiol*, vol. 116, no. 10, pp. 2266-2301, 2005.
- [95] A. Wolf, J. Swift, H. Swinney and J. Vastano, "Determining Lyapunov exponents from a time series," *Physica D: Nonlinear Phenomena*, vol. 16, no. 3, pp. 285-317, 1985.
- [96] E. Hanavan, "A Mathematical Model of the Human Body," Aerospace Medical Research Laboratories Tech. Rep., Dayton, OH: Wright Patterson Air Force Base, AMRL,, 1964.
- [97] <http://www.speakingimage.org/images/human-anatomy-planes>, . [Online].
- [98] P. McGinnis, *Biomechanics of sport and Exercise*, 2 ed., : Human Kinetics, 2005.
- [99] [http://professionals.epilepsy.com/page/generalized\\_tonic.html](http://professionals.epilepsy.com/page/generalized_tonic.html), . [Online].
- [100] R. L. Huston, *Principle of Biomechanics*, CRC press, 2009, p. 148.
- [101] H. Hatze, "A mathematical model for the computational determination of parameter values of anthropometric segments," *Journal of Biomechanics*, vol. 13, p. 833-843, 1980.
- [102] F. C. Anderson, "A dynamic optimization solution for a complete cycle of normal gait: An analysis of muscle function and joint contact force," PhD dissertation, University of Texas at Austin, Austin, Texas, 1999.

- [103] M. Audu and D. Davy, "The influence of muscles model complexity in musculoskeletal motion modeling," *J. Biomech. Engrg.*, vol. 107, pp. 147-157, 1985.
- [104] D. Davy and M. Audu, "A dynamic optimization technique for predicting forces in the swing phase of gait," *J. Biomechanics*, vol. 20, pp. 187-202, 1987.
- [105] G. Yamaguchi, "Feasibility and Conceptual design of functional neuromuscular stimulation systems for the restoration of natural gait to paraplegics based on dynamic musculoskeletal models," Ph.D. Thesis, Department of Mechanical Engineering, Stanford University, , Stanford, CA, 1989.
- [106] A. Hill, *First and last experiments in muscle mechanics*, Cambridge: Cambridge University Press, 1970.
- [107] T. McMahon, *Muscles, reflexes, and locomotion*, Princeton, N.J.: Princeton University Press, 1984.
- [108] D. Winter, *Biomechanics and motor control of human gait: normal, elderly and pathological*, 2. Ed., Ed., Waterloo, Canada: Univ. Waterloo Press, 1991, pp. 224-230.
- [109] D. Green, "A Note on Modeling Muscle in Physiological Regulators," *Med. & Biol. Engrg.*, vol. 7, pp. 41-48, 1969.
- [110] W. T. Latt, U.-X. Tan, C. N. Riviere and W. T. Ang, "Placement of accelerometers for high sensing resolution in micromanipulation," *Sens. Actuators: A Phys.*, 2011.
- [111] J. H. Holland, *Adoption in neural and artificial systems*, The University of Michigan Press, Ann Arbor, Michigan, 1975.
- [112] L. Kun, Y. Inoue, K. Shibata and C. Enguo, "Ambulatory estimation of knee-joint kinematics in anatomical coordinate system using accelerometers and magnetometers," *IEEE Trans Biomed Eng*, vol. 58, pp. 435-442, 2011.
- [113] C. M. van den Bleek and J. C. Schouten, "Deterministic chaos: a new tool in fluidized bed design and operation," *Chem. Eng. J.*, vol. 53, p. 75-87, 1993.
- [114] F. Amirouche, *Fundamentals of Multibody Dynamics Theory and Applications*, 1 ed., Boston: Birkhauser/Springer, 2005.
- [115] J. J. Craig, *Introduction to Robotics: Mechanics and Control*, 3rd ed., Englewood Cliffs: Prentice Hall, 2004.
- [116] D. Goldberg, "Genetic Algorithms in Search, Optimization and Machine Learning,"

Addison-Wesley, New York, 1989.

[117] A. J. Wheeler and A. R. Ganji, Introduction to Engineering Experimentation, 2nd ed., :  
Prentice Hall,, 2004.



## Appendices

### Appendix A: An example of application of Kane's method

#### A.1 Kane's Method Formulation

In this section, first the procedure to develop Kane's method is briefly reviewed [114]. Then, employing Kane's method, dynamical governing equations are developed especially for a simple example to briefly illustrate the overall procedure of deriving the equations of motion and also providing an insight into comparison between Kane's method and Newton-Euler's.

Kane's equation as discussed in section (1.2.3) of chapter one, is a dynamical approach to deal with the multi-body systems with high degrees of freedom. An open-chain, tree-like multi-body system of  $N$  interconnected rigid bodies is an example of such systems (Figure A. 1). As it was mentioned earlier one of the advantages of Kane's method over Newton-Euler's is the elimination of the interactive forces, so each segment is subject to the external and constraint forces. The external forces can be converted into an equivalent force and torque of the form  $\vec{F}_j^e$  and  $\vec{M}_j^e$ ; passing through the center of mass of each segment  $j$ , where  $j$  denotes the number of interconnected rigid bodies. Similar to the external forces, the constraint forces also may be indicated as  $\vec{F}_j^c$  and  $\vec{M}_j^c$ . Using D'Alembert's principle for the force equilibrium of body  $j$ , the following is obtained:

$$\vec{F}_j^e + \vec{F}_j^* + \vec{F}_j^c = 0, \quad \text{A. 1}$$

where  $\vec{F}_j^* = -m_j a_j$  is the inertia force associated with body  $j$ .

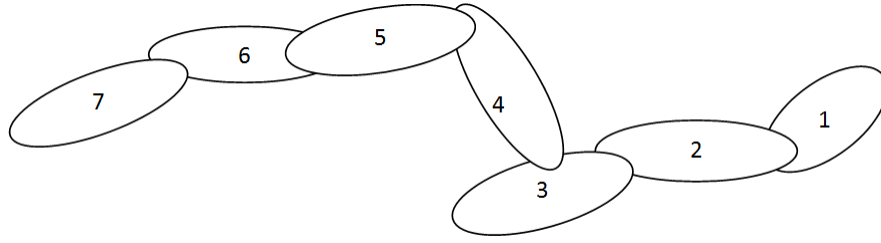


**Figure A. 1: A general treelike multi-body systems**

In general, the system  $S$  shown in Figure A. 1 possesses  $3N$  degrees of freedom in a fixed inertial reference frame. Further,  $N$  interconnected bodies have  $3N$  generalized coordinates in the form of  $x_1, x_2, x_3, \dots, x_{3N}$ . If the force components  $F_1, F_2, \dots, F_{3N}$  are applied at the particles along the corresponding coordinates, then the virtual work denoted by  $\delta W$  of these forces with a virtual displacement  $\delta r$  is described as

$$\delta W = \sum_{j=1}^{3N} \vec{F}_j \cdot \delta r_j, \quad \text{A. 2}$$

where  $\vec{F}_j$  is the resultant force acting on the  $j$ th segment and  $r_j$  is the position vector of the segment in global reference frame (R). Extending the principle of virtual work to Eq. A. 1 yields to:

$$\delta W = (\vec{F}_j^e + \vec{F}_j^* + \vec{F}_j^c) \cdot \delta \vec{r}_j = 0 \quad (j = 1, 2, \dots, N), \quad \text{A. 3}$$

The constraints that are commonly encountered are known as workless constraints so:

$$\vec{F}_j^c \cdot \delta r_j = 0, \quad \text{A. 4}$$

which simplifies the work equation to

$$\delta W = (\vec{F}_j^e + \vec{F}_j^*) \cdot \delta \vec{r}_j = 0 \quad (j = 1, 2, \dots, N), \quad \text{A. 5}$$

which can be written as

$$\delta W = (\vec{F}_j^e + \vec{F}_j^*) \cdot \frac{\partial \vec{r}_j}{\partial q_r} \delta q_r = 0 \quad (r = 1, 2, \dots, 3N), \quad \text{A. 6}$$

Now, since the position vector may be written as:

$$\vec{r}_j = \vec{r}_j(q_r, t), \quad \text{A. 7}$$

Performing the differentiation in accordance with multivariable differentiation techniques, the following expression can be derived for velocity vector of segment  $j$ ,

$$\dot{\vec{r}}_j = \frac{\partial \vec{r}_j}{\partial q_r} \frac{dq_r}{dt} + \frac{\partial \vec{r}_j}{\partial t} = \frac{\partial \vec{r}_j}{\partial q_r} \dot{q}_r + \frac{\partial \vec{r}_j}{\partial t}, \quad \text{A. 8}$$

From Eq. A. 8, the partial derivative of  $\dot{\vec{r}}_j$  with respect to  $\dot{q}_r$  can be evaluated to be:

$$\frac{\partial \dot{\vec{r}}_j}{\partial \dot{q}_r} = \frac{\partial \vec{r}_j}{\partial q_r}, \quad \text{A. 9}$$

or simply

$$\frac{\partial \vec{v}_j}{\partial \dot{q}_r} = \frac{\partial \vec{r}_j}{\partial q_r}, \quad \text{A. 10}$$

where  $\vec{v}_j$  is velocity of body  $j$  in  $R$ .

Since the virtual displacement  $\partial q_r$  is arbitrary, without violating the constraint, Eq. A. 6 can be written in the following format:

$$F_r^* + F_r = 0, \quad \text{A. 11}$$

where  $F_r^*$  and  $F_r$  are called the generalized active and inertia forces respectively, and are defined as:

$$F_r^* = \vec{F}_j^* \cdot \frac{\partial \vec{r}_j}{\partial q_r} = \vec{F}_j^* \cdot \frac{\partial \vec{v}_j}{\partial \dot{q}_r}, \quad \text{A. 12}$$

and,

$$F_r = \vec{F}_j \cdot \frac{\partial \vec{r}_j}{\partial q_r} = \vec{F}_j \cdot \frac{\partial \vec{v}_j}{\partial \dot{q}_r}, \quad \text{A. 13}$$

In a similar way it can be shown that using virtual work, the moments can be written as

$$M_r^* + M_r = 0, \quad \text{A. 14}$$

where  $M_r^*$  and  $M_r$  are the generalized active and inertia moments and are defined as follows:

$$M_r^* = -(\vec{\alpha}_j \cdot \vec{\bar{I}} + \vec{\omega}_j \times \vec{\bar{I}} \cdot \vec{\omega}_j) \cdot \frac{\partial \vec{\omega}_j}{\partial \dot{q}_r}, \quad \text{A. 15}$$

and,

$$M_r = \vec{T}_r \cdot \frac{\partial \vec{\omega}_j}{\partial \dot{q}_r}, \quad \text{A. 16}$$

where  $\vec{\alpha}_j$  is the angular acceleration of body  $j$  in  $R$ , and  $\vec{\bar{I}}$  is the inertia dyadic of  $j$  relative to the center of mass  $G_j$  and  $\vec{\omega}_j$  denotes the angular velocity of  $j$  in  $R$ . By superposition of Eqs. A. 11 - A. 14 for a system subjected to both external forces and moments, one can obtain the equations of motion as:

$$f_r + f_r^* = 0. \quad \text{A. 17}$$

Equation A. 17 is known as *Kane's equations*.

## A.2 Arm Dynamic Formulation via Kane's Approaches

Human arm dynamics including the upper arm and forearm parts in considered in this section. The governing equations of the arm are obtained employing Kane's method and is verified by Newton-Euler's method and also compared with the result of the Motion Genesis™ code. The purpose of solving the problem by Kane's approach and Motion Genesis™ is to present the similarities each procedure has for formulating the equations of motion. The mechanism considered in this section as shown in Figure A. 2, consists of two bodies representing arm and forearm parts.

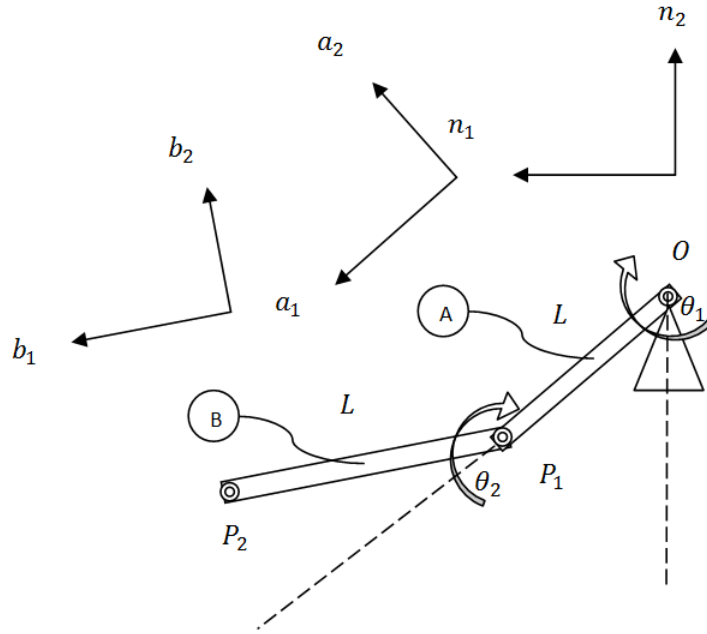


**Figure A. 2: Two DOF model for the human arm with two revolute joints**

To compare two common methods used to solve the multi body problems, Kane's method is presented in this section. According to the procedure presented in [115], it is perceivable that Newton-Euler's method deals with not only the external forces and torques applied to the segments but also the internal interactions between different segments. As shown in Figure A. 2, the mechanism consists of two links with point masses at points P1 and P2. The joint angular changes are presented as  $\theta_1$  and  $\theta_2$ .  $T_{A/B}$  is the net torque applied on joint P1.

Generalized coordinates and speeds for the joints are derived as:

$$u_1 = \dot{\theta}_1, u_2 = \dot{\theta}_2. \quad \text{A. 18}$$

Then, angular velocities and transitional velocities can be written in terms of the angular velocity and in the local coordinate systems as:

$${}^N\omega^A = u_1 \hat{a}_3, \quad {}^N\omega^B = u_1 \hat{a}_3 + u_2 \hat{b}_3 = (u_1 + u_2) \hat{a}_3, \quad \text{A. 19}$$

and

$${}^N V_r^{P_1} = {}^N \omega^{P_1} \times r^{NP_1} = (u_1 \hat{a}_3) \times (l_1 \hat{a}_1) = u_1 L \hat{a}_2, \quad \text{A. 20}$$

Angular acceleration terms for the joints are derived as:

$${}^N \alpha^{P_1} = \frac{d({}^N \omega^{P_1})}{dt} = \dot{u}_1 \hat{a}_3, \quad {}^N \alpha^{P_2} = {}^N \alpha^{P_1} + {}^R \alpha^{P_2} + {}^N \omega^{P_1} \times {}^R \omega^{P_2} = \dot{u}_1 \hat{a}_3 + \dot{u}_2 \hat{a}_3, \quad \text{A. 21}$$

Transitional acceleration terms can be also calculated as:

$$\begin{aligned} {}^N a^{P_1} &= {}^N \alpha^{P_1} \times r^{NP_1} + {}^N \omega^{P_1} \times ({}^N \omega^{P_1} \times r^{NP_1}) = L \dot{u}_1 \hat{a}_2 + L u_1^2 (-\hat{a}_1), \\ {}^N a^{P_2} &= {}^N a^{P_1} + {}^N \alpha^{P_2} \times r^{RP_2} + {}^N \omega^{P_2} \times ({}^N \omega^{P_2} \times r^{RP_2}) \\ &= L \dot{u}_1 \hat{a}_2 + L u_1^2 (-\hat{a}_1) - L(u_1 + u_2)^2 \hat{b}_1 + L(\dot{u}_1 + \dot{u}_2) \hat{b}_2. \end{aligned} \quad \text{A. 22}$$

The definitions for partial velocities are given in Table A-1.

**Table A-1: Partial velocity for the two degree of freedom system**

	r=1	r=2
${}^N \omega_r^A$	$\hat{a}_3$	0
${}^N \omega_r^B$	$\hat{a}_3$	$\hat{b}_3$
${}^N V_r^{P_1}$	$L \hat{a}_2$	0
${}^N V_r^{P_2}$	$L \hat{a}_2 + L \hat{b}_2$	$l \hat{b}_2$

The expressions for the generalized inertia forces and active forces are as follows:

$$F_r = \sum (F_A \cdot {}^N v_r^A + T_A \cdot {}^N \omega_r^A + F_B \cdot {}^N v_r^B + T_B \cdot {}^N \omega_r^B), \quad \text{A. 23}$$

and,

$$\begin{aligned} F_r^* &= \sum (-m_1 \cdot {}^N a^A \cdot {}^N v_r^A - ({}^N \alpha^A \cdot I^A + {}^N \omega^A \times I^A \cdot {}^N \omega^A) \cdot {}^N \omega_r^A \\ &\quad - m_2 \cdot {}^N a^B \cdot {}^N v_r^B - ({}^N \alpha^B \cdot I^B + {}^N \omega^B \times I^B \cdot {}^N \omega^B) \cdot {}^N \omega_r^B. \end{aligned} \quad \text{A. 24}$$

Because of the point-mass assumption, the inertia tensor at the center of mass for each link is the zero matrix:

$$I^{P_1/P_1^*} = 0, I^{P_2/P_2^*} = 0. \quad \text{A. 25}$$

Using Eq. (A. 23) to (A. 24), the expression for generalized inertia and active forces will be:

$$F_1^* = -mL^2(\dot{u}_1(3+2c_2) + \dot{u}_2(1+c_2) + s_2(u_1^2 - (u_1 + u_2))), \quad \text{A. 26}$$

$$F_2^* = -mL^2(\dot{u}_1(1+c_2) + \dot{u}_2 + s_2u_1^2),$$

$$F_1 = T_A + mgL(-2c_1 - c_{12}), F_2 = -mgLc_{12} + T_{A/B}, \quad \text{A. 27}$$

Using these equations, Kane's equation can be derived as follows:

$$0 = -mL^2(\dot{u}_1(3+2c_2) + \dot{u}_2(1+c_2) + s_2(u_1^2 - (u_1 + u_2))) + T_A + mgL(-2c_1 - c_{12}), \quad \text{A. 28}$$

$$0 = -mL^2(\dot{u}_1(1+c_2) + \dot{u}_2 + s_2u_1^2) - mgLc_{12} + T_{A/B}, \quad \text{A. 29}$$

It is noted that Eqs. (A. 28) and (A. 29) can be verified employing the Newton-Euler based solution which is provided in [115] by substituting following parameters:

$$\begin{aligned} \dot{\theta}_1 &= u_1, \ddot{\theta}_1 = \dot{u}_1, \dot{\theta}_2 = u_2, \ddot{\theta}_2 = \dot{u}_2, \\ m_2 &= m_1 = m, l_2 = l_1 = L. \end{aligned} \quad \text{A. 30}$$

Kane's method thus produces simple equations of motion with less computational effort required compared to the Newton-Euler approach. This is the reason that Kane's method is the basis for a variety of multi-body dynamics computer codes.

## Application of Motion Genesis™ for the Example

The Motion Genesis™ code and the output result of the procedure for the example studied in this section is presented in Figure A. 3.

%Motion Genesis™ Code, Babak Kamalizonouzi	p_o_p> = L*a1>
% Define the parts of the system	p_p_q> = L*b1>
Newtonian N	p_o_a0> = L*a1>
Bodies A, B	p_p_bo> = L*b1>

<pre> Points O, P, Q % Define variables and constants that will be used Constants L Constants G Variables q{2}' MotionVariables' u{2}' q1' = u1 q2' = u2 % Define system properties Mass A = m, B = m Inertia A, IA=0,m*L^2/12,IA Inertia B, IB=0,m*L^2/12,IB % Define relative orientation of system Simprot (n,a,3,q1) Simprot (a,b,3,q2) % Define origin v_o_n&gt; = 0&gt; a_o_n&gt; = 0&gt; % Define angular velocity and acceleration w_a_n&gt; = u1*a3&gt; w_b_n&gt; = u2*b3&gt; alf_a_n&gt; = dt(w_a_n&gt;,n) alf_b_n&gt; = dt(w_b_n&gt;,n) % Define the positions of the points </pre>	<pre> % Define the velocity of the system points v_p_a&gt; = 0&gt; v_q_b&gt; = 0&gt; v2pts(n,a,o,P) v2pts(n,b,p,q) v2pts(n,a,o,ao) v2pts(n,b,p,bo) % Define the accelerations of system points a_p_a&gt; = 0&gt; a_q_b&gt; = 0&gt; a_p_n&gt; = dt(v_p_n&gt;,n) a_ao_n&gt; = dt(v_ao_n&gt;,n) a_q_n&gt; = dt(v_q_n&gt;,n) a_bo_n&gt; = dt(v_bo_n&gt;,n) %Forces Gravity (-G*N2&gt;) % Define torques acting on joints Variables TA, TA_B Constants k2, k4, b2, b4 Torque_A&gt; = TA*a3&gt; Torque(A/B, TA_B*b3&gt;) % Form the equations of motion zero = fr() + frstar() Kane() </pre>
--	--

**Figure A. 3: Motion Genesis™ code for the two link structure**

Using the procedure of Figure A. 3, the expressions for the Kane's equation can be derived. The output of the Motion Genesis™ program is:

$$\text{ZERO}[1] = TA - 2 * G * L * m * \cos(q1) - G * L * m * \cos(q1+q2) - m * L^2 * \sin(q2) * (u1^2 - (u1+u2)^2) - 2 * m * L^2 * (1.5 + \cos(q2)) * u1' - m * L^2 * (1 + \cos(q2)) * u2' \quad \text{A. 31}$$

and,

$$\text{ZERO}[2] = TA_B - G * L * m * \cos(q1+q2) - m * L^2 * \sin(q2) * u1^2 - m * L^2 * u2' - m * L^2 * (1 + \cos(q2)) * u1' \quad \text{A. 32}$$

which are the same as the answers resulted from Kane's method and Newton-Euler's.



## Appendix B: Joint Torque Estimation Procedure Developed in Motion Genesis™

In this section the output procedure from the Motion Genesis™ software is implemented in order to be used in the symbolic toolbox available in MATLAB™, MuPAD. The following procedure is developed considering the arm of human body which includes arm, forearm and hand parts. Considering three degrees of freedom for each joint (shoulder, elbow and wrist), the total degrees of freedom of the model is nine.

```

z1 = cos(q1);
z2 = sin(q1);
z3 = cos(q2);
z4 = sin(q2);
z5 = cos(q3);
z6 = sin(q3);
z7 = cos(q4);
z8 = sin(q4);
z9 = cos(q5);
z10 = sin(q5);
z11 = cos(q6);
z12 = sin(q6);
z13 = z2.*z3;
z14 = z2.*z4;
z15 = z1.*z3;
z16 = z1.*z4;
z17 = z3.*u1.*u3;
z18 = u1.*u2;
z19 = u2.*u3;
z20 = z1.*z5 - z6.*z14;
z21 = z1.*z6 + z5.*z14;
z22 = z2.*z5 + z6.*z16;
z23 = z2.*z6 - z5.*z16;
z24 = z3.*z6;
z25 = z3.*z5;
z26 = z1.*z20 + z2.*z22;
z27 = z2.*z15 - z1.*z13;
z28 = z1.*z21 + z2.*z23;
z29 = z1.*z22 - z2.*z20;
z30 = z1.*z15 + z2.*z13;
z31 = z1.*z23 - z2.*z21;
z32 = z29.*z18 - z6.*z19 - z26.*z17;
z33 = z30.*z18 - z27.*z17;
z34 = z5.*z19 + z31.*z18 - z28.*z17;
z35 = z7.*z20 - z8.*z13;
z36 = -z7.*z13 - z8.*z20;

```

```

z37 = z7.*z22 + z8.*z15;
z38 = z7.*z15 - z8.*z22;
z39 = z4.*z8 - z7.*z24;
z40 = z4.*z7 + z8.*z24;
z41 = z1.*z35 + z2.*z37;
z42 = z1.*z36 + z2.*z38;
z43 = z1.*z37 - z2.*z35;
z44 = z1.*z38 - z2.*z36;
z45 = z3.*z43 + z4.*z39;
z46 = z3.*z44 + z4.*z40;
z47 = z3.*z31 + z4.*z25;
z48 = z3.*z39 - z4.*z43;
z49 = z3.*z40 - z4.*z44;
z50 = z3.*z25 - z4.*z31;
z51 = z9.*z36 + z10.*z21;
z52 = z9.*z21 - z10.*z36;
z53 = z9.*z38 + z10.*z23;
z54 = z9.*z23 - z10.*z38;
z55 = z9.*z40 + z10.*z25;
z56 = z9.*z25 - z10.*z40;
z57 = z8.*z9;
z58 = z8.*z10;
z59 = z7.*z9;
z60 = z7.*z10;
z61 = z1.*z51 + z2.*z53;
z62 = z1.*z52 + z2.*z54;
z63 = z1.*z53 - z2.*z51;
z64 = z1.*z54 - z2.*z52;
z65 = z3.*z63 + z4.*z55;
z66 = z3.*z64 + z4.*z56;
z67 = z3.*z55 - z4.*z63;
z68 = z3.*z56 - z4.*z64;
z69 = u4.*(u3+z4.*u1+z27.*u2);
z70 = u4.*(z24.*u1-z26.*u2);
z71 = u5.*(z40.*u1+z42.*u2+z46.*u3);
z72 = u6.*(z9.*u4+z56.*u1+z62.*u2+z66.*u3);
z73 = u5.*(u4+z25.*u1+z28.*u2+z47.*u3);
z74 = u6.*(u5+z39.*u1+z41.*u2+z45.*u3);
z75 = z11.*z35 - z12.*z52;
z76 = z11.*z52 + z12.*z35;
z77 = z11.*z37 - z12.*z54;
z78 = z11.*z54 + z12.*z37;
z79 = z11.*z39 - z12.*z56;
z80 = z11.*z56 + z12.*z39;
z81 = z20.*z75 + z22.*z77 - z24.*z79;
z82 = z20.*z51 + z22.*z53 - z24.*z55;

```

```

z83 = z20.*z76 + z22.*z78 - z24.*z80;
z84 = z4.*z79 + z15.*z77 - z13.*z75;
z85 = z4.*z55 + z15.*z53 - z13.*z51;
z86 = z4.*z80 + z15.*z78 - z13.*z76;
z87 = z21.*z75 + z23.*z77 + z25.*z79;
z88 = z21.*z51 + z23.*z53 + z25.*z55;
z89 = z21.*z76 + z23.*z78 + z25.*z80;
z90 = z7.*z81 + z8.*z84;
z91 = z7.*z82 + z8.*z85;
z92 = z7.*z83 + z8.*z86;
z93 = z7.*z84 - z8.*z81;
z94 = z7.*z85 - z8.*z82;
z95 = z7.*z86 - z8.*z83;
z96 = z1.*z75 + z2.*z77;
z97 = z1.*z76 + z2.*z78;
z98 = z1.*z77 - z2.*z75;
z99 = z1.*z78 - z2.*z76;
z100 = z3.*z98 + z4.*z79;
z101 = z3.*z99 + z4.*z80;
z102 = z3.*z79 - z4.*z98;
z103 = z3.*z80 - z4.*z99;
z104 = z81.*z69 + z84.*z70 + z93.*z73 + z98.*z18 + z102.*z19 - z12.*z74 - z87.*z71 - z90.*z72 - z96.*z17;
z105 = z63.*z18 + z67.*z19 + z82.*z69 + z85.*z70 + z94.*z73 - z61.*z17 - z88.*z71 - z91.*z72;
z106 = z11.*z74 + z83.*z69 + z86.*z70 + z95.*z73 + z99.*z18 + z103.*z19 - z89.*z71 - z92.*z72 - z97.*z17;
z107 = CM_A.*z25;
z108 = CM_A.*z28;
z109 = CM_A.*z24;
z110 = CM_A.*z26;
z111 = L_AF.*z25;
z112 = L_AF.*z28;
z113 = L_AF.*z24;
z114 = L_AF.*z26;
z115 = -z81.*z111 - z87.*z113;
z116 = z87.*z114 - z81.*z112;
z117 = -z82.*z111 - z88.*z113;
z118 = z88.*z114 - z82.*z112;
z119 = -z83.*z111 - z89.*z113;
z120 = z89.*z114 - z83.*z112;
z121 = CM_AF.*z80;
z122 = CM_AF.*z89;
z123 = CM_AF.*z92;
z124 = CM_AF.*z97;
z125 = CM_AF.*z101;
z126 = CM_AF.*z79;
z127 = CM_AF.*z87;
z128 = CM_AF.*z90;

```

```

z129 = CM_AF.*z96;
z130 = CM_AF.*z100;
z131 = z115 - z121;
z132 = z116 - z124;
z133 = z119 + z126;
z134 = z120 + z129;
z135 = L_A.*z80;
z136 = L_A.*z89;
z137 = L_A.*z92;
z138 = L_A.*z97;
z139 = L_A.*z101;
z140 = L_A.*z79;
z141 = L_A.*z87;
z142 = L_A.*z90;
z143 = L_A.*z96;
z144 = L_A.*z100;
z145 = z115 - z135;
z146 = z116 - z138;
z147 = z119 + z140;
z148 = z120 + z143;
z149 = -z107.*u1 - z108.*u2;
z150 = z110.*u2 - z109.*u1;
z151 = -z3.*z6.*u3 - z4.*z5.*u2;
z152 = z1.*z4.*u1 + z2.*z3.*u2;
z153 = z1.*z5.*u3 + z5.*z152 - z2.*z6.*u1 - z6.*z14.*u3;
z154 = z1.*z3.*u2 - z2.*z4.*u1;
z155 = z1.*z6.*u1 + z2.*z5.*u3 + z6.*z16.*u3 - z5.*z154;
z156 = z1.*z23.*u1 + z1.*z153 + z2.*z155 - z2.*z21.*u1;
z157 = CM_A.*(u1.*z151+u2.*z156);
z158 = -z1.*z6.*u3 - z2.*z5.*u1 - z5.*z14.*u3 - z6.*z152;
z159 = z1.*z5.*u1 + z5.*z16.*u3 + z6.*z154 - z2.*z6.*u3;
z160 = z1.*z22.*u1 + z1.*z158 + z2.*z159 - z2.*z20.*u1;
z161 = z3.*z5.*u3 - z4.*z6.*u2;
z162 = CM_A.*(u1.*z161-u2.*z160);
z163 = (u3+z4.*u1+z27.*u2).*z150 - z157;
z164 = (z25.*u1+z28.*u2).*z149 + (z24.*u1-z26.*u2).*z150;
z165 = -z162 - (u3+z4.*u1+z27.*u2).*z149;
z166 = z131.*u1 + z132.*u2 - z122.*u4 - z123.*u5 - z125.*u3;
z167 = z117.*u1 + z118.*u2;
z168 = z127.*u4 + z128.*u5 + z130.*u3 + z133.*u1 + z134.*u2;
z169 = z1.*z3.*u1 - z2.*z4.*u2;
z170 = z7.*z158 - z7.*z13.*u4 - z8.*z20.*u4 - z8.*z169;
z171 = z8.*z13.*u4 - z7.*z20.*u4 - z7.*z169 - z8.*z158;
z172 = z9.*z153 - z9.*z36.*u5 - z10.*z21.*u5 - z10.*z171;
z173 = z11.*z170 - z11.*z52.*u6 - z12.*z35.*u6 - z12.*z172;
z174 = -z1.*z4.*u2 - z2.*z3.*u1;

```

$$\begin{aligned}
z175 &= z7.*z15.*u4 + z7.*z159 + z8.*z174 - z8.*z22.*u4; \\
z176 &= z7.*z174 - z7.*z22.*u4 - z8.*z15.*u4 - z8.*z159; \\
z177 &= z9.*z155 - z9.*z38.*u5 - z10.*z23.*u5 - z10.*z176; \\
z178 &= z11.*z175 - z11.*z54.*u6 - z12.*z37.*u6 - z12.*z177; \\
z179 &= z3.*z8.*u2 + z4.*z7.*u4 + z8.*z24.*u4 - z7.*z161; \\
z180 &= z3.*z7.*u2 + z7.*z24.*u4 + z8.*z161 - z4.*z8.*u4; \\
z181 &= z9.*z151 - z9.*z40.*u5 - z10.*z25.*u5 - z10.*z180; \\
z182 &= z11.*z179 - z11.*z56.*u6 - z12.*z39.*u6 - z12.*z181; \\
z183 &= z20.*z173 + z22.*z178 + z75.*z158 + z77.*z159 - z24.*z182 - z79.*z161; \\
z184 &= z21.*z173 + z23.*z178 + z25.*z182 + z75.*z153 + z77.*z155 + z79.*z151; \\
z185 &= -z111.*z183 - z113.*z184 - L_AF.*z81.*z151 - L_AF.*z87.*z161; \\
z186 &= z11.*z39.*u6 + z11.*z181 + z12.*z179 - z12.*z56.*u6; \\
z187 &= z185 - CM_AF.*z186; \\
z188 &= z114.*z184 + L_AF.*z87.*z160 - z112.*z183 - L_AF.*z81.*z156; \\
z189 &= z11.*z35.*u6 + z11.*z172 + z12.*z170 - z12.*z52.*u6; \\
z190 &= z11.*z37.*u6 + z11.*z177 + z12.*z175 - z12.*z54.*u6; \\
z191 &= z1.*z78.*u1 + z1.*z189 + z2.*z190 - z2.*z76.*u1; \\
z192 &= z188 - CM_AF.*z191; \\
z193 &= z21.*z189 + z23.*z190 + z25.*z186 + z76.*z153 + z78.*z155 + z80.*z151; \\
z194 &= z20.*z189 + z22.*z190 + z76.*z158 + z78.*z159 - z24.*z186 - z80.*z161; \\
z195 &= z3.*z80.*u2 + z4.*z186 + z15.*z190 + z78.*z174 - z13.*z189 - z76.*z169; \\
z196 &= z7.*z86.*u4 + z7.*z194 + z8.*z195 - z8.*z83.*u4; \\
z197 &= z1.*z190 - z1.*z76.*u1 - z2.*z78.*u1 - z2.*z189; \\
z198 &= z3.*z80.*u2 + z3.*z197 + z4.*z186 - z4.*z99.*u2; \\
z199 &= u1.*z187 + u2.*z192 - CM_AF.*u3.*z198 - CM_AF.*u4.*z193 - CM_AF.*u5.*z196; \\
z200 &= z9.*z21.*u5 + z9.*z171 + z10.*z153 - z10.*z36.*u5; \\
z201 &= z9.*z23.*u5 + z9.*z176 + z10.*z155 - z10.*z38.*u5; \\
z202 &= z9.*z25.*u5 + z9.*z180 + z10.*z151 - z10.*z40.*u5; \\
z203 &= z20.*z200 + z22.*z201 + z51.*z158 + z53.*z159 - z24.*z202 - z55.*z161; \\
z204 &= z21.*z200 + z23.*z201 + z25.*z202 + z51.*z153 + z53.*z155 + z55.*z151; \\
z205 &= -z111.*z203 - z113.*z204 - L_AF.*z82.*z151 - L_AF.*z88.*z161; \\
z206 &= z114.*z204 + L_AF.*z88.*z160 - z112.*z203 - L_AF.*z82.*z156; \\
z207 &= u1.*z205 + u2.*z206; \\
z208 &= z3.*z79.*u2 + z4.*z182 + z15.*z178 + z77.*z174 - z13.*z173 - z75.*z169; \\
z209 &= z7.*z84.*u4 + z7.*z183 + z8.*z208 - z8.*z81.*u4; \\
z210 &= z1.*z178 - z1.*z75.*u1 - z2.*z77.*u1 - z2.*z173; \\
z211 &= z3.*z79.*u2 + z3.*z210 + z4.*z182 - z4.*z98.*u2; \\
z212 &= -z111.*z194 - z113.*z193 - L_AF.*z83.*z151 - L_AF.*z89.*z161; \\
z213 &= z212 + CM_AF.*z182; \\
z214 &= z114.*z193 + L_AF.*z89.*z160 - z112.*z194 - L_AF.*z83.*z156; \\
z215 &= z1.*z77.*u1 + z1.*z173 + z2.*z178 - z2.*z75.*u1; \\
z216 &= z214 + CM_AF.*z215; \\
z217 &= u1.*z213 + u2.*z216 + CM_AF.*u3.*z211 + CM_AF.*u4.*z184 + CM_AF.*u5.*z209; \\
z218 &= z199 + (u6+z55.*u1+z61.*u2+z65.*u3+z88.*u4+z91.*u5).*z168 - \\
& (z80.*u1+z89.*u4+z92.*u5+z97.*u2+z101.*u3).*z167; \\
z219 &= z207 + (z80.*u1+z89.*u4+z92.*u5+z97.*u2+z101.*u3).*z166 -
\end{aligned}$$

```

(z79.*u1+z87.*u4+z90.*u5+z96.*u2+z100.*u3).*z168;
z220 = z217 + (z79.*u1+z87.*u4+z90.*u5+z96.*u2+z100.*u3).*z167 -
(u6+z55.*u1+z61.*u2+z65.*u3+z88.*u4+z91.*u5).*z166;
z221 = 0;
z222 = exp(-21.88.*q1);
z223 = exp(5.05.*q1);
z224 = 20.*t.*z221 + 5.162573E-05.*z222 - 2.616502E-05.*z223 - 20.*u1;
z225 = exp(-21.88.*q2);
z226 = exp(5.05.*q2);
z227 = 5.162573E-05.*z225 - 2.616502E-05.*z226 - 20.*u2;
z228 = exp(-21.88.*q3);
z229 = exp(5.05.*q3);
z230 = 5.162573E-05.*z228 - 2.616502E-05.*z229 - 20.*u3;
z231 = exp(-21.88.*q4);
z232 = exp(5.05.*q4);
z233 = 5.162573E-05.*z231 - 2.616502E-05.*z232 - 20.*u4;
z234 = exp(-21.88.*q5);
z235 = exp(5.05.*q5);
z236 = 5.162573E-05.*z234 - 2.616502E-05.*z235 - 20.*u5;
z237 = exp(-21.88.*q6);
z238 = exp(5.05.*q6);
z239 = 5.162573E-05.*z237 - 2.616502E-05.*z238 - 20.*u6;
z240 = 9.81.*m_A.*(z22.*z107+z23.*z109) + z224 - 9.81.*m_AF.*(z53.*z117+z77.*z131+z78.*z133);
z241 = 9.81.*m_A.*(z22.*z108-z23.*z110) + z227 - 9.81.*m_AF.*(z53.*z118+z77.*z132+z78.*z134);
z242 = 9.81.*m_AF.*(z77.*z125-z78.*z130) + z230;
z243 = 9.81.*m_AF.*(z77.*z122-z78.*z127) + z233;
z244 = 9.81.*m_AF.*(z77.*z123-z78.*z128) + z236;
z245 = z26.*u2 - z24.*u1;
z246 = u3 + z4.*u1 + z27.*u2;
z247 = z25.*u1 + z28.*u2;
z248 = I_A11.*z245;
z249 = I_A22.*z246;
z250 = I_A33.*z247;
z251 = I_A11.*z26;
z252 = I_A11.*z24;
z253 = I_A11.*z32;
z254 = I_A22.*z4;
z255 = I_A22.*z27;
z256 = I_A22.*z33;
z257 = I_A33.*z25;
z258 = I_A33.*z28;
z259 = I_A33.*z34;
z260 = z245.*z249 - z246.*z248;
z261 = z247.*z248 - z245.*z250;
z262 = z246.*z250 - z247.*z249;
z263 = z79.*u1 + z87.*u4 + z90.*u5 + z96.*u2 + z100.*u3;

```

```

z264 = u6 + z55.*u1 + z61.*u2 + z65.*u3 + z88.*u4 + z91.*u5;
z265 = z80.*u1 + z89.*u4 + z92.*u5 + z97.*u2 + z101.*u3;
z266 = I_AF11.*z263;
z267 = I_AF22.*z264;
z268 = I_AF33.*z265;
z269 = I_AF11.*z79;
z270 = I_AF11.*z84;
z271 = I_AF11.*z87;
z272 = I_AF11.*z90;
z273 = I_AF11.*z96;
z274 = I_AF11.*z104;
z275 = I_AF22.*z55;
z276 = I_AF22.*z61;
z277 = I_AF22.*z85;
z278 = I_AF22.*z88;
z279 = I_AF22.*z91;
z280 = I_AF22.*z105;
z281 = I_AF33.*z80;
z282 = I_AF33.*z86;
z283 = I_AF33.*z89;
z284 = I_AF33.*z92;
z285 = I_AF33.*z97;
z286 = I_AF33.*z106;
z287 = z263.*z267 - z264.*z266;
z288 = z265.*z266 - z263.*z268;
z289 = z264.*z268 - z265.*z267;
z290 = z4.*z254 + z24.*z252 + z25.*z257 + z55.*z275 + z79.*z269 + z80.*z281 + m_A.*(z107.^2+z109.^2) +
m_AF.*(z117.^2+z131.^2+z133.^2);
z291 = z4.*z255 + z25.*z258 + z55.*z276 + z79.*z273 + z80.*z285 + m_A.*(z107.*z108-z109.*z110) +
m_AF.*(z117.*z118+z131.*z132+z133.*z134) - z24.*z251;
z292 = I_A22.*z4 + z55.*z277 + z79.*z270 + z80.*z282 - m_AF.*(z125.*z131-z130.*z133);
z293 = z55.*z278 + z79.*z271 + z80.*z283 - m_AF.*(z122.*z131-z127.*z133);
z294 = z55.*z279 + z79.*z272 + z80.*z284 - m_AF.*(z123.*z131-z128.*z133);
z295 = z4.*z256 + z4.*z261 + z25.*z259 + z25.*z260 + z55.*z280 + z55.*z288 + z79.*z274 + z79.*z289 +
z80.*z286 + z80.*z287 + m_AF.*(z117.*z219+z131.*z218+z133.*z220) - z24.*z253 - z24.*z262 -
m_A.*(z107.*z163+z109.*z165);
z296 = z27.*z254 + z28.*z257 + z61.*z275 + z96.*z269 + z97.*z281 + m_A.*(z107.*z108-z109.*z110) +
m_AF.*(z117.*z118+z131.*z132+z133.*z134) - z26.*z252;
z297 = z26.*z251 + z27.*z255 + z28.*z258 + z61.*z276 + z96.*z273 + z97.*z285 + m_A.*(z108.^2+z110.^2)
+ m_AF.*(z118.^2+z132.^2+z134.^2);
z298 = I_A22.*z27 + z61.*z277 + z96.*z270 + z97.*z282 - m_AF.*(z125.*z132-z130.*z134);
z299 = z61.*z278 + z96.*z271 + z97.*z283 - m_AF.*(z122.*z132-z127.*z134);
z300 = z61.*z279 + z96.*z272 + z97.*z284 - m_AF.*(z123.*z132-z128.*z134);
z301 = z26.*z253 + z26.*z262 + z27.*z256 + z27.*z261 + z28.*z259 + z28.*z260 + z61.*z280 + z61.*z288 +
z96.*z274 + z96.*z289 + z97.*z286 + z97.*z287 + m_AF.*(z118.*z219+z132.*z218+z134.*z220) -
m_A.*(z108.*z163-z110.*z165);

```

```

z302 = l_A22 + z65.*z277 + z100.*z270 + z101.*z282 + m_AF.*(z125.^2+z130.^2);
z303 = z254 + z65.*z275 + z100.*z269 + z101.*z281 - m_AF.*(z125.*z131-z130.*z133);
z304 = z255 + z65.*z276 + z100.*z273 + z101.*z285 - m_AF.*(z125.*z132-z130.*z134);
z305 = z65.*z278 + z100.*z271 + z101.*z283 + m_AF.*(z122.*z125+z127.*z130);
z306 = z65.*z279 + z100.*z272 + z101.*z284 + m_AF.*(z123.*z125+z128.*z130);
z307 = l_AF22.*z65;
z308 = z256 + z261 + z65.*z280 + z65.*z288 + z100.*z274 + z100.*z289 + z101.*z286 + z101.*z287 -
m_AF.*(z125.*z218-z130.*z220);
z309 = z87.*z269 + z88.*z275 + z89.*z281 - m_AF.*(z122.*z131-z127.*z133);
z310 = z87.*z270 + z88.*z277 + z89.*z282 + m_AF.*(z122.*z125+z127.*z130);
z311 = z87.*z271 + z88.*z278 + z89.*z283 + m_AF.*(z122.^2+z127.^2);
z312 = z87.*z272 + z88.*z279 + z89.*z284 + m_AF.*(z122.*z123+z127.*z128);
z313 = z87.*z273 + z88.*z276 + z89.*z285 - m_AF.*(z122.*z132-z127.*z134);
z314 = z87.*z274 + z87.*z289 + z88.*z280 + z88.*z288 + z89.*z286 + z89.*z287- m_AF.*(z122.*z218-
z127.*z220);
z315 = z90.*z269 + z91.*z275 + z92.*z281 - m_AF.*(z123.*z131-z128.*z133);
z316 = z90.*z270 + z91.*z277 + z92.*z282 + m_AF.*(z123.*z125+z128.*z130);
z317 = z90.*z271 + z91.*z278 + z92.*z283 + m_AF.*(z122.*z123+z127.*z128);
z318 = z90.*z272 + z91.*z279 + z92.*z284 + m_AF.*(z123.^2+z128.^2);
z319 = z90.*z273 + z91.*z276 + z92.*z285 - m_AF.*(z123.*z132-z128.*z134);
z320 = z90.*z274 + z90.*z289 + z91.*z280 + z91.*z288 + z92.*z286 + z92.*z287- m_AF.*(z123.*z218-
z128.*z220);
z321 = z280 + z288;
z322 = z240 - z295;
z323 = z241 - z301;
z324 = z242 - z308;
z325 = z243 - z314;
z326 = z244 - z320;
z327 = z239 - z321;
ze1 = z322 - z275.*a6 - z290.*a1 - z291.*a2 - z292.*a3 - z293.*a4- z294.*a5;
ze2 = z323 - z276.*a6 - z296.*a1 - z297.*a2 - z298.*a3 - z299.*a4- z300.*a5;
ze3 = z324 - z302.*a3 - z303.*a1 - z304.*a2 - z305.*a4 - z306.*a5- z307.*a6;
ze4 = z325 - z278.*a6 - z309.*a1 - z310.*a3 - z311.*a4 - z312.*a5- z313.*a2;
ze5 = z326 - z279.*a6 - z315.*a1 - z316.*a3 - z317.*a4 - z318.*a5- z319.*a2;
ze6 = z327 - l_AF22.*a6 - z275.*a1 - z276.*a2 - z277.*a3 - z278.*a4 - z279.*a5;

```



### Appendix C: Experimental plots and Poincaré Plots

In this section, plots of the magnitude value of the accelerometers and gyroscopes located on the forearm and leg are presented. As sensors are located near the joints, the following figures may become useful in further studies for determination of involvement of each joint in a specific activity. In addition, Poincaré maps are also presented in this section for Node number 2, 3, and 4.

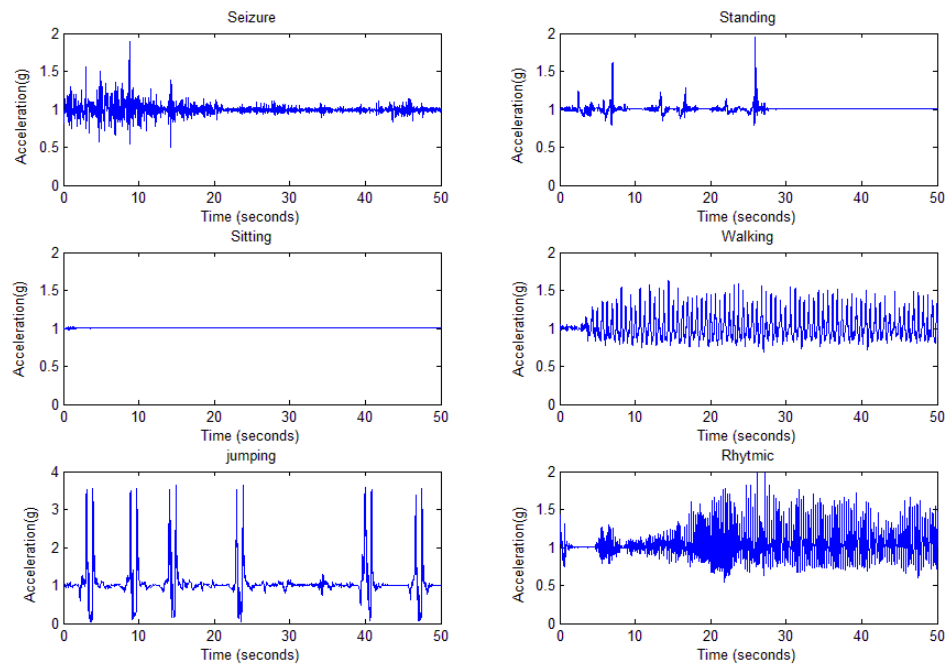


**Figure B. 1: Acceleration magnitude of the Node 2 attached to the forearm**

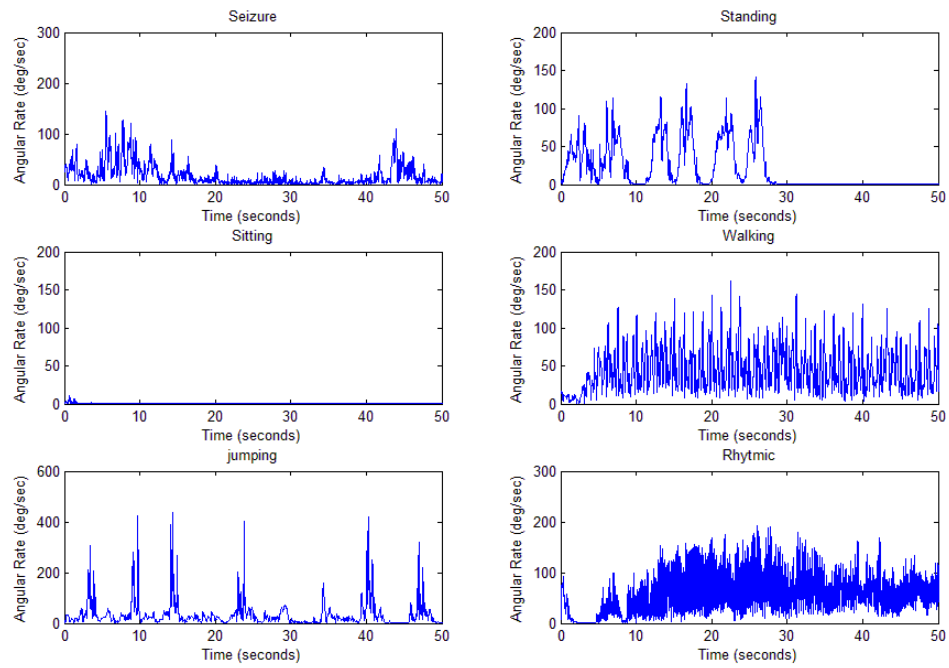


**Figure B. 2: Gyroscope magnitude of the Node 2 attached to the forearm**

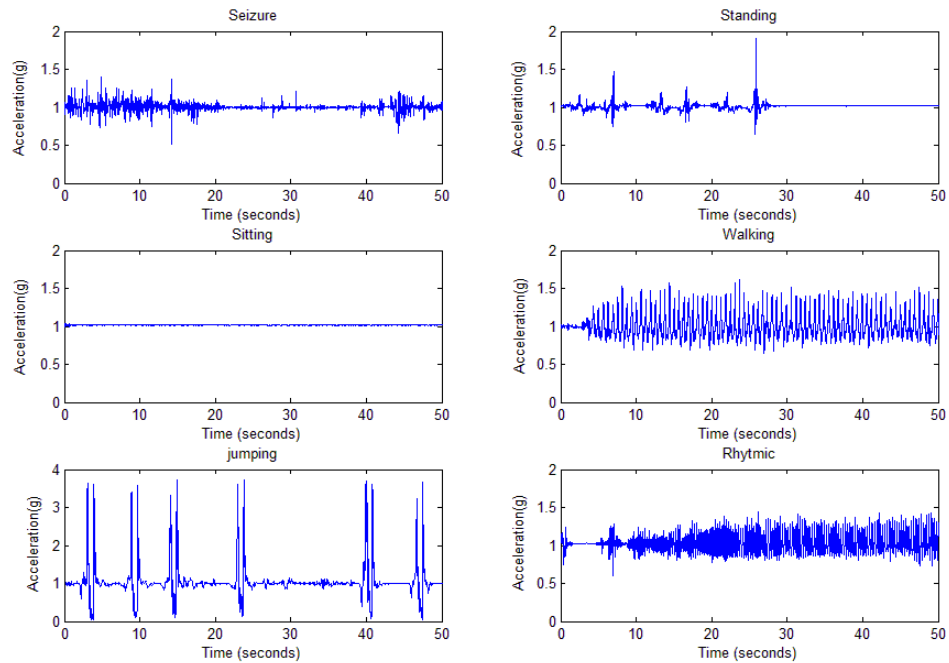


**Figure B. 3: Acceleration magnitude of the Node 3 attached to the forearm**

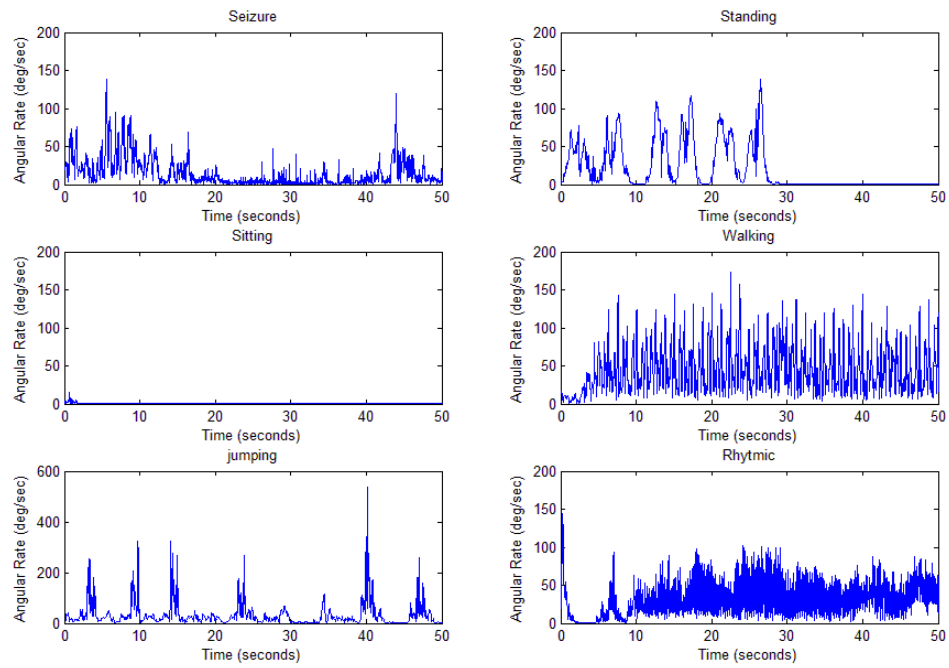


**Figure B. 4: Gyroscope magnitude of the Node 3 attached to the forearm**

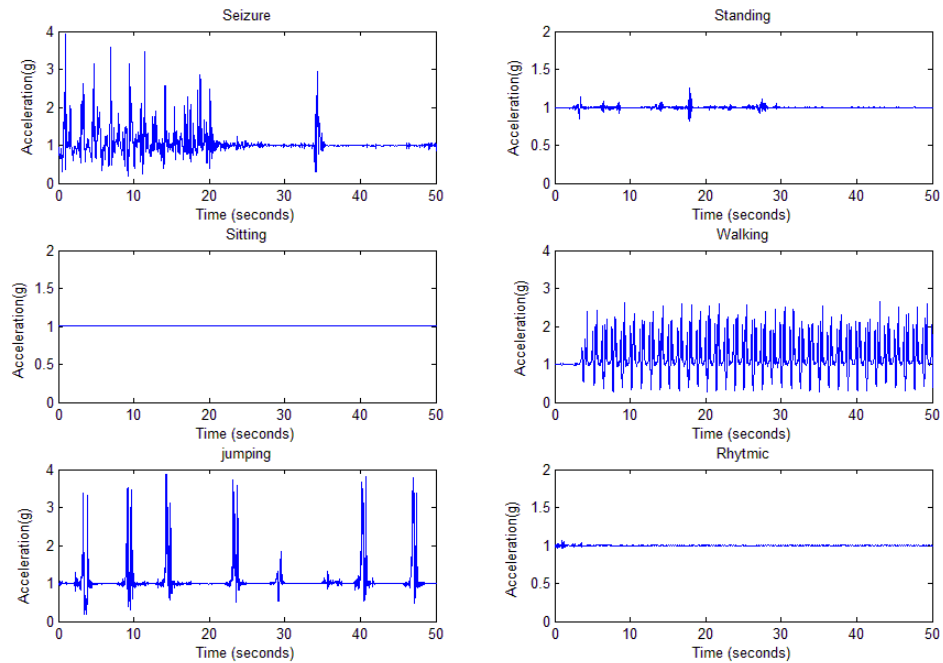


**Figure B. 5: Acceleration magnitude of the Node 4 attached to the leg**

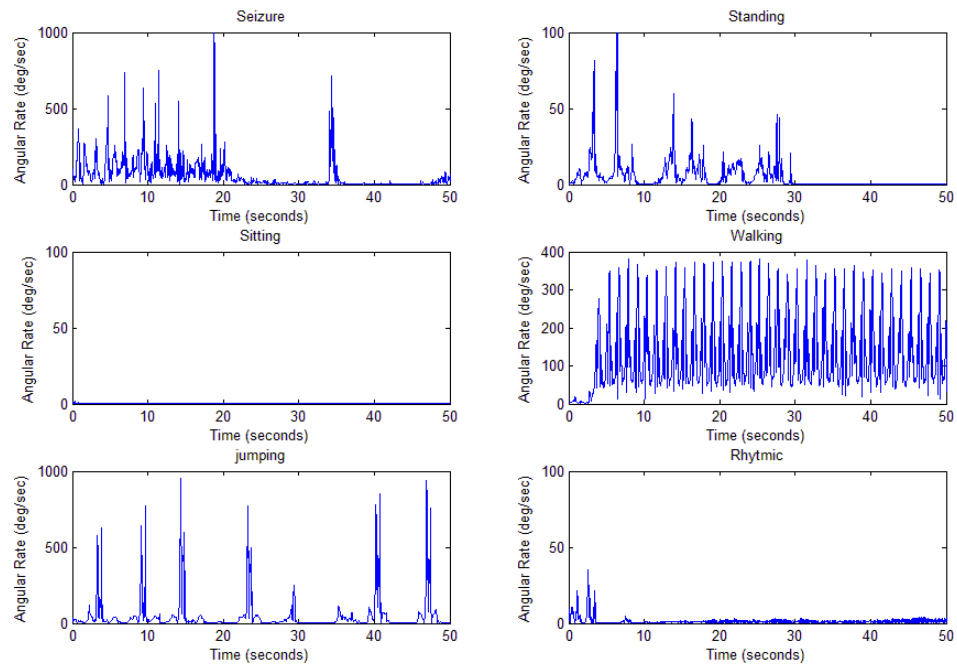


**Figure B. 6: Gyroscope magnitude of the Node 4 attached to the leg**

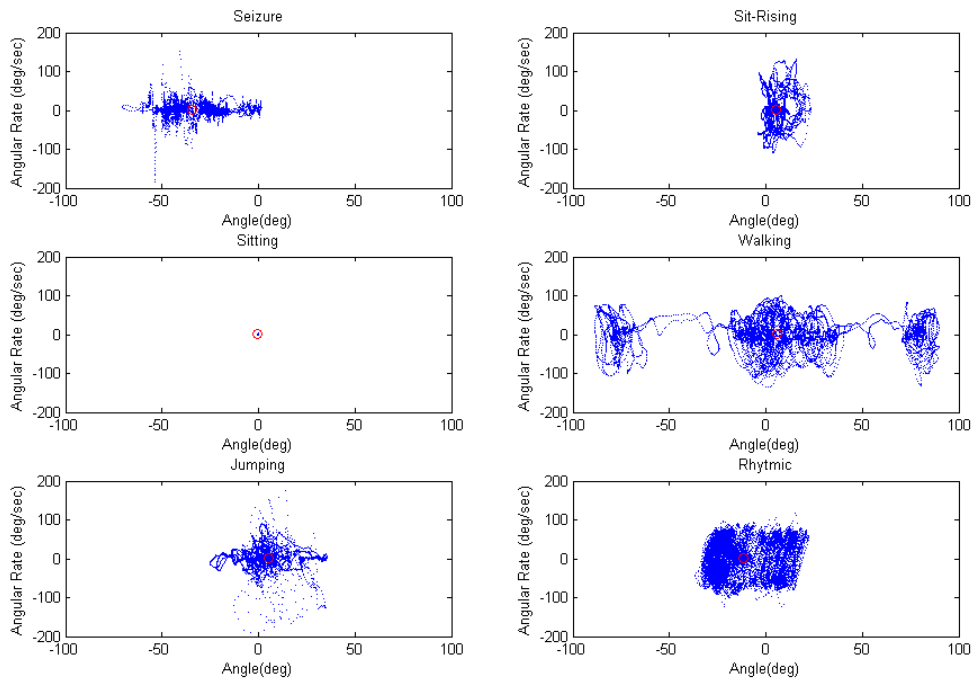


**Figure B. 7: Poincaré map for the Node 02 on the arm**

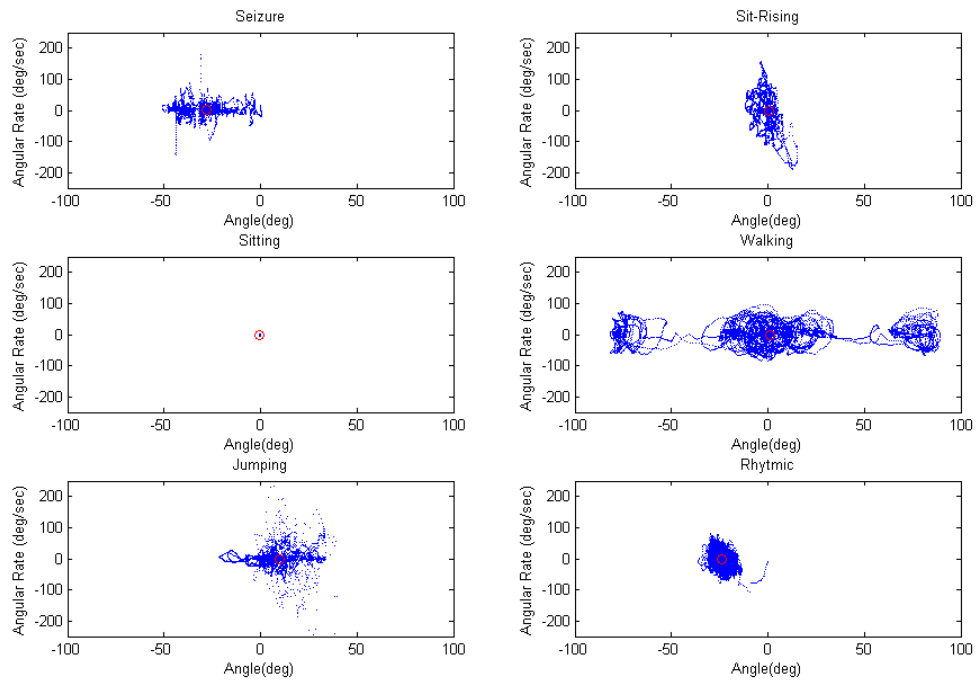


**Figure B. 8: Poincaré map for the Node 03 on the arm**

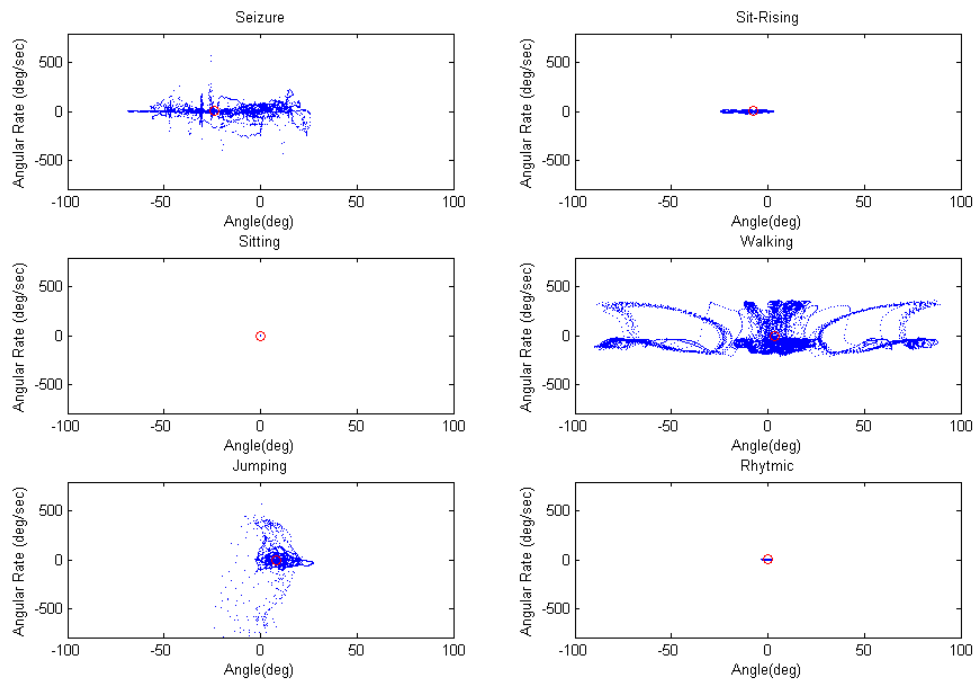


**Figure B. 9: Poincaré map for the Node 04 on the leg**

## Curriculum Vitae

- Name:** Babak Kamalizonouzi
- Post-secondary Education and Degrees:** The University of Western Ontario  
London, Ontario, Canada  
2011-2012 M.E.Sc. Mechanical and Materials Engineering
- Sharif University of Technology  
Tehran, Iran  
2006-2010 B.Sc. Mechanical Engineering
- Honours and Awards:** Western Graduate Research Scholarship (WGRS)  
The University of Western Ontario  
2011-2012
- Related Work Experience:** Teaching Assistant  
The University of Western Ontario  
2011-2012
- Publications:**
- B. Kamalizonouzi, S. F. Asokanthan, "Inertial Sensor Dynamics, Selection and Applications for Epileptic Seizure Detection", Proceedings of ASME 2012 International Mechanical Engineering Congress & Exposition, IMECE2012-88371, Nov. 9-15 2012, Houston, Texas
  - B. Kamalizonouzi, S. F. Asokanthan, " Numerical Simulation of MDOF Human Body Dynamics VIA Motion Genesis™", CSB/SCB 2012 International Conference, Jun. 6-9 2012, Burnaby, British Columbia